Quantifying the Hydrological Impact of Landscape Re-greening Across Various Spatial Scales

Raha Hakimdavar

Submitted in partial fulfillment of the
requirements for the degree of
Doctor of Philosophy
in the Graduate School of Arts and Sciences

COLUMBIA UNIVERSITY

2016

ABSTRACT

Quantifying the Hydrological Impact of Landscape Re-greening Across Various Spatial Scales

Raha Hakimdavar

The conversion of natural landscapes for human use over the past century has led to significant ecological consequences. By clearing tropical forests, intensifying agriculture and expanding urban centers, human actions have transformed local, regional and global hydrology. Urban landscapes, designed and built atop impervious surfaces, inhibit the natural infiltration of rainfall into the subsurface. Deforestation, driven by the demand for natural resources and food production, alters river flow and regional climate. These land cover changes have manifested into a number of water management challenges, from the city to the watershed scale, and motivated investment into landscape re-greening programs. This movement has prompted the need for monitoring, evaluation and prediction of the hydrological benefits of re-greening. The research presented in this dissertation assesses the contribution of different re-greening strategies to water resources management, from multiple scales. Specifically, re-greening at the city scale is investigated through the study of vegetated rooftops (*green roofs*) in a dense urban environment. Re-greening at the watershed scale is investigated through the study of forest regeneration on deforested and ecologically degraded land in the tropics.

First, the benefits of city re-greening for urban water management are investigated through monitoring and modeling the hydrological behavior of a number of green roofs in New York City (NYC). Influence of green roof size and rainfall characteristics on a green roof's ability to retain/ detain rainwater are explored and the ability of a soil

infiltration model to predict green roof hydrology is assessed. Findings from this work present insight regarding green roof design optimization, which has utility for scientific researchers, architects, and engineers.

Next, a cost effective tool is developed that can be used to evaluate green roof hydrologic performance, citywide. This tool, termed the Soil Water Apportioning Method (SWAM), generates green roof runoff and evapotranspiration based on minimally measured parameters. SWAM is validated using measured runoff from three extensive green roofs in NYC. Additional to green roofs, there is potential for SWAM to be used in the hydrologic performance evaluation of other types of green infrastructure, making SWAM a relevant tool for city planners and agencies as well as for researchers from various disciplines of study.

Finally, the impact of degraded landscape re-greening is investigated using a case study of 15 watersheds in Puerto Rico that have experienced extensive reforestation. The study provides evidence of improved soil conditions following reforestation, which in effect positively impacts streamflow generation processes. Findings from this work fill a gap in knowledge regarding the hydrological benefits of forest regeneration in mesoscale watersheds and provide guidance for future investment into reforestation programs.

Land cover will inevitably continue to change to meet the needs of a growing and increasingly urban population. Yet there is potential to offset some of the ecological effects – especially those on hydrology – that result from land cover change. As a whole, this dissertation aims to contribute knowledge that can be used to make the re-greening of altered landscapes more realizable.

Table of Contents

List of Figures

List of Tables

Acknowledgements

It is a rare gift to wake up each morning full of ideas, excited for the prospects of work that lay ahead. The past four years have broadened my perspective about science, the world at large and about my own abilities. These years have been some of the most transformative and exhilarating of my adult life. For affording me this gift, I have many to thank.

First, I cannot thank my PhD advisor Dr. Patricia Culligan enough for giving me the opportunity to discover my love for scientific research. Dr. Culligan's enthusiasm for challenging conventional disciplinary boundaries and constant encouragement to follow my ideas, big and small, through to the end are what gave me the confidence to begin and complete my doctoral studies. I thank Dr. Wade McGillis for showing me how to make even the most complicated research topics and tasks fun and for constantly challenging me to consider the broader implications of my work. I owe a great deal to Professors Pierre Gentine and Maria Uriarte for furthering my interdisciplinary education and for providing me with guidance in carrying out the research on tropical land cover change and hydrology. I acknowledge my PhD committee members, Patricia Culligan, George Deodatis, Pierre Gentine, Wade McGillis and Steve WaiChing Sun for their contributions to the final product of my work.

To my research group members, Tyler Carson, Rebecca Gibson, Diana Hsueh, Po-Chieh Liu, Daniel Marasco, and Nandan Shetty, thank you for your valuable feedback and for creating a supportive environment for the sharing of ideas. I especially thank my officemate Robert Elliott for his friendship through the good and difficult times of the past years. For feeding my curiosity about all research topics under the sun (and even

some beyond it), I extend gratitude to my IGERT colleagues, faculty and administrators. Having the freedom to explore the language and culture of different academic disciplines has been one of the most fulfilling aspects of my education and an experience that I will continue to cherish and cultivate.

I thank the United Nations Environment Program (UNEP), the Center for International Earth Science Information Network (CIESIN), and again Dr. Wade McGillis for affording me the unique opportunity to contribute to their projects in Haiti over the past five years. The research summarized in Chapter 4 of this dissertation was, without a doubt, carried out to address one of the most critical environmental challenges facing Haiti – deforestation. It is my sincere hope that the findings from the work can be expanded upon in the future and used to make more informed decisions regarding investment into reforestation programs in Haiti. I also thank everyone that I had the pleasure to work with and meet on my trips to Haiti – *mesi anpil*.

The chance to spend a year of my graduate studies as a visiting scholar at the Technical University of Delft (TU Delft) in the Netherlands contributed immensely to my professional and personal development. For granting me the opportunity to work with exceptionally talented researchers at TU Delft, I pay a debt of gratitude to the William J. Fulbright foundation, the Fulbright commission in the Netherlands, and the Netherlands America Foundation. I thank Dr. Nick van de Giesen for supporting my work at TU Delft and for sharing the inspired work of the Trans African Hydro-Meteorological Observatory with me. I also extend a warm thank you to the all of the wonderful people that I met at TU Delft, many of whom have become lifelong collaborators and friends.

To my amazing friends from near and far: thank you for always reminding me of the important things in life. To my best friends Allison Howard and Kristi Bergstrom, I don't think that I could have gotten through the last year without you – thank you.

Finally, there is little appreciation that can be expressed with words about the unconditional love and support given to me by my family over these years. To my sister, Golnoosh Hakimdavar, thank you for your fearless strength and unwavering kindness. There is no one in this world that I aspire to be more like than you. To my mother, Atoofeh Hakimdavar, thank you for helping me to find beauty and optimism in every aspect of life and for encouraging me to work hard while living life to the fullest. To my father, Houshang Hakimdavar, I owe everything. Thank you for instilling in me a drive to excel not for personal gain but for the betterment of society and those around me; thank you for teaching me to stand up for what is right and fair; thank you for teaching me the value of hard work and sacrifice; thank you for seeing potential in me when I could not see it myself. Most of all, thank you for being my greatest teacher. Although you are not here to see the final product of my work, in this dissertation and beyond it, you have inspired every single aspect of it.

The research presented in this dissertation was made possible with the financial support of the National Science Foundation (NSF) grant CMMI-0928604, the Environmental Protection Agency grant AE-83481601-1, the NSF Integrative Graduate Education and Research Training (IGERT) Fellowship #DGE-0903597, the William J. Fulbright Foundation / Netherlands America Foundation, and the United Nations Environment Program.

I dedicate this dissertation, wholeheartedly, to my father
Houshang Hakimdavar

Chapter 1

Introduction

The rapid conversion of land cover over the past century has had significant local and regional consequences on hydro-climate systems (Foley et al., 2005; Grimm et al., 2008). The demand for clearing otherwise natural landscapes has stemmed from the need to support the unprecedented rates of urban population growth (Grimm et al., 2008). Today, more than half of the globe is considered urban, a number that is projected to grow to 66% by 2050 (United Nations, 2014). The flourishing need for agricultural products to support the world's urban population, along with the exodus of greater numbers of people into cities, have been the largest drivers of global deforestation, urban sprawl and subsequently a growing number of water management challenges (Brown, 2001; DeFries et al., 2010; Vörösmarty et al., 2000). The consequences of land cover change (LCC) on local and regional hydro-climatology may in some cases even outweigh those from climate change, making region-specific data and modeling driven studies vital for future water and land use planning decisions (DeFries and Eshleman, 2004; Lovett et al., 2007; Pielke, 2005; Vörösmarty et al., 2000).

LCC can disrupt the surface water balance by affecting the partitioning of precipitation into evapotranspiration, runoff and groundwater flow. Locally, at the sub-watershed scale, the conversion of otherwise pervious surfaces into impervious cover, through clearing vegetation and trees and leveling and compacting of natural soils,

inhibits the infiltration of rainwater into the sub-surface, resulting in greater surface runoff than would have been experienced during a pre-clearing and/ or pre-urbanization period (Paul and Meyer, 2001). Regionally, at the watershed scale, river flow generally increases post clearing (Costa et al., 2003), although quantifying the impact of LCC on hydrology at this scale often requires region-specific studies that can discern between differences in geology, soils, topography and climate as well as heterogeneities in land cover (Andressian, 2004). Increased impervious cover through forest clearing and urbanization at both scales also affects water quality by funneling accumulated pollutants, including nutrients, metals and pesticides, from buildings, roadways, and agricultural lands into streams (Grimm et al., 2008; Paul and Meyer, 2001). Thus, the clearing and re-defining of land cover has a direct impact on the lives of people and their environments, potentially leading to greater risks of flooding due to less soil water storage capacity (Bradshaw et al., 2007) and water resources contamination, among other things. Considering this, mitigating the water management challenges brought on by LCC requires a holistic approach that simultaneously considers solutions across various spatial scales (Blöschl et al., 2007).

Increasingly, focus has been placed on utilizing natural measures to combat the water management challenges brought on by LCC. Among the different options, re-greening strategies such as reforestation programs and the incorporation of vegetated, or 'green', infrastructure into urban landscapes prove the most attractive at both the sub-watershed and watershed scale, due to their benefits beyond ameliorating water quantity and quality issues (Chazdon, 2008; Lamb et al., 2005; Laurance, 2007; Tzoulas et al., 2007). While neither strategy can replace the ecological functions of the original

landscape (Hobbs et al., 2006), these new systems can potentially help to establish a new hydrologic balance amidst our increasingly urbanizing world. For this reason, quantifying the benefits – in the case of this dissertation, the hydrological benefits – of re-greening programs in urban and non-urban environments is vital for making more cognizant land use and water management planning decisions that can better assess the costs as well as the benefits of different available options (Gartner et al., 2013).

1.1. Dissertation objective

The overarching objective of this dissertation is to advance the current state of knowledge regarding landscape re-greening strategies at various spatial scales by: 1) quantifying the impact of vegetated rooftop (*green roof*) drainage size on its ability to control stormwater runoff at the rooftop-scale, 2) developing a widely applicable and cost-effective method for quantifying green roof hydrology at a city-scale, and 3) quantifying the impact of reforestation on watershed scale hydrology in degraded landscapes. To achieve this three-pronged objective, the research draws on case studies in New York City and Puerto Rico. Section 1.2 provides background information regarding each case study.

1.2. Background

1.2.1. Re-greening in New York City

Recently, much focus has been placed on incorporating non-traditional, decentralized stormwater management infrastructure – such as those using vegetation, soils and natural processes – into urban spaces to help combat water management issues arising from increasing urbanization and shifting climate patterns. These green

infrastructure systems aim to mimic pre-development hydrology (Coffman, 2000) by capturing rainwater at its source, promoting evapotranspiration, and leading to a slow release of the remaining retained water into existing city infrastructure (see Figure 1.1). Green roofs in particular have gained popularity as a subset of green infrastructure that could be implemented in dense urban environments where land availability is scarce.

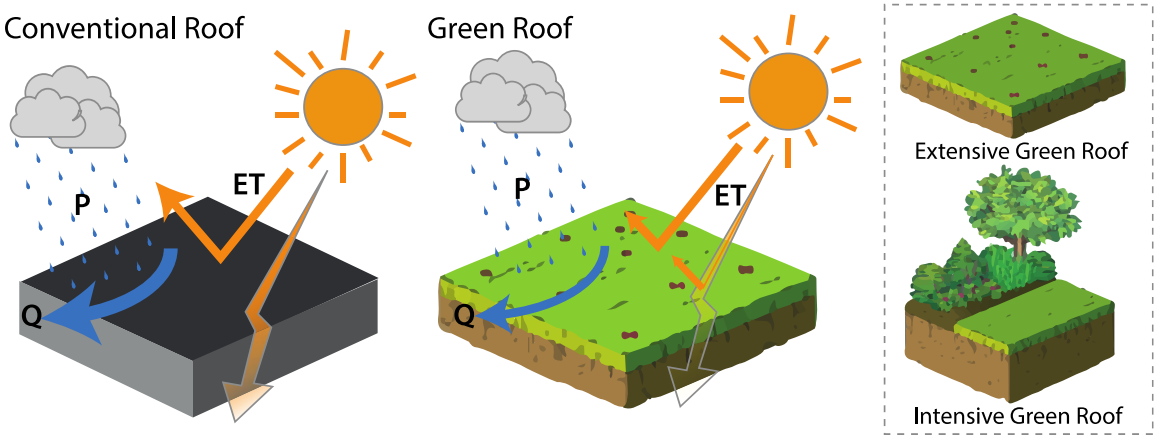

Figure 1.1. Schematic of the hydrologic functionality of green roofs, compared with a conventional blacktop roof. Green roofs are believed to reduce stormwater runoff (Q) by capturing rainwater at its source, promoting evapotranspiration (ET) and leading to a slow release of the remaining precipitation (P).

Green roofs are typically composed of an engineered soil substrate planted with drought tolerant vegetation, and are underlain by a drainage layer that allows for vertically infiltrated rainwater to be transported toward the roof drain. Green roofs are classified as either extensive (<150 mm depth substrate) or intensive (>150 mm depth substrate) (Carson et al., 2013) based on their substrate thickness and the type of vegetation that they can support (see Figure 1.1). The use of one type over the other is most often dependent on cost and rooftop weight restrictions. Due to their lower cost, maintenance requirements, and weight per unit area, extensive green roofs are more widely implemented in established urban areas, and are the focus of the research presented in this dissertation.

The appeal of green roofs for dense urban areas is twofold. First, rooftops are estimated to compose up to 50% of the impervious surface area of many cities (Culligan et al., 2011; Hoffman, 2006; Marsalek et al., 2006), revealing a nearly untapped source for green infrastructure implementation. Second, green roofs can provide many environmental co-benefits in addition to rainwater attenuation. Studies have shown, for example, that green roofs can help to reduce the urban heat island effect (Susca et al., 2011; Takebayashi and Moriyama, 2007; Wong et al., 2003), increase building insulation (Niachou et al., 2001; Wong et al., 2003), control air pollution (Yang et al., 2008) and help manage urban noise (Van Renterghem and Botteldooren, 2011, 2009). These co-benefits, along with the availability of suitable rooftop space in cities provide a strong motivation for investment in green roof systems.

As green roof implementation in urban areas becomes more typical, there is a growing need to quantify their region-specific benefits on water systems using robust and widely applicable physical monitoring and modeling programs. New York City presents an important case study for investigating the impact of urban re-greening because of the city's large planned investments in new green infrastructure installations over the next 20 years, which are projected to be in the thousands (Bloomberg and Lloyd, 2013).

1.2.2. Re-greening in Puerto Rico

Although deforestation can have significant effects on watershed hydrology (see Figure 1.2), the extent of the relationship between forest cover and runoff remains a contentious issue, subject to ongoing discussion (Andressian, 2004; Bruijnzeel, 2004). While in recent years, there has been much attention on the role of forests in mitigating floods (ex. Bradshaw et al., 2007; Van Dijk et al., 2009), the impact of reforestation on

low, high and seasonal flows is also under growing debate as deforested lands are being abandoned, allowing for secondary forest regrowth, and greater investments are being made into reforestation programs (Bruijnzeel, 2004; Chazdon, 2008; Giambelluca, 2002; Lamb et al., 2005). Globally, secondary forests account for 70% of the total forested land in the tropics (Brown and Lugo, 1990; FAO, 2010). In Latin America and the Caribbean, secondary forests account for roughly 66% of the deforested land area (Aide et al., 2012).

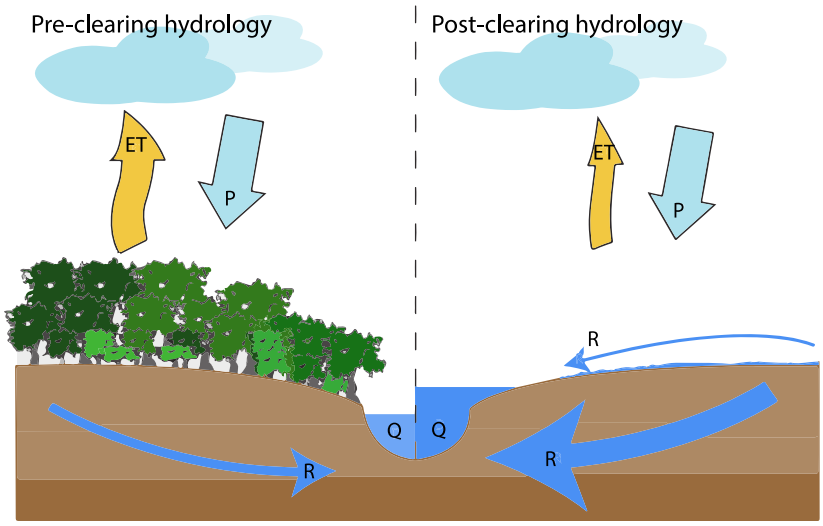

Figure 1.2. Generalized schematic of the impact of deforestation on watershed hydrology. Deforestation reduces local evapotranspiration (ET) through decreased plant water demand from vegetation, as a result total water yield (R) and river runoff (Q) are increased. At a regional scale, precipitation (P) patterns may also be affected. Figure adapted from Wohl et al. (2012).

The regeneration of forests on previously degraded landscapes may lead to improved soil water storage capacity over time, however, the hydrological benefits of forest recovery remain poorly understood (Bruijnzeel, 2004). To date, the general contention is that the impact of reforestation on watershed hydrology depends on the trade-off between increases in runoff due to enhanced soil water recharge and decreases in soil water reserves due to the higher water use of trees compared to crops, pasture, or shrub lands (Bonell and Bruijnzeel, 2005; Bruijnzeel, 2004, 1989). This trade-off is also dependent on the physical environment of the reforested region, namely on the soil type,

underlying geology, climate, topography and land cover, making it difficult to draw general conclusions without undertaking regional studies (Price, 2011; Wohl et al., 2012). The benefits of reforestation may also be further complicated by the degree of degradation that the landscape sustained prior to re-greening efforts (Giambelluca, 2002). Thus, there is an immediate need for greater understanding of reforestation – whether from agricultural land abandonment or from targeted reforestation programs – on regional hydrology. This is an especially important topic for developing countries that have faced severe deforestation and land degradation and are now making large investments into targeted reforestation programs with the aim of rehabilitating the degraded environment (ex. in Haiti Lall, 2013). Unfortunately, however, many of these nations lack the historical record of hydro-climate and land cover data required to conduct robust studies regarding the hydrologic impact of re-greening efforts (FAO, 2010; Wohl et al., 2012).

The Caribbean island of Puerto Rico presents a good opportunity to study the impact of natural forest regeneration on regional hydrology. The island nation has experienced significant changes in land cover over the past 60 years – forest cover rose from less than 10% in the 1930s to approximately 57% in 2003 (Brandeis et al., 2003) and nearly half of the island is estimated to be in some degree of urban sprawl (Martinuzzi et al., 2007). Most of the reforestation in Puerto Rico has occurred on abandoned agricultural lands and coffee plantations (Aide et al., 2012; López et al., 2001). Contrary to its neighboring islands in the Caribbean basin, however, Puerto Rico has a strong record of publically available hydro-climate and historical land cover data, which make it possible to conduct analysis on historical water and LCC dynamics. Thus,

studying the impact of LCC on watershed hydrology in Puerto Rico can help to both advance knowledge of tropical reforestation and to provide critical information for other tropical regions undergoing land cover conversion.

1.3. Research questions & dissertation format

Given the importance of LCC on local and regional hydrology and current limitations in the state of knowledge on this topic, this dissertation aims to quantify the impact of landscape re-greening on water systems across various spatial scales. The dissertation takes a three-paper structure to meet the main objective, in each chapter offering studies representing different scales of re-greening, from the sub-watershed to the watershed scale. Figure 1.3 outlines the format of the dissertation, presenting the key research question addressed in each chapter.

In *Chapter 2*, the research seeks to fill a gap in knowledge regarding the impact of green roof scale on its hydrologic performance. Specifically, this chapter investigates how rainfall characteristics and green roof drainage area impact the peak and cumulative volume of green roof runoff during individual storm events. Hydro-climate data gathered from three extensive green roofs of variable size in New York City is analyzed and the applicability of a one-dimensional infiltration model for future studies is assessed. *Chapter 3* also focuses on quantifying green roof hydrologic performance by developing a low-cost method for the long-term evaluation of green roof runoff and evapotranspiration that can be applied at a citywide scale. The method, termed the Soil Water Apportioning Method (SWAM), relies solely on measurements of local precipitation, substrate soil moisture and knowledge of the substrate maximum water storage capacity, and is validated using measured parameters from three extensive green

roofs in New York City. The final core chapter, *Chapter 4*, investigates the impact of LCC – focusing on reforestation – on 15 mesoscale watersheds in Puerto Rico for the period between1955 to 2015. Various datasets from different sources are utilized to characterize 1) the physical characteristics and changes over time for each watershed, 2) changes in precipitation, total streamflow, and high, low and seasonal streamflow using trend analyses, 3) the influence of a number of biophysical and anthropogenic factors, including land cover, on changing streamflow, and 4) changes in the baseflow recession behavior. The concluding chapter of the dissertation, *Chapter 5*, discusses the contributions and future work. References and appendices are available at the end of the dissertation.

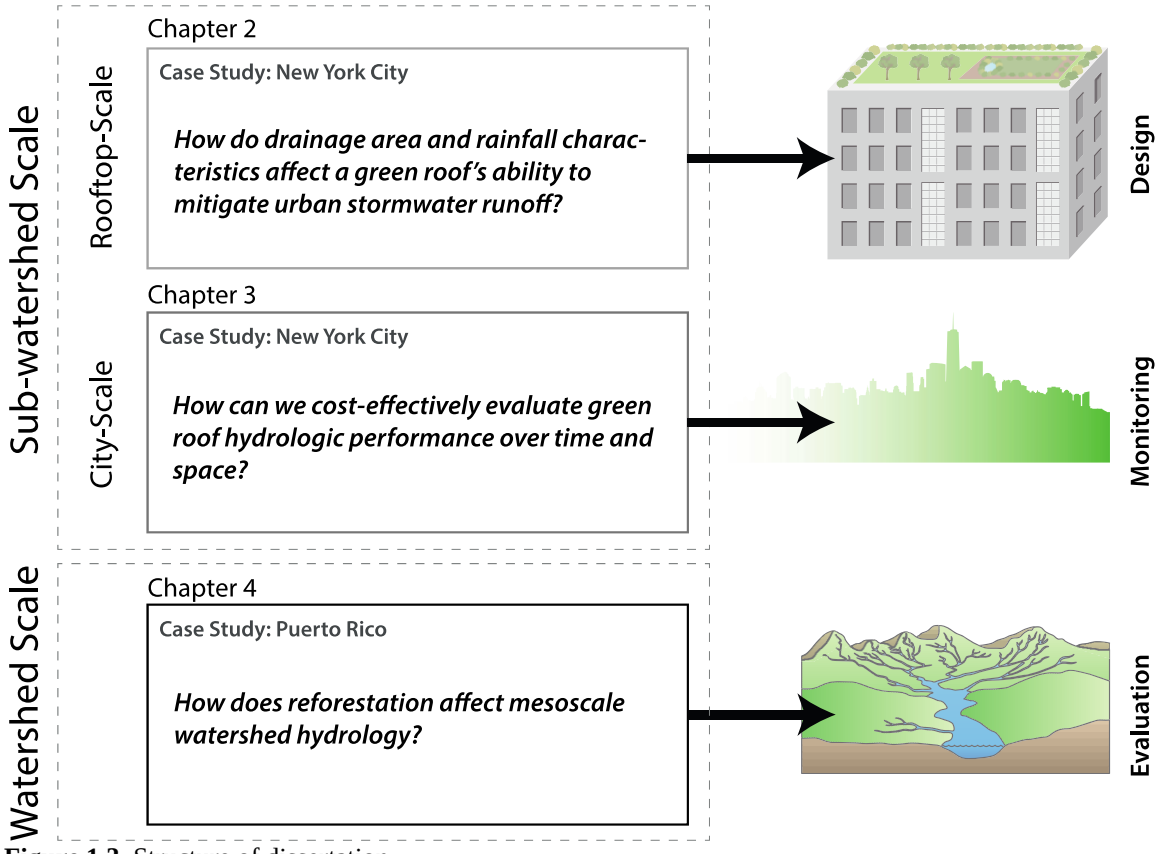

Figure 1.3. Structure of dissertation

Chapter 2

The effect of drainage area and rainfall characteristics on green roof hydrologic performance

Abstract – Green roofs offer many benefits for dense urban environments, one of which is their potential to supplement existing stormwater management infrastructure. The ability of green roof systems to act as a decentralized rainwater retention and detention network has been the topic of many recent studies. While these studies have provided important insight into the hydrologic performance of green roofs, none to date, to the knowledge of the author and her collaborators, have specifically examined the effect of green roof drainage area on system performance in an urban climate. The research summarized in this chapter aims to evaluate how rainfall characteristics and green roof scale impact the peak and cumulative volume of green roof runoff during individual storm events. The hydrologic performance of three extensive green roofs in New York City, each with the same engineered components and age but different drainage areas, are analyzed. It is found that green roof drainage area has the greatest impact on peak runoff reduction, with peak runoff reduction increasing with increasing drainage area, whereas rainfall retention and the time to peak runoff are not greatly influenced by drainage area. Data collected from the three green roofs are used to examine the applicability of a one-dimensional infiltration model, HYDRUS-1D, in predicting hydrologic behavior across the different green roof spatial scales. It is found that model performance improves as the green roof drainage area and rainfall volume increases. However, in general, HYDRUS-1D is only partially able to capture the hydrologic behavior of extensive green roofs across the different rooftop scales examined during this study.

Graphical Abstract – Graphical representation of the main findings regarding A) the influence of green roof drainage area on reductions in peak rainfall runoff and B) the influence of rainfall characteristics on green roof hydrologic performance.

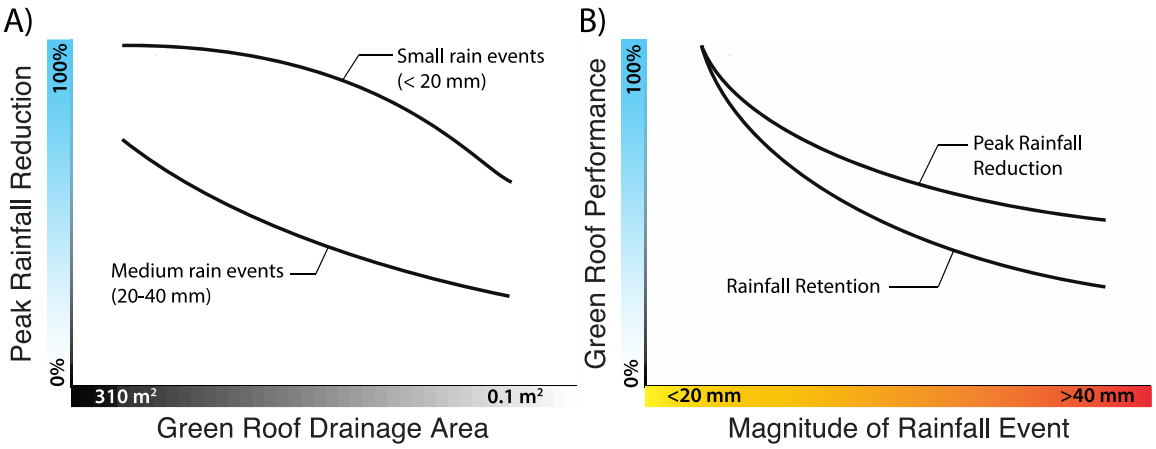

2.1. Introduction

Urbanization poses many challenges for stormwater management in cities. Reductions in pervious land area and vegetative cover, and the leveling and compacting of natural soils, have greatly modified the hydrologic cycle, resulting in higher rainfall runoff peaks, volumes and velocities than would be seen under pre-development conditions (Palla et al., 2012). Greater urban runoff can lead to disruptive flooding and, in many older cities, combined sewer overflows (CSOs) – the overflow of sewage and rainwater from single pipe systems into neighboring water bodies – affecting water quality and habitat health (National Research Council Committee on Reducing Stormwater Discharge Contributions to Water Pollution, 2009). While conveyance and detention infrastructure have traditionally been used for reducing urban flooding and CSO occurrences, these options are becoming increasingly difficult to implement in dense urban environments due to design and cost restrictions associated with city construction, creating a need for low footprint solutions at the ground and in the sub-terrain (Field and Sullivan, 2001). This need has made alternative design solutions, such as low impact development, an attractive option.

With the aim to mimic predevelopment hydrology (Coffman, 2000), low impact development focuses on designs that work with nature to reduce the impact of the built environment by, among other things, increasing pervious land area, managing stormwater as close to its source as possible, and mitigating the urban microclimate. Since in many cities rooftops make up to half of the impervious urban land area (Culligan et al., 2011; Hoffman, 2006; Marsalek et al., 2006; Palla et al., 2009; Villarreal and Bengtsson, 2005), there is a meaningful opportunity for green, or vegetated, roofs to become an important component of low impact development planning strategies (Carson et al., 2013; Guo et

al., 2012; Montalto et al., 2007; Palla et al., 2012). Compared with conventional roofs, the growing substrate and vegetation layers of green roofs attenuate and delay peak rainfall runoff and reduce overall runoff volumes (Berndtsson, 2010; Mentens et al., 2006; Stovin, 2010), thereby diminishing the load on combined and separate sewer systems as well as the likelihood of street flooding.

Green roofs are typically constructed by placing a drainage course, growing substrate, and vegetation on top of a roof's waterproof membrane. In some installations, green roofs may also have additional geo-synthetic layers for preventing plant root penetration damage, limiting sediment intrusion into the drainage course, and/or increasing water storage. It is common for green roofs to be classified as either extensive or intensive based on the thickness of the growing substrate layer (Berndtsson, 2010). Extensive roof substrates are generally classified as being 15 cm thick or less and feature short rooting, drought resistant plants, whereas intensive roof substrates are greater than 15 cm thick and may be sowed with deeper rooting plants including shrubs and trees. Due to their lighter weight and lower maintenance requirements, extensive green roofs are more widely implemented in urban environments than their intensive counterparts and are thus the focus of this study.

Several factors affect the ability of a green roof to mitigate urban runoff, including the hydraulic properties of the growing substrate, the substrate's antecedent moisture conditions – which will be influenced by local evaporation and transpiration potential – rainfall volume, and rainfall intensity (Carson et al., 2013; Hilten et al., 2008). Green roof geometry, including drainage area and configuration, can also influence green roof water retention capacity and runoff dynamics (Berndtsson, 2010). The size of the

drainage area, in particular, can influence rainwater travel times through horizontal drainage layers as well as rainwater detention – temporary storage and eventual slow release of water – which could affect both runoff and evapotranspiration. Thus, there is a need to better identify optimal strategies for green roof design and placement in urban environments that account for the influence of scale on green roof hydrologic performance. Although some research has been undertaken regarding the impact of green roof scale on a regional level (ex. Carter and Jackson, 2007; Villarreal et al., 2004), most studies have focused on the behavior of individual roofs without specifically accounting for the impact of roof size and the role of drainage area on urban green roof runoff characteristics.

The primary objective of this study was to evaluate how drainage area impacts green roof hydrologic performance during individual storm events and explore the applicability of a one-dimensional hydrologic model, HYDRUS-1D, in predicting that performance. Although green roof modeling efforts using HYDRUS-1D have been made in previous studies with relative success (ex. Hilten et al., 2008; Palla et al., 2012), to the best knowledge of the author and her collaborators no studies to date have explored the model's performance across green roofs that have the same engineered characteristics but different drainage areas. The results of this study aim to fill a gap in knowledge regarding the role of scale in urban green roof hydrologic performance, adding to the current body of work building toward effective urban planning of green infrastructure. In the sections that follow, the extensive green roof study sites, which span several orders of magnitude difference in drainage area, instrumentation and data collection protocols are described, together with the HYDRUS-1D model and parameter selection process. The observed

hydrologic behavior of the green roofs is then presented, followed by a comparison of the HYDRUS predictions and observed behavior for the different green roof scales. Finally, the limitations of the work are discussed and conclusions are drawn.

2.2. Methodology

2.2.1. Site descriptions

The three green roof sites that were part of this study are located on buildings around Columbia University's Morningside Campus in Manhattan, New York (Figure 2.1). The 423 West 118th Street building (*W118*) is a graduate student residence; the 635 West 115th Street building (*W115*) is Brownstone housing for Columbia University's Office of Environmental Stewardship, while the S.W. Mudd Building (*Mudd*) is the headquarters of Columbia's School of Engineering and Applied Sciences.

In 2007, the Xero Flor XF301+2FL pre-vegetated sedum mat system was installed on the *W115* and *W118* buildings. This system consists of a 32 mm thick integrated unit of plant material and growing substrate, underlain by two 6 mm thick water retention fleeces, a 19 mm non-woven polymer drainage mat and an 0.5 mm polyethylene root barrier (Figure 2.2). The sedum species grown in the mat include: *Saxifraga granulata, Sedum acre, Sedum album, Sedum ellacombianum, Sedum hybridum* 'Czars Gold', *Sedum oregonum, Sedum pulchellum, Sedum reflexum, Sedum sexangulare, Sedum spurium* var. *coccineum, Sedum stenopetalum*. Hummel & Co (2007) report that the substrate has a water-saturated density of 1.37 g/cm^3, a water storage capacity of 37.1%, and a saturated hydraulic conductivity of 1.26 cm/min, based on tests following the Forschungsgesellschaft Landschaftsentiwicklung Landschaftsbau guidelines (FLL, 2002). The 600 m^2 *W118* roof consists of two watersheds connected to

exterior parapet downspouts (Figure 2.1A), of which the southwest watershed, with a 310 m^2 drainage area, was monitored for rainfall, runoff and substrate moisture content. The smaller *W115* green roof has a single 99 m^2 watershed connected to an exterior parapet downspout (Figure 2.1B): this watershed was also monitored for rainfall, runoff and substrate moisture content. Fifty three percent and fifty eight percent of the *W118* and *W115* roofs are vegetated, respectively, with gravel walkways, parapets, and a raised rooftop above the buildings' elevator/ stairwell shaft comprising non-vegetated areas.

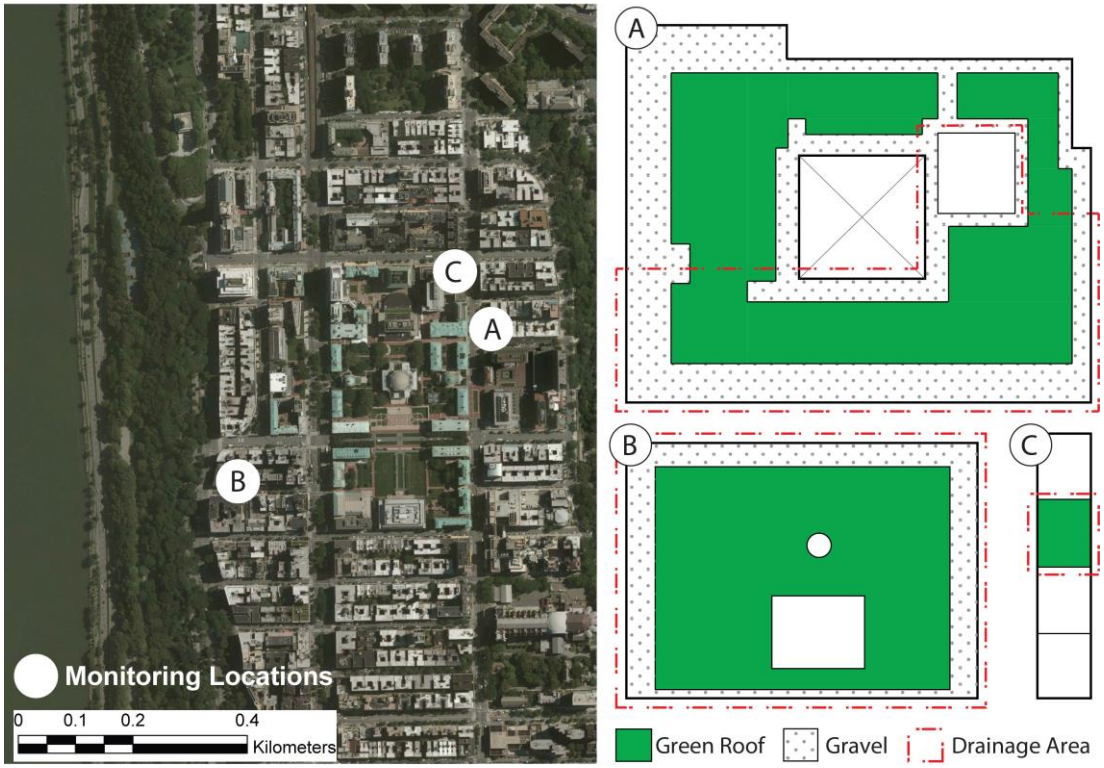

Figure 2.1. Locations and schematics of the studied green roof sites (A) *W118* (600 m^2), (B) *W115* (99 m^2), and (C) *Mudd* (0.09 m^2). Roof schematics are not to scale. The outlined drainage area reflects the monitored area used in this study.

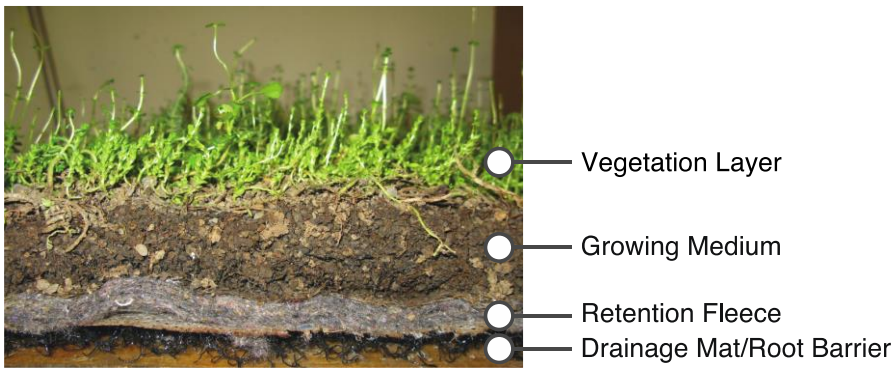

Figure 2.2. Profile and components of the XeroFlor® green roof system.

The *Mudd* site consists of a 30 cm x 30 cm test box assembled on the roof of the S.W. Mudd Building in 2008 as part of an experimental set up described in detail by Peterson (2009) (Figure 2.1C). A segment of the Xero Flor XF301+2FL pre-vegetated sedum mat system with the same stratification adopted for the *W118* and *W115* sites was placed in the test-box and monitored for rainfall and runoff only.

Table 2.1. Characterization of the investigated green roof sites.

Denomination	Location	Type	Monitored Drainage Area (m^2)
W118	423 W 118th Street, Manhattan (NY)	Full-scale	310
W115	646 W 115th Street, Manhattan (NY)	Full-scale	99
Mudd	500 W 120th Street, Manhattan (NY)	Test-box	0.09

2.2.2. Instrumentation and data collection

An Onset Hobo U30 (Hobo) data logger was installed on each of the roofs described above. Readings from equipment connected to the data loggers were taken every second and five minute averages were recorded and wirelessly uploaded to the

Onset Hobolink data service every hour. Data were then accessible on-line via this service.

For the *W118* and *W115* roofs, the Hobo logger recorded rainfall with a tipping bucket rain gauge, while green roof runoff was measured using custom designed weir devices described by Carson et al. (2013). Additional sensors were connected to the logger to record local environmental conditions such as green roof growing substrate moisture content and temperature, air temperature, solar radiation, wind speed, and relative humidity. The *W118* and *W115* data used in this study were recorded at five-minute intervals from August 2011 to July 2012.

For the *Mudd* site, runoff was measured by a tipping bucket that was placed beneath the drain of the test box, while rainfall was recorded with another tipping bucket located close to the test box. The *Mudd* data used in this study were recorded at five-minute intervals between September 2009 and November 2009.

2.2.3. Observed hydrologic performance

Monitored rainfall and corresponding runoff responses were separated into individual storm events following the National Oceanic and Atmospheric Administration (NOAA) minimum 6-hour dry weather period (National Oceanic and Atmospheric Administration, 2007). The separated events were pre-processed to assess suitability for analysis using criteria determined by Carson et al. (2013). Events were removed if (1) the recorded peak runoff rate caused an accumulation in the weir that exceeded 90% of the notch height, and thus was close to the measurement capacity of the weir, (2) precipitation was in the form of snow, (3) the recorded volume of runoff exceeded the volume of rainfall, which occurred when a weir became clogged with debris and leaves,

and (4) storm conditions caused a malfunction in the recording device. The events were then separated by green roof size and placed into three storm categories, representing small events (<20 mm rainfall depth), medium events (20-40 mm rainfall depth) and large events (>40 mm rainfall depth). The storm size categories will henceforth be referred to as small, medium and large events. Table 2.2 lists all available events together with those considered suitable for analysis for each green roof site.

Table 2.2. Characterization of observed storm events at the green roof sites.

Number of Events	W118	W115	Mudd
Total available	113	110	9
Suitable for analysis	63	79	6
0-10 mm	32	53	2
10-20 mm	9	17	1
20-30 mm	11	3	1
30-40 mm	2	2	1
>40 mm	9	4	1
Small	41	70	3
Medium	13	5	2
Large	9	4	1
Selected for Modeling			
Small	7	10	3
Medium	5	4	2
Large	4	2	1

The hydrologic performance of the green roof sites was assessed per unit area of rooftop, to enable comparison across the different roof scales. The assessment was based on three parameters: (1) rainwater retention, (2) lag time between peak rainfall and peak runoff, and (3) the percent reduction from peak rainfall to peak runoff per unit roof area. Per the illustrative hydrographs in Figure 2.3, retention was calculated as:

$$\frac{\sum rainfall - \sum(GR\ runoff)/A}{\sum rainfall} \text{ x } 100 \qquad [2.1]$$

peak reduction as:

$$\frac{P_R - P_Q}{P_R} * 100 \quad [2.2]$$

and lag time as:

$$t_Q - t_R \quad [2.3]$$

where A is the total area of the roof, P_R and P_Q represent peak rainfall and peak runoff per unit roof area, respectively, and t_Q and t_R represent time to peak runoff and time to peak rainfall, respectively.

In what follows, all further references to runoff volume, peak runoff and peak reduction are per unit area of each roof.

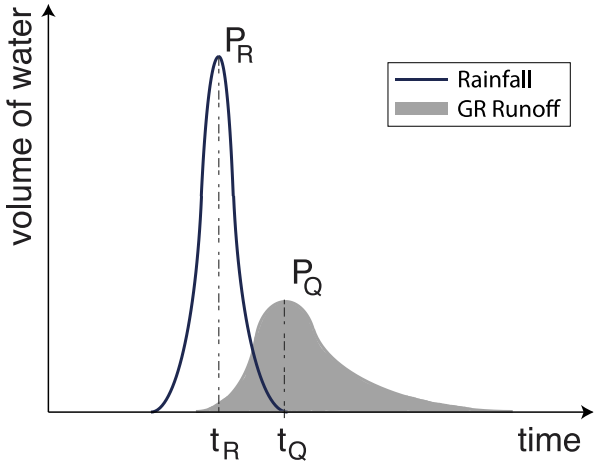

Figure 2.3. Illustrative rainfall and green roof runoff response hydrograph, indicating key parameters used for assessing hydrologic performance from the monitored systems. P_R and P_Q represent peak rainfall and peak runoff, respectively; t_R and t_Q represent time to peak rainfall and time to peak runoff, respectively.

2.2.4. Hydrologic modeling

Thirty-eight representative events, spanning different rainfall depths, durations and intensities, were selected for HYDRUS-1D modeling. Sixteen events each from the *W118* and *W115* roofs and six from the *Mudd* test box were modeled; corresponding to 25%, 20% and 100% of the total number of events recorded, respectively. Because the

number of recorded events was limited for the *Mudd* test box, all of the events were modeled in order to provide the widest range of behavior possible. The proceeding sections provide a discussion of the model, its derived input parameters, and the model validation process.

2.2.4.1. Model description, boundary and initial conditions

Given the relative thinness of the Xero Flor XF301+2FL pre-vegetated system, the dominant process governing water flow during individual storm events was considered to be vertical infiltration through the roof's layers to the base drainage mat. This assumption is also supported by a previous study from Bengtsson (2005). Thus, as per prior studies (ex. Hilten et al., 2008), the HYDRUS-1D finite element flow and solute transport model for variably saturated porous media (Šimůnek et al., 2009) was selected to simulate stormwater runoff behavior from the three green roof study sites.

HYDRUS-1D adopts the Galerkin type linear finite element scheme to numerically solve the one-dimensional form of the Richards equation:

$$\frac{\partial \theta(\psi)}{\partial t} = \frac{\partial}{\partial z}\left[K(\psi)\left(\frac{\partial \psi}{\partial z} + 1\right)\right] \qquad [2.4]$$

where θ is the volumetric water content [L^3L^{-3}], ψ is the tensiometer pressure potential [L], z is the vertical coordinate, positive upward, and K is the unsaturated hydraulic conductivity [LT^{-1}]. In order to obtain an analytical expression for the unsaturated hydraulic conductivity, the van Genuchten (1980) and Mualem (1976) relationships were adopted, viz:

$$\theta(\psi) = \begin{cases} \theta_r + \dfrac{\theta_s - \theta_r}{[1 + |\alpha\psi|^n]^m} & \psi < 0 \\ \theta_s & \psi \geq 0 \end{cases} \qquad [2.5]$$

and

$$K(\psi) = K_s {S_e}^{1/2} \left[1 - \left(1 - {S_e}^{1/m}\right)^m\right]^2 \quad [2.6]$$

where θ_r and θ_s are the residual and the saturated volumetric water content [L^3L^{-3}] of the modeled unit, respectively, α is a fitting parameter [L^{-1}], n and m are dimensionless shape parameters of the soil-water retention curve, being $m = 1 - 1 / n$, $S_e = (\theta - \theta_r)/(\theta_s - \theta_r)$ is the effective saturation, and K_S is the saturated hydraulic conductivity [LT^{-1}].

The 32.5 mm thick integrated unit of plant material and growing substrate and the two 6.25 mm thick water retention fleeces above the green roof's 19 mm thick drainage mat were modeled as a 50 mm thick homogenous unit, discretized into 101 contiguous nodes. The choice of 50 mm was based on observations that the thickness of the integrated unit of plant material was actually as high as 38 mm, thus a rounded average value of 50 mm was selected for the thickness of the integrated unit and water retention fleeces. At the unit's upper boundary a system-dependent boundary condition was imposed, since moisture content in the underlying layers impacts water flux through the unit's upper boundary. When the unit was unsaturated, a prescribed flux (equal to the atmospheric precipitation) was applied at the upper boundary. Conversely, when the unit reached saturation, a zero head condition ($\psi = 0$, no ponding) was applied; above which excess input water was converted into surface runoff. A free drainage boundary condition, corresponding to a zero-gradient pressure head ($\partial\psi/\partial z = 0$), was applied at the base of the modeled unit. This reflected the assumption that vertical drainage dominates flow due to the thinness and quick-draining nature of the green roof substrate.

Green roof hydrological behavior during each storm was then modeled by running simulations starting the hour prior to a storm, through the storm itself, to 6 hours

following the end of the storm. The precipitation data during each storm were input to HYDRUS at five-minute intervals using the relevant observed data from the rooftop tipping buckets.

Analysis was carried out to test the sensitivity of the extensive green roof water balance to evapotranspiration during a single storm event. Evapotranspiration (ET) was simulated for the *W115* roof based on the United Nations Food and Agriculture Organization (FAO) recommended Penman-Monteith combination equation and estimated soil-water availability (Šimůnek et al., 2009) using monitored meteorological data. Several events were modeled both with and without ET input, and the difference between the runoff results was found to be negligible. Based on this, evapotranspiration during storm events was not considered for any of the simulations. ET that would have affected the antecedent soil moisture conditions, however, was included.

The initial boundary conditions in HYDRUS represent the starting saturation of the green roof unit, expressed as a suction head. In all cases, it was assumed that the effective saturation of the unit was equivalent to the effective saturation of the green roof substrate prior to each storm event. Measurements of substrate moisture content were used to calculate the effective saturation of *W118* prior to each storm event and translated to an initial suction head via the medium's water retention curve (see Figure 2.4). Reliable moisture content data were not available for *W115* during the study period due to an instrument malfunction and substrate moisture content was not collected for *Mudd*. Hence, an average initial boundary condition from *W118* of 10% saturation was taken as the initial boundary condition for *W115* and *Mudd* for all storms. A sensitivity analysis on the impact of average versus actual initial boundary conditions was conducted for the

W118 roof. Because the models were able to converge the initial pressure heads within a few times steps, it was found that the difference between the predicted and observed runoff depth associated with using the average substrate saturation, versus measured saturation, was within 5%, which was considered acceptable.

2.2.4.2. Growing substrate water retention curve

The substrate water retention curve was measured in Columbia University's Heffner Hydraulics Laboratory using five samples of the green roof substrate. A 15 bar capacity pressure plate extractor was used to derive the curve (Figure 2.4), which represents the relationship between the volumetric substrate water content, θ, and the suction head in the substrate, ψ. The experimental procedure followed the method set out in ASTM International (2009). Different pressure levels, ranging from 0.1 to 8 bars, were applied to the five samples and the corresponding gravimetric water content of each sample was measured after equilibrium was reached at each pressure. The final substrate curve was then obtained by averaging the gravimetric water content of the five samples at each pressure point.

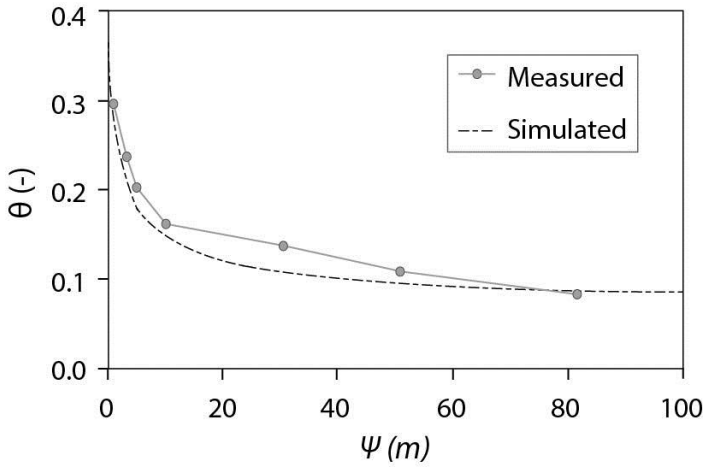

Figure 2.4. Measured and simulated water retention curves for the XeroFlor® growing medium.

2.2.4.3. Selection of model parameters

The solution of Eq. [2.4] in HYDRUS-1D requires the input of five independent parameters: θ_r; θ_s; α; n; K_S. Table 2.3 summarizes the values of these parameters used in this study. The values for α and n were estimated by fitting the experimentally derived water retention curve with the soil hydraulic model of Brooks and Corey (1964):

$$S_e = \left(\frac{\psi}{\psi_b}\right)^{-\lambda} \quad [2.7]$$

where ψ_b is the bubbling pressure [L] and λ is a dimensionless pore-size distribution index; α and n were then calculated from the following relationships (Van Genuchten, 1980):

$$\alpha = \frac{1}{\psi_b} \quad [2.8]$$

$$n = \frac{\lambda}{m} = \frac{n\lambda}{n-1} = \lambda + 1 \quad [2.9]$$

Values of θ_r and θ_s were obtained from the fitted water retention curve (see Figure 2.4), with θ_r taken as the volumetric water content at Ψ=100 m. The difference between θ_s and θ_r indicate an upper bound to the water retention capacity of the growing medium of 30%, which is 7% lower than that reported by Hummel & Co. (2007).

The saturated hydraulic conductivity of the green roof unit, K_S, was taken to be 1.26 cm/min, as reported by Hummel & Co. (2007) based on FLL testing protocol. This value is within the range 0.25 – 2.5 cm/min, which is considered satisfactory for green roof media saturated hydraulic conductivity (Snodgrass and McIntyre, 2010) and also

comparable to values reported by others; for example Sun et al. (2012) report K_s values of 0.7 cm/min and 0.65 cm/min for extensive green roofs located in China and the US, respectively, while van Spengen (2010) reports an average K_s value of 1.8 cm/min for a potting soil mix that was used to form an extensive green roof substrate in Singapore.

Table 2.3. Hydraulic parameters of the Xeroflor® substrate. θ_r, θ_s, α, and n were experimentally derived; K_S was adopted from laboratory test results reported by Hummel & Co (2007).

θ_r	θ_s	α	n	K_S	
(cm^3/cm^3)	(cm^3/cm^3)	(1/cm)	(-)	(cm/min)	(mm/h)
0.058	0.360	0.011	1.519	1.26	756

2.2.4.4. Quantification of model accuracy

The performance of the model simulations with respect to the observed data was assessed by comparing the predicted and observed hydrographs in terms of: total runoff depth, peak runoff rate, and time to peak runoff. In order to quantitatively evaluate the model accuracy in predicting green roof runoff during a single storm event, two statistics were used. Moriasi et al. (2007) recommend the Nash-Sutcliffe efficiency (NSE), ratio of the root mean square error to the standard deviation of measured data (RSR), and percent bias (PBIAS) to evaluate hydrologic model performance. According to their study, a watershed runoff model can be considered satisfactory if NSE > 0.5, RSR ≤ 0.7, and PBIAS ± 25%. Given the small scale of green roofs relative to typical small watersheds, the recommended threshold for PBIAS was not explicitly used as criteria for the HYDRUS-1D model performance, as it was believed that it would provide a false indication of model under-performance. Rather, PBIAS was used as a general indication for runoff bias, and was calculated so that positive values represent a positive bias, or

over-prediction, while negative values represent a negative bias, or an under-prediction. The recommended threshold values for NSE and RSR, however, were used as cutoff points for evaluating model performance.

The Nash-Sutcliffe Efficiency, NSE, index (Moriasi et al., 2007; Nash and Sutcliffe, 1970) was computed from:

$$NSE = 1 - \frac{\sum_{t=1}^{n}(q_t - \hat{q}_t)^2}{\sum_{t=1}^{n}(\mu - \hat{q}_t)^2} \quad [2.10]$$

where q_t and $\hat{q}_t$ are the predicted and the observed runoff values, respectively, *m* is the mean value of the observed outflow data, *t* represents a time step and *n* is the total number of time steps throughout the storm event. The NSE index ranges from $-\infty$ to 1. Negative values indicate that the model returns a less accurate estimation of the roof runoff than the mean value of the observed data, while a NSE index equal to 1 indicates a perfect equivalency between predicted and observed runoff.

2.3. Results and discussion

2.3.1. Rainfall characteristics and green roof hydrologic performance

The key climatic determinants for green roof hydrologic performance have often been identified as: rainfall depth, event intensity, event duration and the antecedent dry weather period (ADWP) (Berndtsson, 2010; Palla et al., 2011; Stovin, 2010). Thus, these four characteristics were used to guide the interpretation of the observed results for this study. Although rainfall intensity can be characterized in different ways, this study considered it to be the total precipitation divided by the duration of each event.

The results from this study (as displayed in Figure 2.5) indicate that, of the four key climatic determinants investigated, rainfall depth and event duration have the greatest

influence on rainfall retention and peak reduction. Across all three green roof scales, the average rainfall retention for events less than 20 mm in depth was 85%, whereas it was 48% for events 20-40 mm in depth, and 32% for events larger than 40 mm in depth. For average peak reduction: events less than 20 mm in depth displayed an average reduction of 89%, whereas an average reduction of 62% was seen for events of 20-40 mm in depth, and 51% for events larger than 40 mm in depth. These results are similar to those reported by others. For example, Carter and Rasmussen (2006) reported 88% retention for small rainfall events (<25.4 mm), 54% for medium rainfall events (25.4 to 76.2 mm) and 48% for large events (>76.2 mm) from a green roof study in Athens, Georgia. Although climate conditions play a factor in the performance of green roofs in different regions, the general finding that green roof retention and peak reduction decrease as rainfall volume increases is also in agreement with a number of other studies (Berghage et al., 2009; Carson et al., 2013; Getter et al., 2007).

The results presented in Figure 2.5C indicate that green roof rainfall retention and peak reduction performance decrease as storm duration increases. The average rainfall retention for events lasting less than 10 hours was 85%, 66% for events between 10-20 hours, and 43% for events lasting longer than 20 hours. With respect to the observed peak reduction: the average peak reduction for events lasting less than 10 hours was 89%, while it was only 67% for events between10-20 hours, and 55% for events lasting longer than 20 hours. These results are explained by the fact that total volume of rain increased as rainfall duration increased. Thus longer duration events reduced the water storage capacity of the substrate and resulted in more runoff. The exception to this was the occurrence of short duration, high intensity storms, which account for the large spread of

green roof performance displayed in Figure 2.5. A study of an extensive green roof in Pennsylvania by Bliss et al. (2009) also found a relationship between storm duration and overall green roof hydrologic performance, where the greatest reductions in total volume of runoff between the monitored green roof and a control roof were recorded for storms under 12 hours in duration.

One surprising trend is that the ADWP does not appear to have a primary influence on the rainfall retention or reduction in peak runoff for the green roofs studied (see Figure 2.5D). This finding differs from the reports of several other studies, which found the ADWP to be a key hydrological determinant for green roof performance (Fioretti et al., 2010; Palla et al., 2011; Stovin, 2010). The fact that similar trends in rainfall retention and peak runoff reduction are seen for ADWP values ranging from less than 50 hours to more than 100 hours is attributed to the observation that rainfall depth and event duration are greater determinants of hydrologic performance during individual storm events than ADWP for the investigated shallow, extensive green roofs. A similar conclusion was also drawn in a study by van Spengen (2010). Van Spengen's study, although based on test box observations and not the monitoring of full scale roofs, found that substrate moisture content is a better predictor for green roof retention than ADWP. This can be explained by the fact that the substrate moisture content is a more direct indicator of green roof retention capacity. Although there is a relationship between ADWP and substrate moisture, the relationship depends on factors that impact green roof evapotranspiration rates, such as growth season, air temperature, relative humidity and wind-speed.

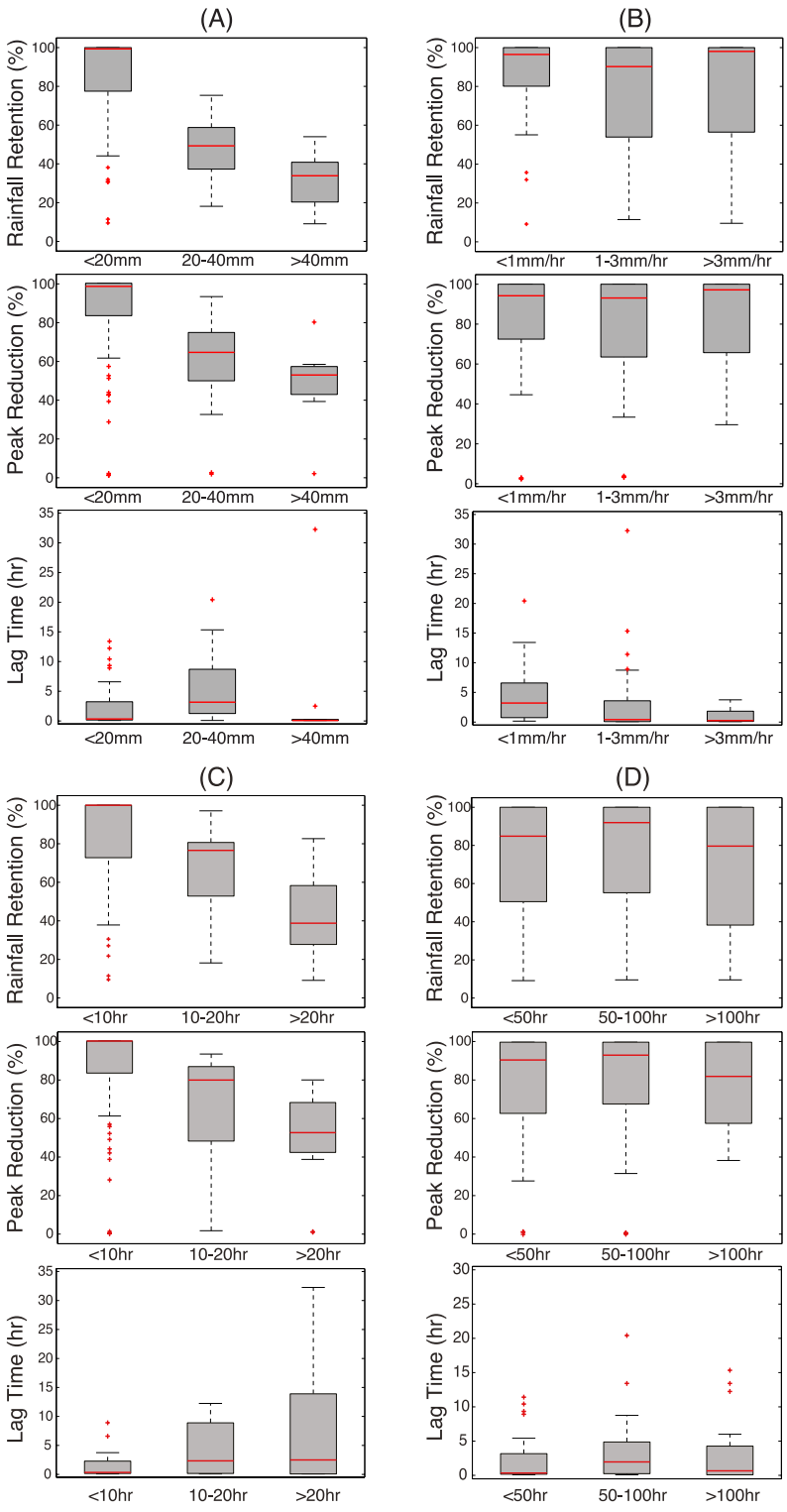

Figure 2.5. Rainfall retention, reduction in peak rainfall, and lag time between peak rainfall and peak runoff for all events from the studied sites broken down into three classes of (A) total rainfall depth, (B) rainfall intensity, calculated as the total precipitation divided by the duration of each event, (C) rainfall event duration and (D) antecedent dry weather period. Table A1 provides summary statistics for this figure.

The highest rainfall retention and peak reduction values were experienced most frequently during events characterized with less than 1 mm/hr of rainfall. Rainfall retention ranged from 55-100% (exclusive of finite outliers) for these events with an average value of 87%, while 25th and 75th quartiles spanned from 81-100%. In addition, peak reduction ranged from 66-100% (exclusive of finite outliers) with an average value of 88%, while 25th and 75th quartiles spanned from 86-100%. Green roof performance was largely consistent beyond 1 mm/hr event intensities. Rainfall retention ranged from 11-100% and 10-100% for event intensities of 1-3 mm/hr and those greater than 3 mm/hr, respectively; while peak reduction ranged from 3-100% and 28-100%. These results indicate that event intensities greater than 1 mm/hr play a much smaller role in predicting the hydrologic behavior of green roofs than rainfall depth and event duration. Bliss et al. (2009) also revealed a weak relationship between intensity and runoff reduction, where a wide range of runoff reductions occurred for storms of similar intensities.

Finally, it was found that lag time is not necessarily impacted by rainfall depth, event duration or ADWP, as no substantial trends between these storm characteristics and lag time were revealed during the analysis. It was, however, observed that lag time is significantly lowered during rainfall depths greater than 40 mm and event intensities greater than 1 mm/hr. The general conclusion that lag time decreases with increasing rainfall depth and intensity is in agreement with findings reported by Berghage et al. (2010).

2.3.2. The impact of drainage area on green roof hydrologic performance

Figure 2.6 displays observed rainfall retention, peak reduction and lag time for each of the three green roofs studied, divided into small (<20 mm rainfall depth), medium

(20-40 mm rainfall depth), and large events (>40 mm rainfall depth). For the large events, only data for *W118* and *W115* are shown due to insufficient data for a statistical analysis of the behavior of *Mudd* during larger storms. For a full range of summary statistics readers can refer to the Appendix section, Table A2.

Regarding rainfall retention, *W118* and *W115* displayed similar responses for small and medium events – average retention of 81% and 46% respectively for *W118*, and 89% and 52% respectively for *W115* – while *W115* had higher retention for large events, with an average retention of 43% versus 25% for *W118*. This could, in part, be due to differences in the number of larger events experienced by the two roofs; because of its location, the *W115* roof experiences a rain shadow effect from adjacent buildings, thus it is generally exposed to lower magnitude, shorter duration storms than the *W118* roof which is not shielded by other buildings (see Figure 2.1). The *Mudd* test box had lower rainfall retention than the other two roofs during small events, and, on average, comparable retention (46%) for the medium events. The limitations with data from this site will be discussed in Section 2.3.4.

As illustrated by Figure 2.6, reduction in peak runoff displays the strongest relationship to green roof scale. Figure 2.7 displays that relationship in the context of average peak reduction versus actual roof drainage area. Generally, as green roof scale increases, the peak reduction also increases, especially for small and medium events. The range of observed peak reductions also decreases as roof area increases. The three green roofs differ in the average distance water needs to travel in the drainage mat to the roof drain, where peak discharge is measured. Although prior work published by Bengtsson (2005) reported no relationship between peak discharge and roof drainage length, work

by Vesuviano and Stovin (2013) demonstrates a clear relationship between drainage length and peak discharge for green roof drainage layers, with peak discharge decreasing as drainage length increases, which is supported by this work.

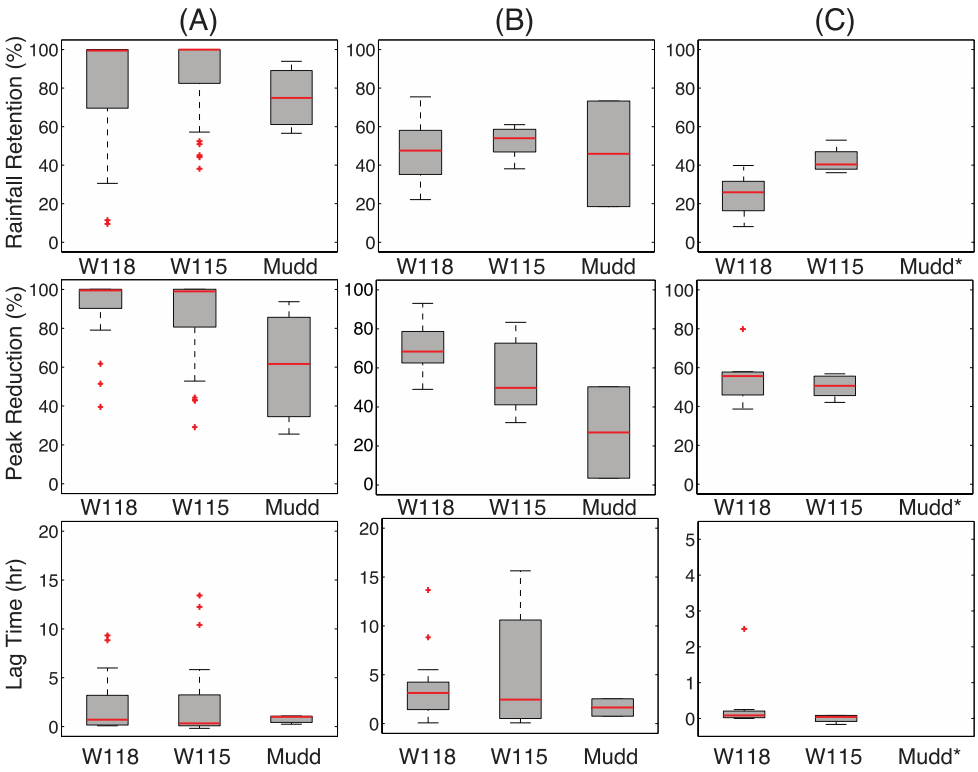

Figure 2.6. Observed rainfall retention, reduction in peak rainfall and lag time between peak rainfall and peak runoff for the three green roof sites for (A) small events (<20mm), (B) medium events (20-40mm), and (C) large events (>40mm). **Mudd* not included because only one large event was recorded during the study period. Table A2 provides summary statistics for this figure.

Lag time between peak rainfall and peak runoff for the *W118* roof ranged (considering 25th to 75th quartiles, and exclusive of lower and upper bounds and finite outliers) from 0.2 to 1.6 hours for small events, 1.4 to 4.2 hours for medium events and 0.1 to 0.2 hours for large events, while *W115* had lag times between 0.1 and 3.2 hours for small events, 0.5 and 10.4 for medium events, and 0 to 0.1 for large events. For the *Mudd* roof, lag time for small events ranged from 0.4 to 1.1 hours and for medium events from 0.8 to 2.5 hours. As might be anticipated, large events yielded the shortest lag times for

the two full-scale roofs. In addition, the *Mudd* roof displayed shorter relative lag times across the small and medium events, which is to be expected given its much smaller drainage area.

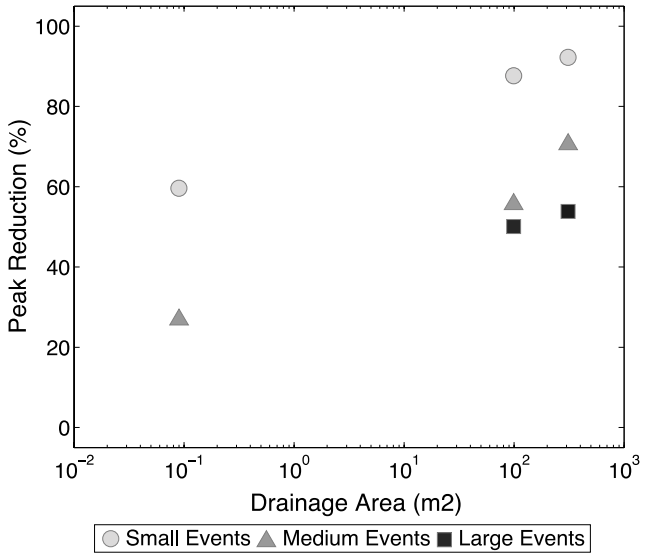

Figure 2.7. Mean peak reduction for different green roof drainage areas for small (< 20mm), medium (20 – 40mm) and large (> 40mm) rainfall events. Note that there were not enough large events to define a mean for the smallest roof size.

2.3.3. Comparisons of observed and modeled green roof performance

Figures A1 to A3 in the Appendix compare HYDRUS predictions with observations of rainfall depth, peak runoff rate and time to peak runoff, respectively; Table A3 provides a detailed summary of the modeling results. Figure 2.8 displays simulation hydrographs from representative events for each roof.

For the event based modeling, HYDRUS-1D captured best the *W118* performance for all storm categories and the *W115* performance for medium and large events. Prediction of the performance of *Mudd* improved with the total rainfall depth during a storm, but was generally not well captured. These findings could be related to the influence of system heterogeneity with spatial scale. For smaller roofs, system

heterogeneities, such as the existence of preferential flow paths, will exert greater influence on overall water flow patterns than for larger roofs. Thus, the hydrologic applicability of a model that assumes uniform system properties, as was the case for the HYDRUS simulations presented here, could reduce with smaller spatial scale.

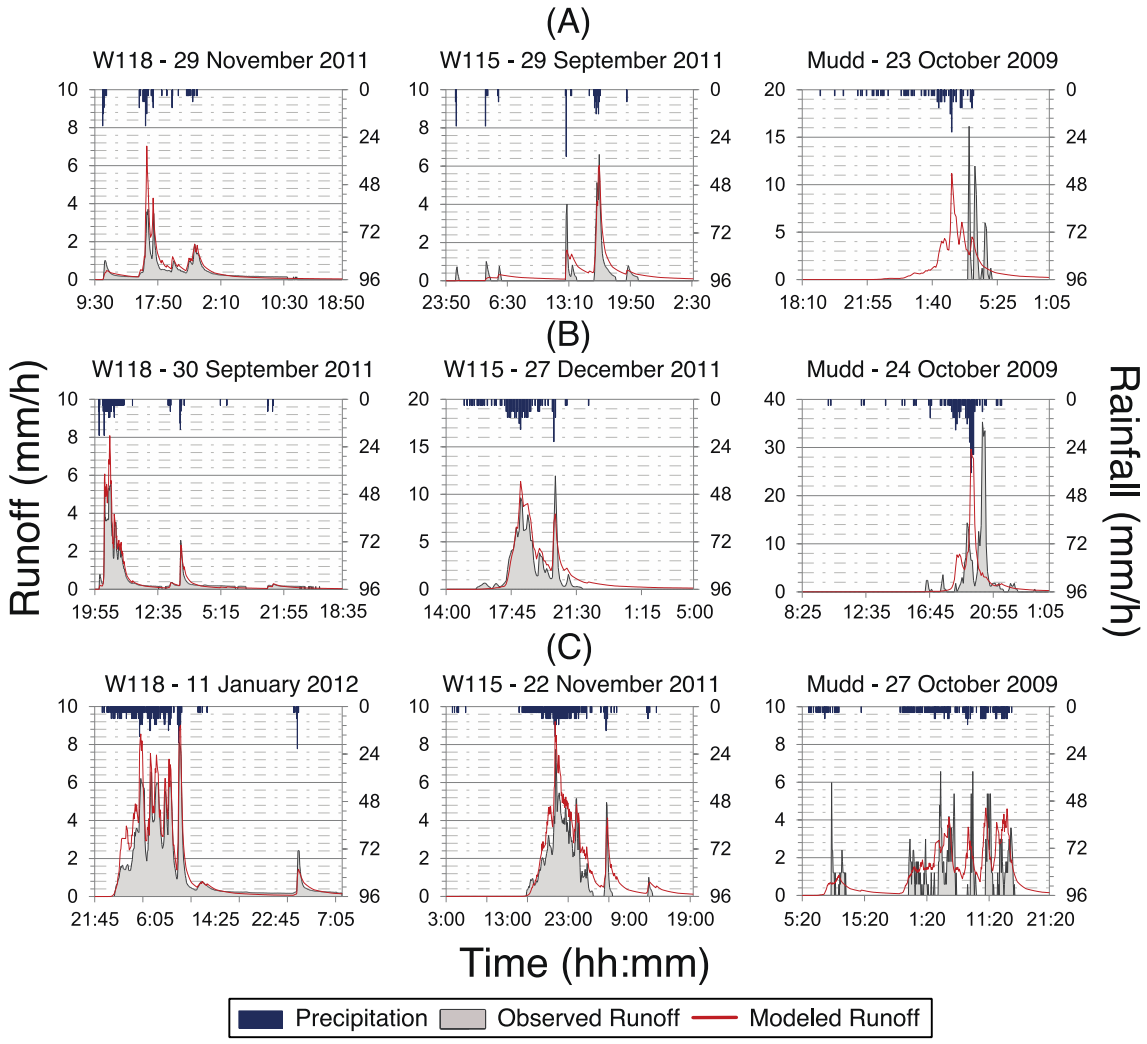

Figure 2.8. The hyetograph and corresponding observed and simulated hydrographs for selected event based models of the investigated green roof sites. The plots are divided into (A) small events (<20mm), (B) medium events (20-40mm), and (C) large events (>40mm).

Except for rainfall events of 2 mm or less, HYDRUS-1D over-predicted the total depth of runoff for all three roofs (Figure A1), with the absolute error in prediction

increasing with the event size. Hilten et al. (2008) also observed that HYDRUS appears to over-predict for large storm events, but report better agreement between HYDRUS and observed total runoff for storms of 20 mm or less. Individual events modeled with HYDRUS in a study by Palla et al. (2012) indicated a mixed bias, with some green roof runoff volumes being over-predicted and others under-predicted with a range of PBIAS (referred to in their paper as relative percent difference) of -13% to 28%.

With respect to peak runoff rate (Figure A2): HYDRUS-1D over-predicted peak runoff for *W118* for all storms, but one, and under-predicted peak-runoff for *Mudd* for all storms but one. Over all of the storm categories, the peak runoff rate was most accurately predicted for the mid-sized roof, *W115*. As per the discussion above, peak runoff displayed the strongest relationship to green roof scale. Thus, differences between the accuracy of the HYDRUS predictions for the different roof sizes are to be expected, especially since the HYDRUS predictions do not account for water flow in each green roof's base drainage mat. Nonetheless, given this, it might also be expected that HYDRUS would best predict the peak runoff rates observed at the *Mudd* site. The fact that the behavior of the *Mudd* system was not well captured by HYDRUS is attributed to the greater influence of system heterogeneity on green roof behavior at small spatial scales, as discussed above. Specifically, the under-prediction of observed peak runoff could indicate the existence of influential preferential pathways in the *Mudd* set-up. For the largest W118 roof site, it is believed that the over-estimation of peak runoff rate is explained by a reduction in peak runoff rate with travel time in a green roof's under-drain, which becomes more notable as roof size increases.

In general, time to peak runoff is well predicted for all storm categories across all green roof scales (Figure A3). For *Mudd,* the largest difference between the observed and predicted time to peak occurs when HYDRUS over-predicts the time to peak, which again might indicate the influence of preferential pathways in *Mudd*. For *W118,* the converse is true, with the greatest difference between observed and predicted time to peak occurring when HYDRUS under-predicts time to peak. Although this difference is not large, it could be related to the travel time in the roof's under-drain slowing the arrival of the peak in the real system, but not the modeled system.

Finally, Figure 2.9 shows variation of NSE, RSR and PBIAS with total rainfall depth for the predicted versus observed results. Generally, the event based models had a positive PBIAS for the total runoff depth when compared with observed values, translating to model over-prediction of runoff; however, this bias decreased as rainfall depth increased. Similarly, the model performance improved as the roof system drainage area increased. The *W118* roof had the highest overall performance indicators with an average NSE value of 0.49, RSR value of 0.51and PBIAS of 21% based on all modeled events, *W115* followed with an average NSE of 0.16, RSR of 0.84, and PBIAS of 71%, while *Mudd* had the poorest performance of the three with an average NSE of -0.45, RSR of 1.45 and PBIAS of 111% (see Table A3). Based on the modified hydrologic model performance criteria recommended by Moriasi et al. (2007), 10 modeled events from the *W118* roof, 7 from the *W115* roof and zero from the *Mudd* test box performed sufficiently, as these events were the only ones to satisfy the thresholds set by the two statistics, NSE and RSR (see Table A3). With the exception of one event from the *W115* roof and one event from *Mudd,* the models that under-performed were all simulations for

rain events of less than 20 hours. One reason for this is that initial boundary conditions play a larger role in overall model performance for shorter duration events than they do for longer ones, thus if actual substrate saturation conditions before a rain event differ from the estimated or assumed value, the model is likely to produce higher or lower runoff than is observed. Although the influence of preferential pathways in the different roofs is believed to be contributing, in part, to the error in runoff depth predictions as drainage area decreases, another contributing source of error may be the lack of actual substrate moisture observations for the *W115* and *Mudd* sites, as these sites also had the poorest performing models. Limitations due to the lack of reliable observed saturation conditions for the *W115* and *Mudd* sites are discussed below.

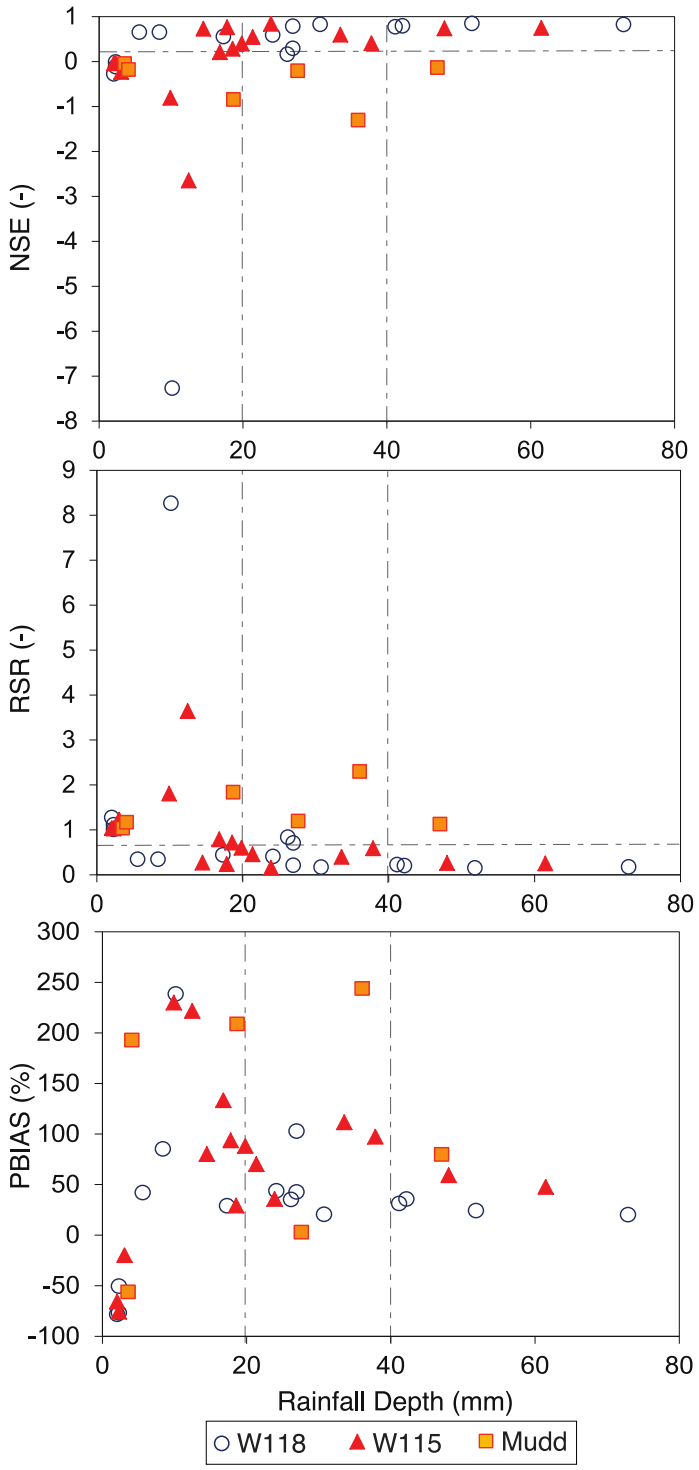

Figure 2.9. Variations of NSE, RSR and PBIAS with total rainfall depth, as calculated for predicted versus observed total runoff depth. The vertical dashed-dotted lines separate the storm size categories for (A) small events (<20mm), (B) medium events (20-40mm), and (C) large events (>40mm). The horizontal dashed lines indicate statistic threshold limits.

2.3.4. Study limitations

One limitation to this study is the small number of available storms for the *Mudd* site. Although the data that are available enabled the comparison of general response patterns across the different green roof drainage areas, particularly for the small and medium sized events, a greater number of observations from the *Mudd* test box would increase the robustness of the conclusions. Similarly, a greater number of observations of large events (those greater than 40 mm in total depth) across all study sites would shed light on green roof performance for the three roof scales during more severe storms.

Because an aim of this study was to assess the capacity of the HYDRUS-1D model to predict the hydrologic behavior of the same green roof system installed at different spatial scales, the hydraulic parameters used in HYDRUS were obtained from independent laboratory measurements, which were then assumed to be universally applicable at each field site. In practice, due to system heterogeneities, differences between laboratory and field measurements of hydraulic properties might be expected, as well as differences across the three roof sites themselves. This also extends to the choice of 50 mm average depth, which was selected in order to better represent the variations in the measured thickness of the substrate. An extension of the work to include a sensitivity study of model results to variability in the hydraulic input parameters would provide further insight on this.

Finally, although the use of average versus actual substrate saturation conditions as an initial boundary condition for the HYDRUS predictions was associated with an error of 5% or less for predictions of the *W118* site (see Section 2.4.1), it is believed that this assumption may be leading to additional error for the *W115* and *Mudd* predictions. It

is therefore recommended that future modeling efforts using HYDRUS include, where possible, actual observations of substrate saturation prior to a storm as an input parameter.

2.4. Conclusions and Recommendations

Green roofs have the potential, if implemented on a wide scale and with proper foresight, to become an important component of future urban water management infrastructure. As a result, research on green roof hydrological behavior has been rapidly growing over the past decades. Recent studies report the effectiveness of green roof systems in reducing and delaying runoff generation during rainfall events, in the context of different climate conditions and design types. However, many studies to date have not addressed the impact of spatial configuration on green roof hydrology, which is believed to be an important design consideration. This research aimed to quantify how rainfall characteristics and green roof size (i.e. drainage area) impact the hydrologic performance of the same extensive green roof system implemented at different spatial scales. It also explored the applicability of a one-dimensional infiltration model, HYDRUS-1D, in predicting shallow and extensive green roof hydrologic behavior at different spatial scales.

From measurements at the three field sites it is concluded that rainfall depth and event duration have the greatest influence on overall green roof rainfall retention and peak runoff reduction per unit rooftop area, with rainfall intensity and antecedent dry weather period (ADWP) having little influence on the aggregate performance of the green roof systems studied. The finding that green roof retention and peak reduction generally decrease as rainfall volume increases agrees with previous studies. However,

the findings regarding ADWP and rainfall intensity differ from prior reported results. It is hypothesized that the influence of ADWP and rainfall intensity on green roof hydrological performance are dependent on individual storm characteristics as well as conditions influencing green roof evapotranspiration; thus these two parameters are not always primary indicators of an extensive green roof's aggregate performance. Finally, a decrease in runoff lag time with increasing rainfall depth and intensity for storms with rainfall depths greater than 40 mm and event intensities greater than 1 mm/hr was observed. Others have also reported that lag time decreases with rainfall depth and intensity.

Based on observations from three green roof systems with drainage areas spanning from 0.09 m^2 to 310 m^2, it is found that drainage area has the largest effect on the peak reduction of runoff per unit rooftop area, with peak runoff reduction increasing as green roof scale increases. The overall rainfall retention performance of the green roofs studied was not affected by scale. The average runoff lag time did increase with green roof scale, but not significantly.

Only 17 out of the 38 HYDRUS-1D simulations of storm events met the statistical performance criteria. This is believed, in part, to be due to the lack of observed substrate moisture conditions at two of the sites, *W115* and *Mudd*, which led to the assumption of an initial average moisture condition at these sites of 10% based on the average observed value at *W118*. In particular, this assumption is believed to explain some of the discrepancy between model output and observations on *W115* and *Mudd* for short duration storms, whose modeling is more sensitive to initial substrate saturation than longer duration storms. Another issue believed to contribute to poor model

performance is that of scale and green roof heterogeneity, whereby system heterogeneity has a greater influence on green roof hydrologic behavior as drainage area decreases. Notably, HYDRUS-1D generally performed better as drainage area increased, with simulations of *Mudd* showing the poorest performance out of the three sites studied. Almost all of the HYDRUS simulations had a positive bias for runoff depth, where runoff was over-predicted. Peak runoff rates were underestimated for the green roof with the largest drainage area and under-estimated for the smallest installation. This observation was attributed to the influence of spatial heterogeneity in small green roof installations and travel time in a roof's under-drain in larger installations on observed peak runoff rates that are not accounted for in the model.

From the work presented in this paper it is concluded that green roof scale and configuration are important determinants of green roof hydrologic performance and should be considered during future planning and modeling efforts. This study has also revealed that a one-dimensional infiltration model, in order to capture event-based dynamics for a shallow, stratified and highly conductive green roof layer needs field specific data, such as substrate saturation conditions. Future modeling efforts should account in more detail for green roof heterogeneity and flow routing variables.

Chapter 3

The Soil Water Apportioning Method (SWAM): An approach for widespread monitoring of green roof hydrologic performance

Abstract – As cities increasingly adopt green infrastructure strategies to combat water management challenges, there is a growing need to develop cost-effective approaches for the long-term monitoring and performance evaluation of these systems. In this study, a water balance approach – termed the Soil Water Apportioning Method (SWAM) – was developed to enable economic assessment of the long-term, hydrologic performance of green roofs, an important component of many urban green infrastructure strategies. SWAM provides estimates of green roof runoff and evapotranspiration based solely on measurements of local precipitation, substrate moisture, and the substrate maximum water storage capacity. To validate the approach, SWAM generated values of runoff and ET were compared with 30-months of runoff and ET data obtained from an extensive, vegetated mat system located in New York City. Accurate runoff and ET estimates were obtained using as few as one substrate moisture measurement per day, although various other data logging frequencies were tested, with best results achieved with data logged every 6 to 24-hours (NSEs of 0.85-0.91 and 0.73-0.78, for runoff and ET respectively). A study of the variance of SWAM runoff and ET estimates based on the location of the substrate moisture reading also indicated that accurate estimates could be obtained using only one soil moisture sensor per green roof drainage area, provided the sensor location is chosen with care. For further validation, SWAM-generated runoff values were compared to 14 months of runoff data obtained at two other extensive green roof sites located in New York City, one a built-in-place system and the other a modular tray system. Overall, results from this study indicate that SWAM provides a viable, low-cost approach for the widespread monitoring of green roof hydrologic performance with nominal instrumentation and implementation costs.

Graphical Abstract – Graphical illustration of SWAM's algorithm. SWAM generates runoff (Q) and ET based on 3 conditions during any time period (t) from 1 to 24 hours: 1) no precipitation (P), 2) soil-storage (S) is greater than P, and 3) S is less than P.

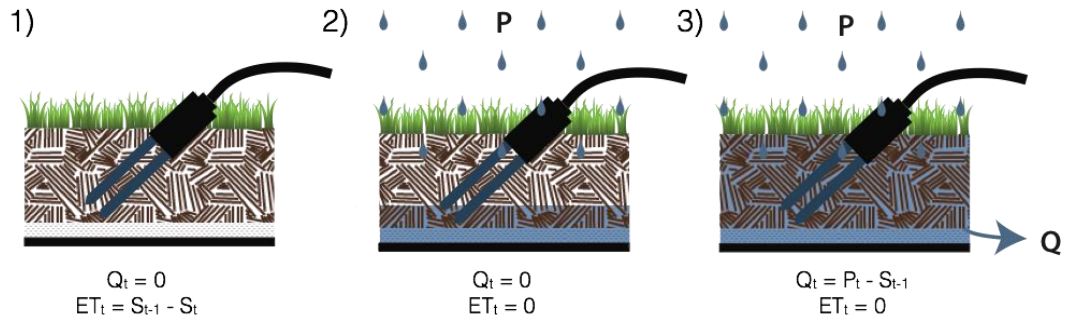

3.1. Introduction

It is projected that 66% of the world's population will be urban by 2050, and already today over half of the globe, including 82% of North Americans, are living in urban areas (United Nations, 2014). These trends place severe demands on existing centralized water management systems and create new challenges for areas being affected by urban sprawl, where naturally pervious land is rapidly being replaced by impervious built surfaces. By inhibiting the infiltration of rainwater into the sub-surface, impervious areas modify the natural hydrologic response; resulting in greater surface runoff than would have been experienced during a pre-urbanization period. While many cities have been designed to handle this additional runoff with a network of underground pipes and sewers, the capacity of these systems is becoming increasingly overwhelmed, leading to problems with flooding and water pollution when stormwater spills into streets and local water bodies. More and more, emphasis has been placed on incorporating non-traditional stormwater management tools, such as green infrastructure, into urban spaces to help combat issues with flooding and water pollution. In New York City alone, the Department of Environmental Protection is planning to invest $2.4 billion over the next 20 years in new green infrastructure installations, which are projected to be in the thousands (Bloomberg and Lloyd, 2013).

Vegetated, or green roofs, in particular, have gained popularity as a subset of green infrastructure for stormwater management that could be implemented in dense urban environments where land availability is scarce. Conventional green roofs are composed of an engineered soil substrate planted with drought tolerant vegetation, and are underlain by a drainage layer that allows for vertically infiltrated rainwater to be

transported toward the roof drain. Green roofs are classified as either extensive (<150 mm depth substrate) or intensive (>150 mm depth substrate) (Carson et al., 2013) based on their substrate thickness; the use of one type over the other is most often dependent on cost and rooftop weight restrictions. Due to their lower cost, maintenance requirements, and weight per unit area, extensive green roofs are more widely implemented in established urban areas. As such, the validation of the method presented in this study focused on data from three common extensive green roof systems, namely the vegetated mat, built-in-place and tray systems, respectively (Carson et al., 2013).

The performance monitoring of green infrastructure, such as green roofs, is an essential component of assessing the functionality and effectiveness of green infrastructure stormwater controls, and guiding future planning, implementation and maintenance efforts (Bloomberg and Strickland, 2012). Numerous studies have quantified a green roof's ability to reduce stormwater runoff based on model or full-scale green roof monitoring. Monitoring studies typically employ a water balance approach, where the water fluxes going into and out of the system are measured. For most green roofs, rainfall determines the inlet flux while runoff and evapotranspiration (ET) determine the outlet fluxes. While the monitoring of rainfall can be easily achieved using a commercial rain gauge, the monitoring of runoff and ET are more challenging. In previous studies, runoff from model-scale green roofs has been measured using weighing lysimeters or tipping buckets (Van Spengen, 2010; VanWoert et al., 2005), while for full-scale green roofs runoff has been measured using a variety of custom-made weir devices coupled with a known or calibrated depth-runoff relationship (Carson et al., 2013; Carter and Rasmussen, 2006; Fassman-Beck et al., 2013; Simmons et al., 2008). Direct

measurements of ET for model-scale green roofs have also been made using weighing lysimeters (ex. Digiovanni et al., 2013) and more recently with atmospheric enclosure chambers on full-scale green roofs (ex. Coutts et al., 2013; Marasco et al., 2014). Although the monitoring of full-scale roofs is believed to better capture the dynamics of their hydrology, obtaining reliable, continuous data on roof runoff and ET performance has proven to be challenging (Carson et al., 2013; Fassman-Beck et al., 2013). Furthermore, the cost and labor requirements for custom designed, calibrated and maintained monitoring systems can inhibit their large-scale implementation.

Efforts have also been made to model extensive green roof stormwater performance using various hydrologic modeling platforms. Physically based models such as EPA's SWMM, SWMS-2D, HYDRUS 1-D, and PROM have been successful in predicting green roof hydrologic behavior (Alfredo et al., 2010; Hilten et al., 2008; Palla et al., 2009; Sun et al., 2013), but require calibration parameters and site and soil specific information that can be difficult to obtain or measure (Hakimdavar et al., 2014). Simpler and less data intensive conceptual water balance models have also been developed to predict green roof runoff, ET and water storage. Table 3.1 provides a summary of these models, which, in addition to rainfall, have used a number of different parameters for their analyses, including potential or actual ET, dew, and certain roof and soil specific routing parameters. The less intensive data requirements of the water-balance models presented in Table 3.1 is encouraging for the development of cost-effective protocols for widespread evaluation of green roof performance. Specifically, the simpler models present opportunities for surrogate based monitoring on the basis of a minimal amount of physically measured data.

Table 3.1. Summary of previous water balance models used to predict green roof hydrologic performance parameters. Columns from left to right identify the name of the model, the model prediction outputs, model inputs, simulation time-scale and the associated publication. 'N/A' is used for models that did not have a designated name.

Model Name	Modeled Outputs	Model Inputs	Simulation Timescale	Publication
N/A	Runoff	1. Rainfall, 2. Field capacity, 3. Wilting point, 4. Daily water storage capacity	Daily	(Bengtsson et al., 2004)
GreenRoof Water Balance	Runoff, ET	1. Rainfall, 2. Potential ET, 3. Roof characteristics (orientation, slope, area)	Daily	(Timmerman, Raes et al., 2006)
AGRR	Runoff, water storage	1. Rainfall, 2. Actual ET, 3. Maximum water holding capacity	Daily	(Berghage et al., 2007)
SGRR	Runoff	1. Rainfall, 2. Actual ET, 3. Dry weather period	6 - 60 min	(Berghage et al., 2007)
N/A	ET	1. Soil moisture or weighing lysimeter data	Daily	(DiGiovanni et al., 2010)
N/A	Runoff	1. Rainfall, 2. Field capacity, 3. Wilting point, 4. Two roof specific routing parameters	Any	(Kasmin et al., 2010)
VR-WBM	Runoff, ET, water storage	1. Rainfall, 2. Dew, 3. Potential ET, 4. Hygroscopic saturation, 5. Soil water content at stomatal closure, 6. Crop coefficient, 7. Maximum water holding capacity, 8. Field capacity	Daily	(Sherrard and Jacobs, 2012)
N/A	ET	1. Soil moisture, 2. Irrigation information	Daily	(Jim and Peng, 2012)
N/A	Runoff, water storage	1. Rainfall, 2. Potential ET, 3. Crop coefficient, 3. ET reduction factor, 4. Two roof specific routing parameters	Any	(Locatelli et al., 2014)
N/A	ET	1. Soil moisture, 2. Field capacity, 3. Crop coefficient, 4. Potential ET	Daily	(Berretta et al., 2014)

The goal of this study was to develop and validate a cost-effective method for assessment and monitoring of the hydrologic performance of green roofs. Utilizing findings from previous green roof monitoring and modeling studies, this study presents a water balance based monitoring and hind-cast modeling approach, termed the Soil Water Apportioning Method (SWAM), to estimate green roof runoff and evapotranspiration based solely on measurements of local precipitation, substrate moisture and the substrate maximum water storage capacity. In the sections below, the development of SWAM is

presented, followed by a description of the three instrumented extensive green roof sites, all located in New York City, that were used for validation of the method. Results from SWAM are then compared with runoff observations and ET values obtained via a modified form of the Soil Moisture Extraction Function model for the green roof site with the longest record of data; a vegetated mat system. This comparison includes an assessment of the optimum data collection frequency, referred to as the SWAM estimation time-step, an investigation of sources of error for the SWAM generated runoff and ET values, and an appraisal of how soil moisture sensor location impacts SWAM runoff and ET estimations. Next, SWAM runoff estimates are further validated using recorded data from the two other green roof sites; one a built-in-place system and the other a modular tray system. Finally, the potential of SWAM as an effective, and resource-efficient, approach for wide-scale green roof monitoring is discussed.

3.2. SWAM description and validation

3.2.1. Back-end modeling framework and assumptions

Soil (or substrate) water balance for non-irrigated extensive green roofs can be described by the following simplified expression (Hilten et al., 2008):

$$\Delta S = P - Q - ET \quad [3.1]$$

where ΔS [L] is the change in soil water storage, and P [L], Q [L], and ET [L] are the precipitation, runoff per unit area, and evapotranspiration, respectively. Note, for the duration of the paper, green roof substrate moisture content will be referred to as soil moisture content.

Equation [3.1] can be adapted to represent a specific time-step, Δt, viz:

$$S_{t-1} - S_t = \sum_{i=1}^{n} P_i - \sum_{i=1}^{n} Q_i - \sum_{i=1}^{n} ET_i \quad [3.2]$$

where S_t is the available soil water storage capacity at the end of the time-step and S_{t-1} is the available soil water storage capacity at the start of the time-step, P_i, Q_i and ET_i are the precipitation, runoff per unit area and ET during the time-step, respectively, and n is the number of observations during the time-step.

Equation [3.2] can then be re-written, for simplicity, to reflect only totals at the end of the time-step, Δt, such that:

$$S_{t-1} - S_t = P_t - Q_t - ET_t \quad [3.3]$$

where the terms on the right hand side of the equation represent summations of all observation points during the time-step, Δt.

To estimate runoff and ET for a given time-step, SWAM makes two basic assumptions. First, SWAM supposes that ET is negligible during periods of rainfall. Following findings from Bengtsson et al. (2004), SWAM also assumes that runoff on a green roof will not occur until the substrate's water content reaches the roof's maximum water storage capacity, S_{max} [L] (DeNardo et al., 2005). The green roof manufacturer typically provides values for the maximum water storage capacity of a green roof.

SWAM obtains values for the available soil water storage capacity of the green roof substrate at the beginning of each time-step, S_{t-1} [L], from readings of green roof soil moisture, θ, viz:

$$S_{t-1} = S_{max} - (S_{max} \text{ x } \frac{\theta_{t-1}}{\theta_{max}}) \quad [3.4]$$

where θ_{t-1} is the soil moisture reading at the beginning of each time-step and θ_{max} is soil moisture reading at S_{max}. Note that $\theta_{t-1} = 0$ is associated with the driest observed field conditions. The available soil water storage capacity at the beginning of each time step, S_{t-1}, determines the amount of rainfall that can be stored in the substrate before runoff occurs.

Based on Equation [3.3] and the assumptions noted above, SWAM uses the following algorithms to calculate Q_t and ET_t during any one time-step:

$$if\ P_t = 0:\ Q_t = 0, ET_t = S_{t-1} - S_t \quad [3.5]$$

$$if\ P_t > 0\ \&P_t \leq S_{t-1}:\ Q_t = 0, ET_t = 0 \quad [3.6]$$

$$if\ P_t > 0\ \&P_t > S_{t-1}:\ Q_t = P_t - S_{t-1}, ET_t = 0 \quad [3.7]$$

Figure 3.1 provides a flow-chart description of SWAM, including data inputs. Note, that in cases where the green roof is not irrigated (as is the case for all of the green roofs in this study), if water gain is present during dry periods where ET is generated, resulting in a negative value for ET, ET is set to zero.

It is important to note that SWAM is not explicitly a *predictive* hydrologic model, in that it cannot make predictions of green roof runoff based on specified design storms without the availability of recorded soil moisture data. Instead, SWAM is an approach that uses a simplified water balance model to enable hind-cast predictions of green roof runoff and ET based on measured values of soil moisture and rainfall, and a knowledge of the green roof substrate's maximum water storage capacity.

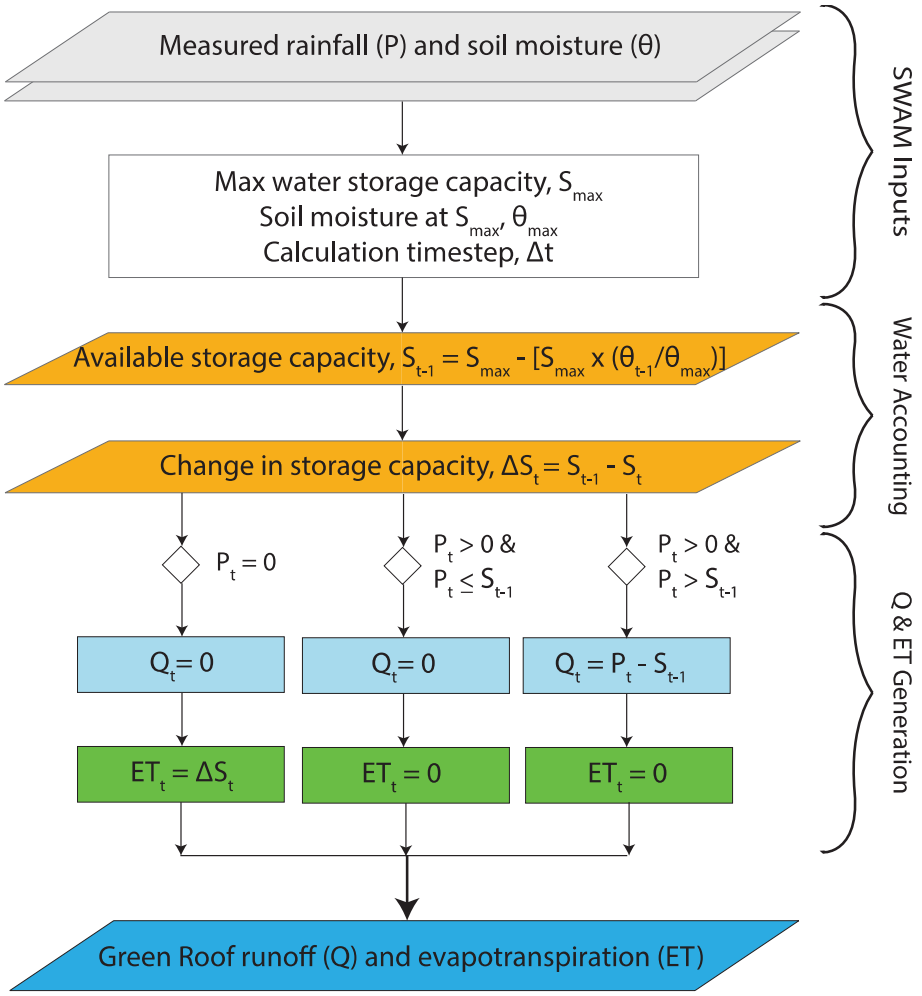

Figure 3.1. SWAM algorithm for calculating green roof runoff and evapotranspiration. Note, P_t, Q_t and ET_t represent the total summations over each time-step, Δt.

3.2.2. Validation sites and data

3.2.2.1. Validation of runoff

SWAM generated runoff values were initially validated using monitored runoff data from a custom designed weir placed in the drain of an extensive, full-scale, vegetated mat green roof located in New York City, herein referred to as *W118*. A comparison of SWAM-generated runoff values with observations from two other extensive green roof types in New York City, namely a built-in-place system, termed *USPS*, and a modular tray system, termed *ConEd*, was then undertaken to explore the

applicability of SWAM across a range of extensive green roof types. Table 2 provides an overview of the characteristics of the *W118*, *USPS* and *ConEd* extensive green roofs used for SWAM validation, while Figure 3.2 illustrates their spatial locations and relevant features. Soil moisture data from the CS615 Campbell Scientific water content reflectometers installed on the *W118* and *ConEd* green roofs, and the Onset EC5 SMC-005 soil moisture sensor installed on the *USPS* green roof, were all soil temperature corrected before use by SWAM using the recommended procedures by Campbell Scientific (1996) and Cobos and Chambers (2010), respectively. A detailed description of the instrumentation and data-loggers installed on each roof, as well as the adopted calibration and data collection protocols, is provided in Culligan et al. (2014). All measured parameters, including rainfall, runoff, and substrate moisture, were sampled every minute and recorded as 5-minute averages. The runoff validation portion of the study utilized runoff monitoring data collected from 2011 to 2014. Exact dates for the study period of each extensive green roof are provided in Table 3.2. For SWAM validation purposes, data from only one soil moisture sensor per green roof was used.

To assess the impact of soil moisture sensor location on SWAM generated values of runoff, nine additional EC5 SMC-005 soil moisture sensors were installed on the *W118* green roof in June 2015. The location of these sensors is shown in Figure 3.2A. The sensor locations were selected to provide a range of different distances from the rooftop drain, as well as a range of different elevations along flow drainage path lines.

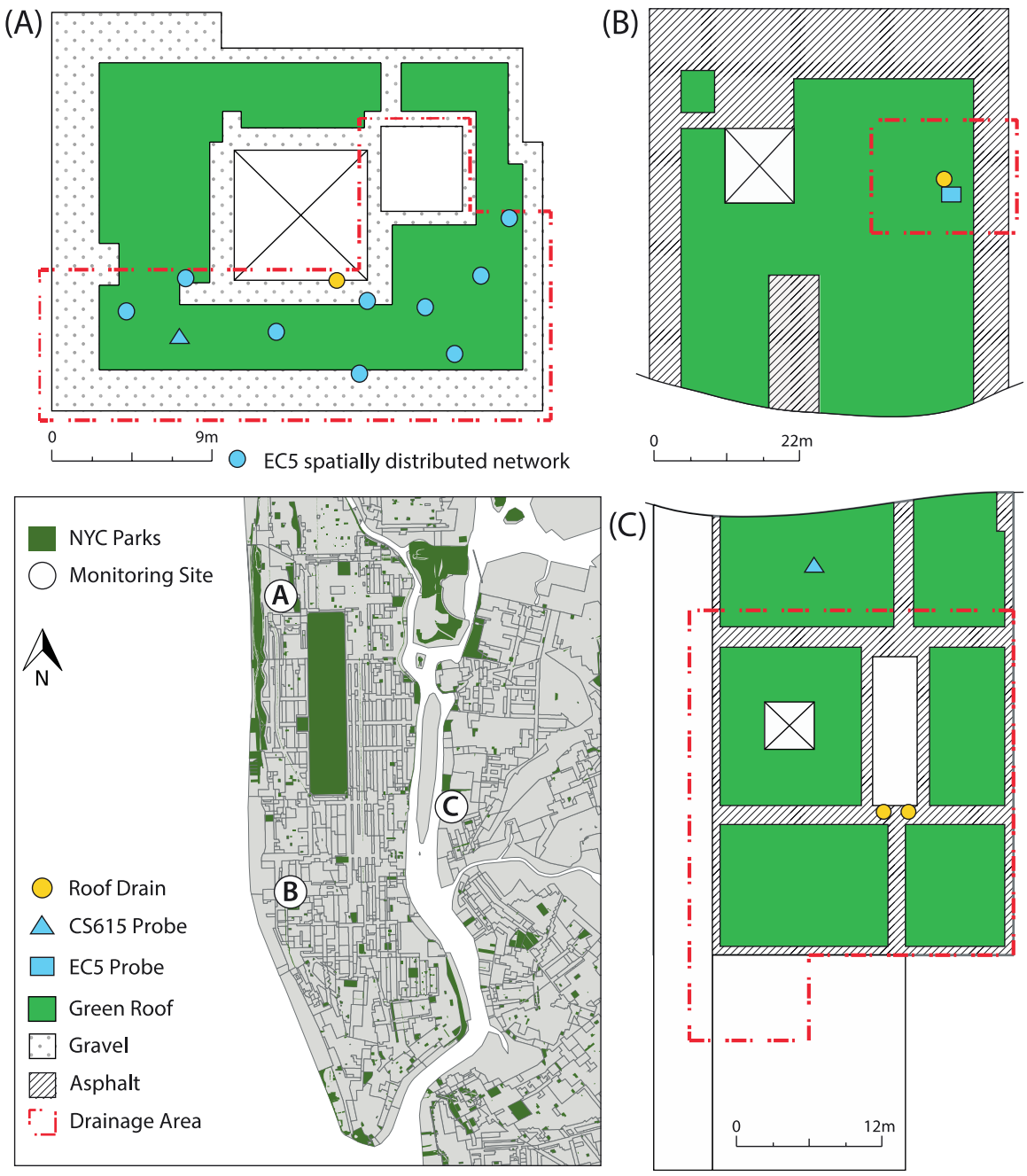

Figure 3.2. Spatial distribution of studied green roof sites in New York City with schematics of the (A) *W118*, (B) *USPS* and (C) *ConEd* roofs. The boundaries of the monitored drainage area for each roof are highlighted via the dotted line, alongside approximate locations for the instrumented roof drains and the soil moisture sensors. Note, that only partial areas from the *USPS* and *ConEd* green roofs are displayed.

Table 3.2. Summary of physical characteristics, study period and number of days used for analysis for each of the studied green roofs. *The study periods for *USPS* and *ConEd* roofs contain gaps due to periods of instrumentation malfunction and runoff weir re-calibrations. **Total number of days excludes the winter months of December, January and February. [1]Campbell Scientific, Logan, Utah, USA [2]Onset Computer Corporation, Bourne, MA, USA

Roof ID	**W118**	**USPS**	**ConEd**
Construction Type	Vegetated mat	Built-in-place	Modular tray
Manufacturer	Xero Flor America	Tecta Green	GreenGrid Roofs
Year built	2007	2009	2008
Total Roof Area (m^2)	600	10 000	2 700
Monitored Drainage Area (m^2)	310	390	940
Vegetation type	Sedum mix	Sedum mix & natives	Sedum mix
Drainage type	Geo-composite course	Geo-composite course	Geo-composite course
Substrate Depth (mm)	32	100 - 200	100
Smax (mm)	12	35 - 65	32
Study Period	06/2011 - 09/2014	08/2012 - 09/2014*	09/2011 - 09/2014*
Soil Moisture Sensor Type	CS615 water content reflectometer[1]	EC5 SMC-005 soil moisture sensor[2]	CS615 water content reflectometer[1]
Total # days**	880	408	409
# Days rainfall recorded	265	117	131

3.2.2.2. Validation of ET

Because direct measurements of green roof ET were not undertaken at the green roof sites during the same period that runoff was monitored, SWAM generated ET values for the roof with the longest record of monitored data, *W118*, were validated using a modified form of the Soil Moisture Extraction Function (SMEF) model (Zhao et al., 2013). The SMEF model was adapted and used by Stovin et al. (2013) and Berretta et al. (2014) to predict ET from green roofs in the U.K.. The adapted model was used in this study to calculate what will be referred to as SMEF ET:

$$\text{SMEF ET} = \text{PET}\left[\frac{\theta_t}{\theta_{max}}\right] K_c \qquad [3.8]$$

where K_c is the crop coefficient and PET is potential evapotranspiration. The cited papers can provide further justification for the applicability and accuracy of the adapted SMEF model in predicting green roof ET.

Hourly potential evapotranspiration was calculated using the Penman-based American Society of Civil Engineering Standardized Reference Evapotranspiration (ASCE ET_{ref}) equation and parameterized with available climate data from the *W118* roof. A crop coefficient of 1.35 was used based on average reported findings from two years of data gathered by Shalikaran et al. (2011) from a study of green roof evapotranspiration in Pennsylvania, which shares a similar climate region to New York (Karl and Koss, 1984).

3.2.2.3. Study period exclusions

Winter months, including December, January and February, were not considered in the comparative analysis between SWAM estimated runoff and monitored runoff in order to exclude runoff due to snowmelt. Further, in order to reduce soil moisture reading biases due to the sensitivity of the soil moisture sensor's to near freezing conditions, time-steps with these conditions, defined as periods where soil temperatures dipped below 5 degrees Celsius, were also excluded from the study. The exclusion of winter months from multi-year green roof hydrologic monitoring studies is not atypical (ex. Carson et al., 2013).

During all rooftop runoff-monitoring campaigns, debris occasionally collected in the weir devices, causing water buildup that resulted in runoff exceeding the recorded precipitation. To account for this issue, storm events that resulted in measured runoff exceeding measured precipitation were also excluded from the analyses.

3.2.3. Validation process

To explore whether the choice of time-step impacts SWAM's ability to provide accurate estimates of green roof runoff and ET, SWAM was run at time-steps, Δt, of 1, 3, 6, 12, and 24-hours, respectively, using the *W118* data. In a physical sense, these time-steps represent the sampling and/or logging frequency (ex. $\Delta t = 1$ hr translates to one recorded measurement of soil moisture and rainfall per hour). Although data used in this study was recorded at 5-minute intervals, for each time-step considered the soil moisture reading at the end of the time-step, and not the averaged value during the time-step, was utilized. In order to compare runoff estimates from SWAM to runoff measured with the *W118* weir, direct measurements of green roof runoff were normalized to a 1 m^2 area and individual storm events were separated using an inter-storm dry period of 24-hours, with measured rainfall, runoff and SWAM estimated runoff summed over each event. SWAM estimated ET for the *W118* roof during the inter-storm periods was compared with SMEF ET at the aforementioned different time-steps by summing values over each 24-hour dry period.

In order to investigate the sensitivity of soil moisture sensor location to SWAM based estimates, data from the nine additional soil moisture sensors installed on the W118 green roof were used (see Figure 3.2A). The SWAM algorithm was run using data from each of the installed soil moisture sensors at a 24-hour time-step, using an inter-storm dry period of 24-hours to separate individual events, and an analysis was undertaken to investigate if sensor elevation and/ or distance to the rooftop drain biased the estimated runoff or ET values.

The Nash-Sutcliffe efficiency (NSE) index, the ratio of the root mean square error to the standard deviation of measured data (RSR), and percent bias (PBIAS) were used to evaluate SWAM's ability to provide robust estimates of runoff and ET. Per recommendations from Moriasi et al. (2007), the following values were used to indicate acceptable performance for both runoff and ET: NSE > 0.5, RSR ≤ 0.7, and PBIAS ± 25%.

Further validation of SWAM's capacity to predict green roof runoff was undertaken by comparing SWAM estimated runoff values with measured runoff values from the *USPS* and *ConEd* green roofs at time-steps, Δt, of 1, 3, 6, 12, and 24-hours, respectively.

3.3. SWAM performance assessment and discussion

3.3.1. Calculation time-step and overall performance

Figures 3.3 and 3.4 and Table 3.3 provide a summary of SWAM performance outcomes for the *W118* green roof. SWAM generated runoff and evapotranspiration values for *W118* were generally well correlated with the measured runoff and SMEF ET results, respectively, for all calculation time-steps/ soil moisture logging frequencies, with the exception of a large PBIAS for runoff at Δt = 1-hour.

For runoff, SWAM estimates progressively improved as the calculation time-step increased, with a slight decrease in performance noted for the daily time-step. The relatively large under-estimation bias of -50% for the 1-hourly time-step was greatly improved with longer processing time-steps (see Figure 3.3), although a consistent over-estimation of several events was observed regardless of the chosen time-step.

Overall, SWAM ET performance was consistently high, as all calculation time-steps investigated were well within the acceptable performance metrics – with NSE and RSR values ranging from 0.73 to 0.78 and 0.52 to 0.47, respectively. An over-estimation bias was observed at shorter time-steps, which decreased with increasing time-step, eventually leading to an under-estimation of ET. The specific sources of SWAM predicted runoff and ET error are discussed in the proceeding two sections.

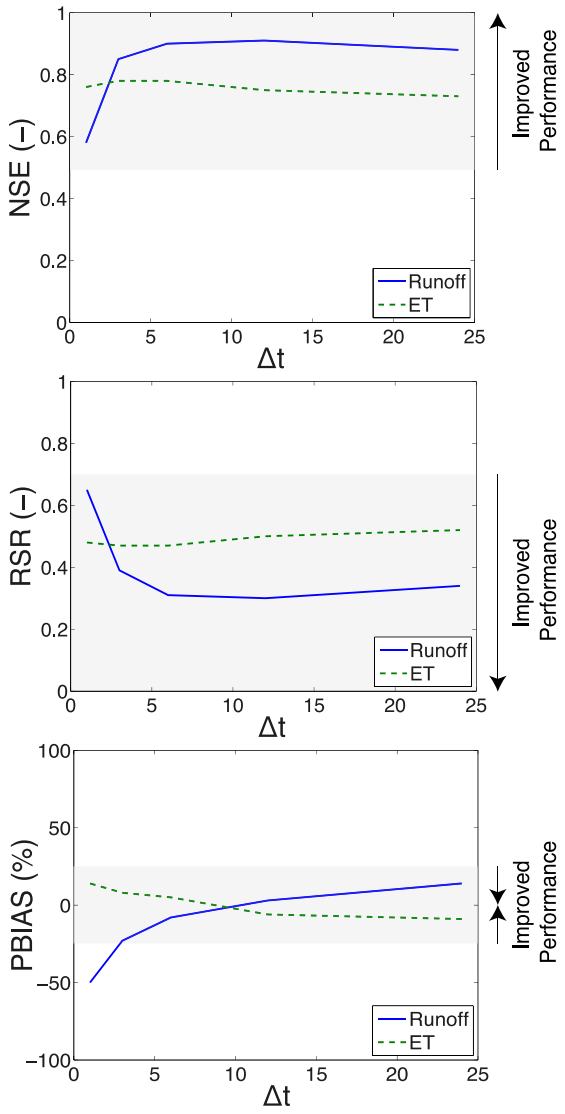

Figure 3.3. Summary of performance statistics, NSE, RSR and PBIAS for SWAM generated runoff and evapotranspiration at different processing time-steps, Δt, for the *W118* green roof. Highlighted areas represent regions of acceptable model performance.

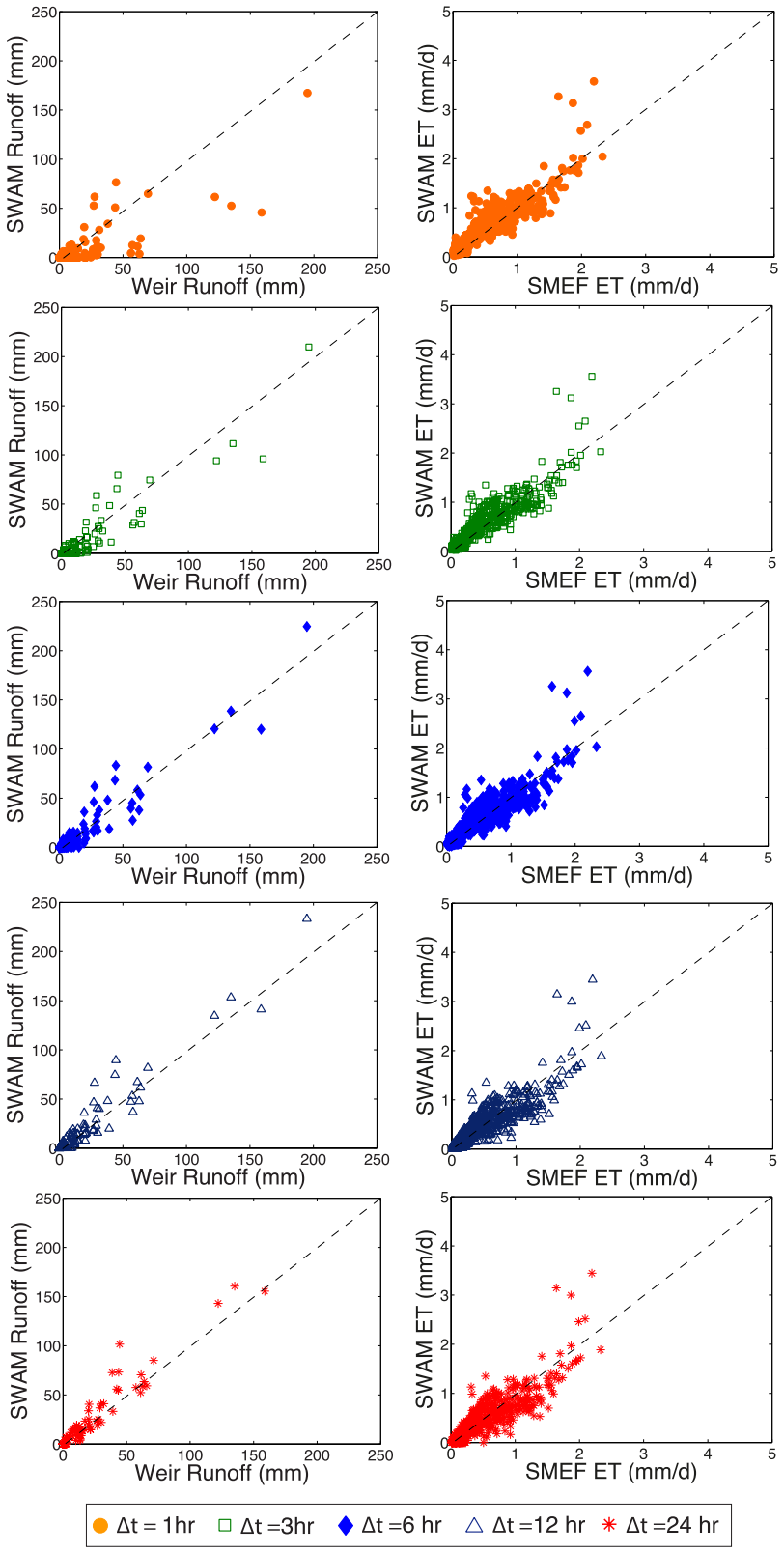

Figure 3.4. SWAM generated runoff and evapotranspiration versus recorded normalized weir runoff and SMEF model evapotranspiration for processing time-steps, Δt, ranging from 1-hour to 24-hours for the *W118* green roof.

Table 3.3. Summary statistics, NSE, RSR and PBIAS, for SWAM predicted runoff and evapotranspiration values for the *W118* extensive green roof. Highlighted areas represent regions of acceptable SWAM performance.

Δt (hr)	Runoff			Evapotranspiration		
	NSE (-)	RSR (-)	PBIAS (%)	NSE (-)	RSR (-)	PBIAS (%)
1	0.58	0.65	-50	0.76	0.48	14
3	0.85	0.39	-23	0.78	0.47	8
6	0.90	0.31	-8	0.78	0.47	5
12	0.91	0.30	3	0.75	0.50	-6
24	0.88	0.34	14	0.73	0.52	-9

3.3.2. Sources of model error

3.3.2.1. Runoff error

Shorter time-steps resulted in a higher runoff under-estimation bias due to the nature of the SWAM model, which assumes that runoff will not be generated until substrate water storage reaches the maximum water storage capacity, S_{max}. Thus, the model does not explicitly take into account time lag in the green roof runoff generation process. This issue reduces as the processing time-step is increased. Additionally, because SWAM assumes no runoff until substrate water storage reaches the maximum water storage capacity, small rainfall events often resulted in predictions of zero runoff (see Figure 3.4), whereas in reality, runoff was observed to occur at less than the manufacturer provided maximum water storage depth.

In order to better identify the source of runoff over-estimation error in the SWAM algorithms, SWAM was run at a time-step, Δt, of 1-hour over each Julian day during the study period for the *W118* green roof, and these results were used to estimate cumulative runoff over each Julian day. The outcome of this analysis is presented in Figures 3.5 and 3.6.

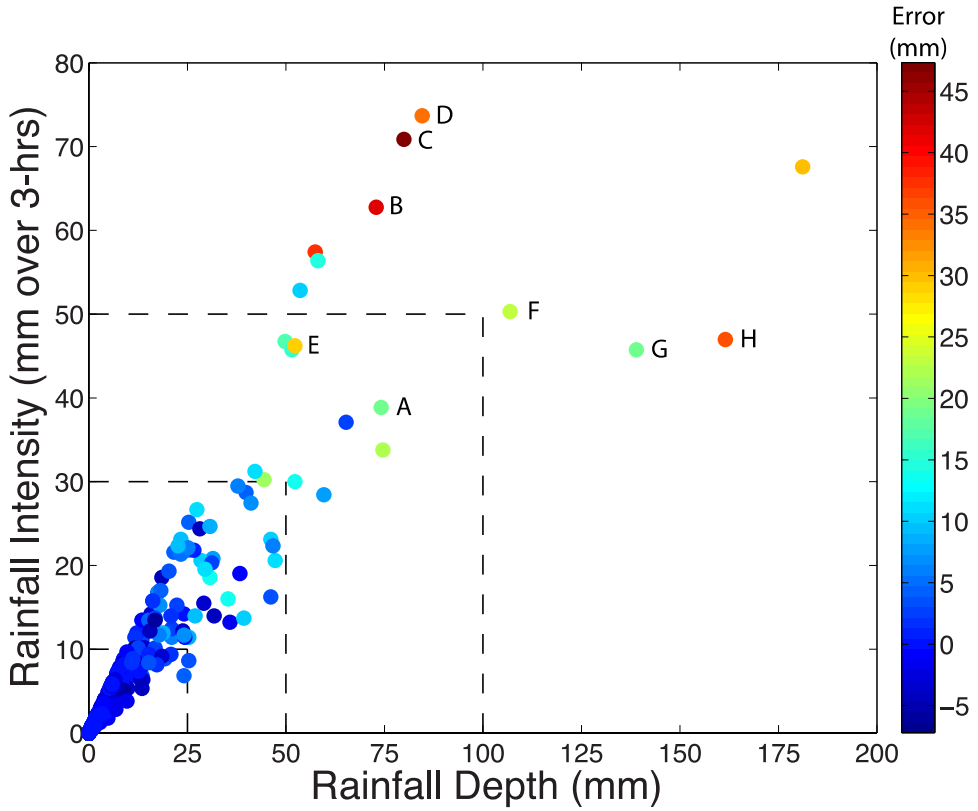

Figure 3.5. Absolute error distribution of SWAM generated runoff versus measured weir runoff for the *W118* green roof, plotted as a function of rainfall depth and intensity. Rainfall intensity was calculated as the maximum amount of rainfall that fell during any consecutive 3-hour period within each Julian day. The cumulative rainfall and runoff hydrographs for points marked with a letter A thru H are shown in Figure 3.6.

Figure 3.5 shows the distribution of absolute runoff error as a function of total rainfall depth per Julian day and maximum rainfall intensity, where maximum rainfall intensity is defined as the greatest amount (in mm) of rainfall that falls during any consecutive 3-hour period for each Julian day. As illustrated, SWAM runoff over-estimation errors generally increase with rainfall depth. However, the greatest observed over-estimation errors are associated with the highest-intensity rainfall events. Figure 3.6 explores the role of rainfall depth and intensity in SWAM over-estimation error. In sub-figures A to D, hourly SWAM generated runoff values are compared to hourly runoff and precipitation data for events with a similar daily runoff depth but with increasingly higher

rainfall intensity. In sub-figures E to H, comparisons involve events with similar rainfall intensity and increasingly greater rainfall depth. As shown in Figure 3.6, large SWAM over-estimation biases are associated with events involving a large amount of recorded rainfall falling in a short period of time. Under these circumstances, SWAM's algorithms convert rainfall to runoff, whereas in reality it is believed that ponding occurs on a green roof during high intensity events, adding depression storage to the water holding capacity of the roof – something that SWAM does not account for. Bengtsson et al. (2004) also reported increased water storage capacity during more intense rain events on a green roof site in Sweden.

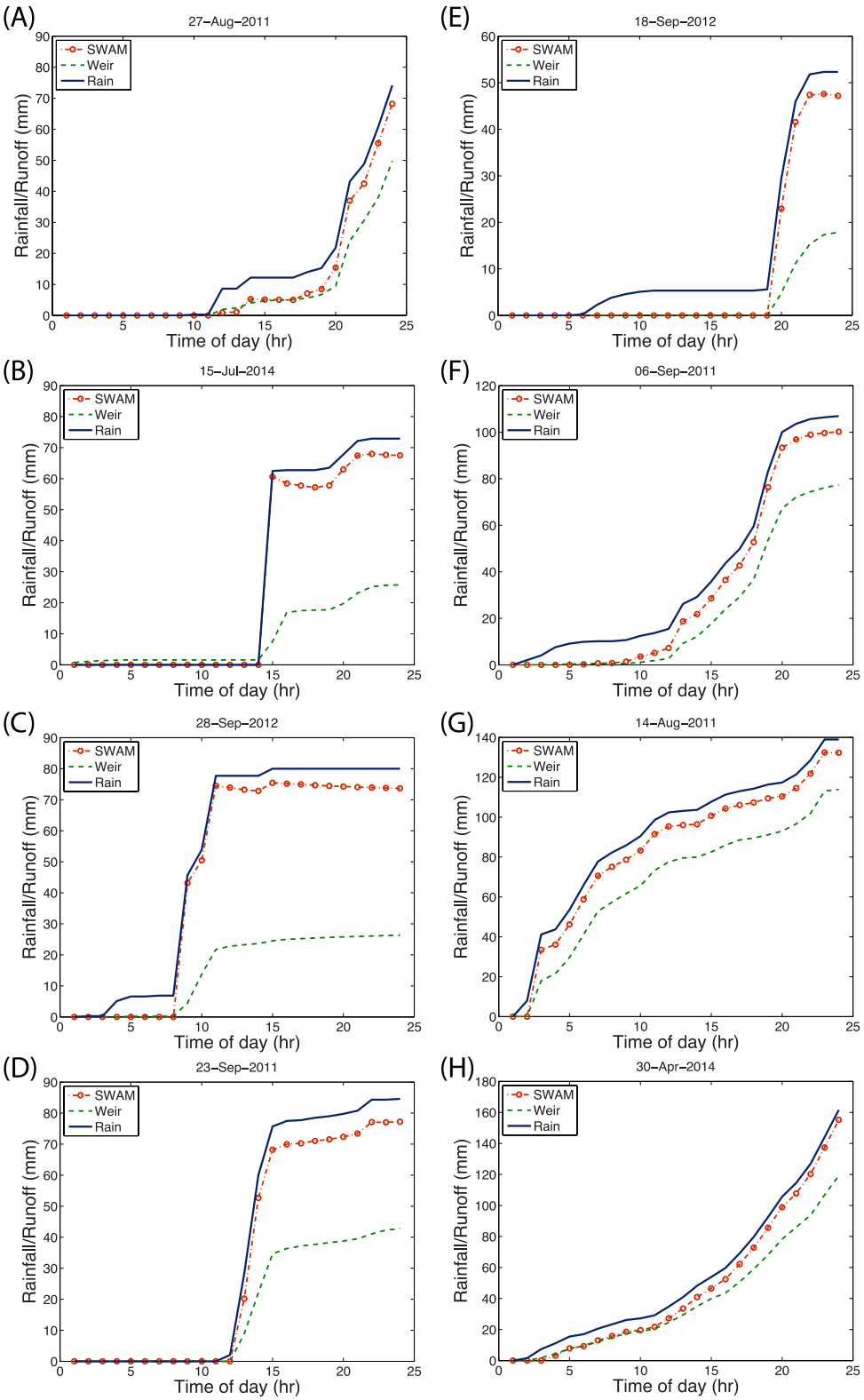

Figure 3.6. Cumulative rainfall and runoff hydrographs for selected Julian days from Figure 3.5. Sub-figures (A) to (D) represent periods of similar rainfall volume, with progressively higher rainfall intensity (A being the lowest and D being the highest). Sub-figures (E) to (H) represent periods of similar rainfall intensity, with progressively greater rainfall volume (E being the lowest and H being the greatest).

3.3.2.2. ET error

Based on prior knowledge of green roof ET diurnal fluctuations (ex. Berretta et al., 2014; Marasco et al., 2014), it was expected that higher temporal resolution data, reflected in SWAM as shorter processing time-steps involving more frequent measurements of soil moisture, would provide the most accurate estimation of green roof ET, with performance decreasing with increasing time-step. The outcome of the ET analysis, however, diverged from this expected result, with SWAM estimated ET at a time-step of 1-hour amounting to slightly lower performance metrics than estimates associated with time-steps of 3 and 6-hours. To investigate the source of this error, SWAM and SMEF ET values were averaged across three different states of water availability and by season. Figure 3.7 presents average SMEF ET and SWAM ET for calculation time-steps of 1-hour, 6-hours and 24-hours, as a function of water availability (sub-figures A to C) and season (sub-figures D to F). Water availability was estimated based on the amount of SMEF ET, with values exceeding 1.5 mm/d signifying water-abundant conditions, values between 0.5 mm/d and 1.5 mm/d signifying average conditions, and those less than 0.5 mm/d signifying water-limited conditions. Seasonal averages were calculated for the spring months of March-April-May (MAM), summer months of June-July-August (JJA), and fall months of September-October-November (SON), for non-water-limited days only.

Most of the divergence between the SMEF and SWAM ET values occurred during water-limited conditions, particularly at shorter time-steps. SWAM over-estimated ET at all processing time-steps during these conditions, although the bias decreased with increasing time-step. It is believed that this bias might, in part, be due to a limitation in

the application of the SMEF ET model for comparison during water-limited states. As observed by Jim and Peng (2012) in their study of an extensive green roof in Singapore, soil evaporation increases in dry substrates on sunny days because the thinness of extensive green roofs allows solar energy to heat up the entire substrate layer, driving up soil temperatures and leading to greater water depletion. The SMEF ET model does not account for this phenomenon.

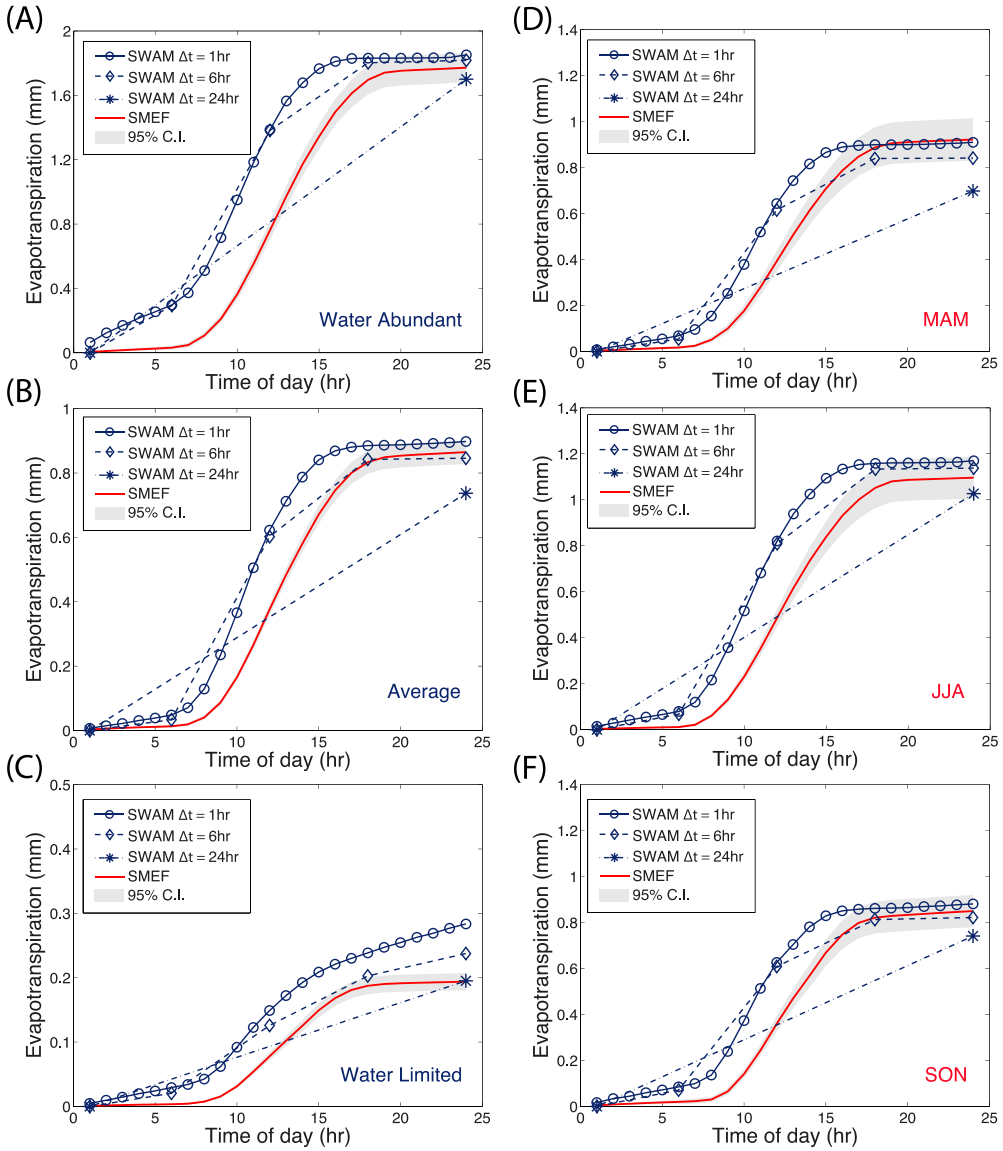

Figure 3.7. Average cumulative SWAM and SMEF evapotranspiration for the *W118* green roof, calculated at three different processing time-steps for: (A) water abundant conditions when ET is greater than 1.5 mm/d, (B) average conditions when ET is between 0.5 mm/d and 1.5 mm/d, (C) water limited conditions when ET is less than 0.5 mm/d, (D) spring months of March-April-May, (E) summer months of June-July-

August, (F) fall months of September-October-November. All averages were calculated over inter-storm Julian days where no rainfall was recorded. Seasonal average do not include water-limited days. 95% Confidence Intervals (C.I.) for SMEF ET are highlighted in grey.

For water-abundant conditions, ET during the first 6-hours of the day was greatly over-estimated by SWAM. This bias occurred on days when a large amount of rainfall fell a short time before the start of the dry Julian day over which SWAM ET was generated. Thus, as shown in Figure 3.8, the observed SWAM over-estimation bias is caused by continued runoff in the first few hours of the day, which the SWAM algorithms attribute to ET (see Equation 3.5). The bias caused by this phenomenon is greatest at a calculation time-step of 1-hour. This issue could be overcome by re-writing Equation 3.5 such that the SWAM ET calculation is disabled until several hours following precipitation. Besides this divergence, SWAM ET during average and water-abundant conditions displayed similar behavior, with an over-estimation bias during the mid-day hours and generally good agreement in the total amount of incurred ET at the end of the day, except at a time-step of 24-hours which, on average, under-estimated ET. The under-estimation bias at the daily time-step is attributed to the inability of SWAM to capture the diurnal pattern of ET using this time-step.

Comparative analyses for seasonal averages of non-water-limited ET indicated that the largest under-estimation bias for 24-hour processing time-steps occurred during spring. This is mainly due to the large temperature fluctuations experienced in New York City during the months of March, April and May, which can lead to large fluctuations in available moisture throughout any 24-hour period. The seasonal behavior of green roof ET was, otherwise, well captured by SWAM, which provided the highest ET estimates in the summer months followed by the spring and fall months.

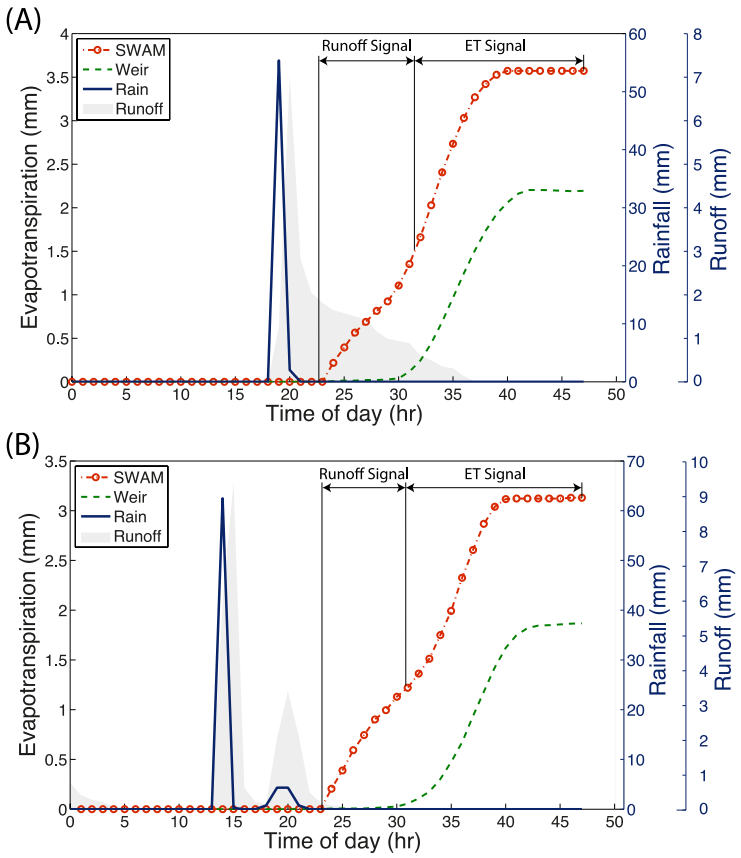

Figure 3.8. Comparison of SWAM and SMEF evapotranspiration calculated at hourly time-steps on two sample Julian days immediately following a large rainfall event. Weir recorded runoff is shaded in grey. In sub-figure (A) peak rainfall occurred 5-hours prior to SWAM ET generation on 19-Aug-2011 and in sub-figure (B) peak rain occurred 11-hours prior to SWAM ET generation with a smaller peak recorded 5-hours prior to SWAM ET generation on 15-Jul-2014. Since ET was only compared on dry Julian days, ET on days where rainfall was recorded was set to zero.

3.3.3. Location of soil moisture sensors

Figure 3.9 displays trends in SWAM estimated runoff and ET on *W118* for the nine, spatially distributed EC5 sensors installed on the roof in June 2015 (see Figure 3.2A) for the months of June, July and August 2015; during this period five runoff generating storms were recorded.

SWAM estimated runoff versus rainfall depth at each of the nine EC5 sensors is compared to a linear regression of SWAM estimated runoff versus rainfall depth obtained from the original CS615 sensor in Figure 3.9A. For all five storms, the runoff estimates

obtained from each of the nine EC5 sensors fell within the 95% confidence interval of the estimate obtained from the single CS615 sensor. Nonetheless, there was variability between the runoff estimates of the individual EC5 sensors, which was caused by differences in the recorded value of θ_{t-1} (the soil moisture at the start of each storm) between the sensors. The magnitude of these differences was found to be a function of both the antecedent dry weather period (ADWP) prior to a storm, and sensor location.

In Figure 3.9B, the variance in SWAM estimated runoff at each sensor, defined as the estimated runoff at the sensor minus the average of estimated runoff from all sensors, is shown as a function of ADWP. As displayed, the overall variance in estimated runoff decreased as the ADWP increased. This is because longer ADWPs allowed time for the green roof substrate to drain to field capacity ($\theta_{t-1} = 0$) at most locations, which minimized differences in θ_{t-1} between the sensors. For shorter ADWPs, the green roof substrate was still undergoing drainage from the prior storm, so θ_{t-1} varied with location.

Figure 3.9C shows SWAM estimated runoff variance as a function of sensor elevation for storms which had relatively short (< 3 days) ADWPs during June, July and August, 2015, and storms which had longer (> 3 days) ADWPs during June, July and August, 2015. Trends with sensor distance to the roof drain were similar, so are not shown. As seen, the SWAM estimated runoff was lowest at the two sensors located at the highest elevations in the monitored watershed for storms with shorter ADWPs. This is because water routing led to a lower θ_{t-1} at these sensor locations than those located further downstream in the drainage area. Hence, SWAM estimated a greater substrate storage of rainfall depth at these two sensors, and thus less runoff. The over-estimation of runoff at the sensor located at an elevation of 97.5m was found to be associated with a

local rooftop depression at this point, which led to water ponding after a storm, and hence higher than average values of θ_{t-1} for the smaller ADWPs. For all of the other six sensors, overall estimated runoff variance was within +/- 1mm, which is considered acceptable. For the storms that had longer ADWPs, SWAM estimated runoff variance was within +/- 0.5 mm for all nine sensors.

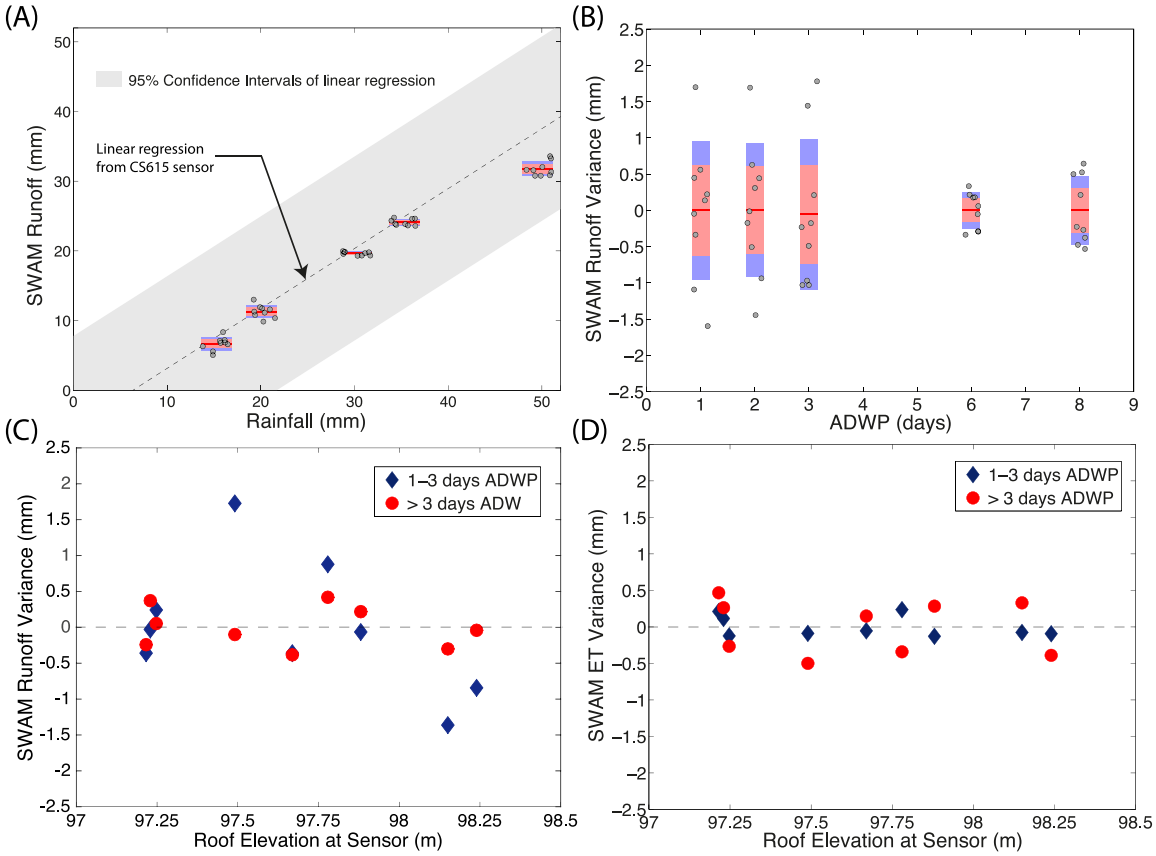

Figure 3.9. (A) SWAM runoff from individual soil moisture sensors on the W118 green roof versus rainfall depth. The linear regression line and 95% confidence intervals of the original data from the W118 green roof SWAM predictions using the CS615 soil moisture sensor are displayed for reference. (B) Variance of runoff from individual sensors from mean runoff per rainfall event versus Antecedent Dry Weather Period (ADWP). (C) Variance of SWAM runoff from individual sensors from mean runoff per rainfall event versus roof elevation at the sensor, binned for two different ADWP conditions. (D) Variance of SWAM ET from individual sensors from mean ET versus roof elevation at the sensor, binned for two different ADWP conditions. Note that boxplots in (A) and (B) have been modified to show predictions from individual sensors, the mean and standard deviation of the predictions, and the 95% confidence intervals.

Figure 3.9D shows SWAM estimated ET variance as a function of sensor elevation. Because SWAM estimated ET is related to change in soil moisture content, rather than absolute values of soil moisture content, there was less variability in estimated values between sensor locations. The variance in estimated ET is within +/- 0.5 mm at all nine sensor locations for both ADWP conditions, which is considered acceptable.

Based on the comparative analysis above, it was concluded that SWAM runoff and ET estimates based on data acquired from one soil moisture sensor can be adequate for many performance monitoring applications, provided the sensor location is chosen with care. To reduce biases that might exist due to local rooftop heterogeneities and rooftop elevation, which most impact SWAM runoff estimates, soil moisture sensors should optimally be placed at mid-elevations in a green roof monitored drainage area, and in areas where local ponding would likely not occur. Although not a problem on the *W118* roof, areas that receive above average exposure to sunlight or shading should probably also be avoided, to reduce potential bias in SWAM ET estimates.

3.3.4. Reproducibility of runoff results

In order to test the reproducibility of SWAM for different extensive green roof types, SWAM estimated runoff values were also compared to measured weir runoff data from *USPS* and *ConEd*. Results for this portion of the study are summarized in Table 3.4 and Figure 3.10.

The results from the *USPS* roof are similar to those from the *W118* roof, with SWAM performance improving with increasing calculation time-step, and generally high performance achieved at calculation time-steps of 3-hours and greater. There was a high PBIAS for most of the time-steps, which is attributed to the fewer number of rainfall

events available for validation purposes. The *ConEd* SWAM runoff estimations were less robust, especially for rainfall events that generated less than 40 mm of runoff, which resulted in estimates of zero runoff from SWAM compared to observations of actual runoff in the field. In general, the greater monitored drainage area for the *ConEd* roof, together with the fact that the moisture sensor on this roof was not within the monitored drainage area, are believed to be confounding factors for this roof. However, the comparisons overall for both extensive green roofs show promise that SWAM can effectively estimate runoff based on a single soil moisture reading across three different extensive green roof types.

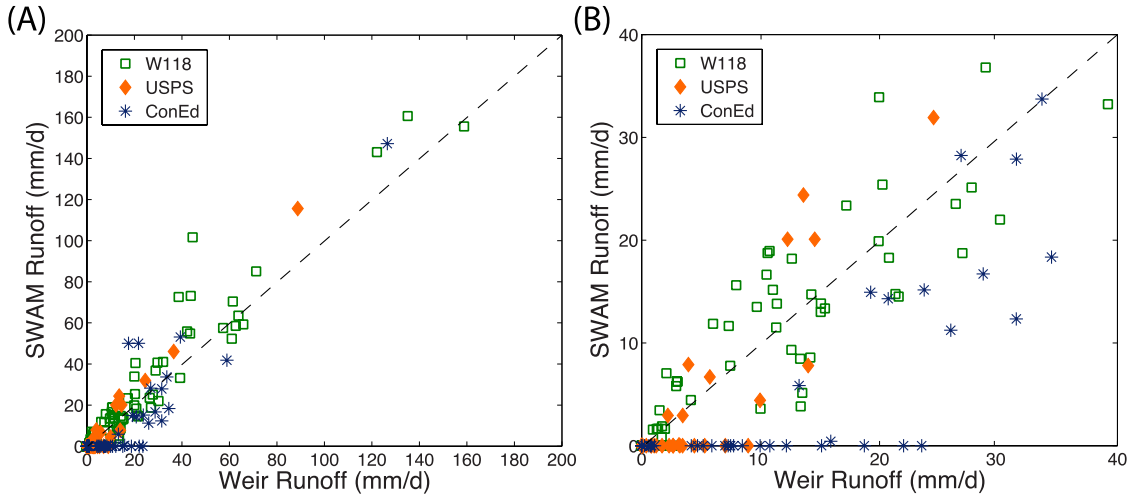

Figure 3.10. SWAM generated runoff versus recorded normalized weir runoff using a processing time-step, Δt, of 24 hours for the three extensive green roof types studied. A and B represent all rain events and rainfall events that generated less than 40 mm of runoff, respectively.

Table 3.4. Summary statistics, NSE, RSR and PBIAS, for SWAM predicted runoff values for the *USPS* and *ConEd* extensive green roofs. Highlighted areas represent regions of acceptable SWAM performance.

Δt (hr)	USPS			ConEd		
	NSE (-)	**RSR (-)**	**PBIAS (%)**	**NSE (-)**	**RSR (-)**	**PBIAS (%)**
1	0.23	0.88	-86	-0.3	1.14	-91
3	0.77	0.48	-58	0.31	0.83	-78
6	0.92	0.29	-36	0.61	0.62	-61
12	0.9	0.32	-18	0.65	0.59	-49
24	0.84	0.39	4	0.65	0.59	-27

3.3.5. Study limitations

A limitation in this study was the lack of physically measured ET data for SWAM validation, leading to the choice of using the SMEF model for comparison. Nonetheless, successful previous application of the SMEF ET model to capture extensive green roof ET (Berretta et al., 2014; Stovin et al., 2013) indicated that this model would be a good benchmark for assessing SWAM performance in lieu of physically monitored data.

Another limitation of the study was the lack of monitored runoff data from larger rainfall events for the *ConEd* and *USPS* green roofs, which precluded validation of SWAM performance for these green roof systems over a wide range of storm conditions. Furthermore, as noted above, the location of the *ConEd* soil moisture sensor in relation to the monitored roof drains is considered non-ideal, although if there was uniformity between each green roof tray on the *ConEd* roof, soil moisture measurements could hypothetically take place in any tray without bias.

3.3.6. Comparison of monitoring approaches

A comparison of set-up costs for monitoring green roof performance based on a conventional weir system and parameterization of ET models such as the SMEF, with the set-up costs associated with the SWAM method is provided in Table 3.5. Conventional

green roof monitoring costs are based on estimates from a green roof monitoring campaign that was undertaken by the author and her collaborators in 2013. As shown, the set-up costs for performance monitoring via SWAM is about half that associated with current day, conventional approaches. In addition to the cost, the custom-designed weir system requires at least 14 hours of labor for the initial installation alone. Based on the experience of the authors in monitoring 6 full-scale green roofs in New York City, the direct runoff monitoring devices also require regular maintenance following installation, as the sensors and weirs can malfunction and/or become filled with debris, leading to the loss of data. In these cases, the weirs and sensors often have to be completely removed from the green roof, laboratory re-calibrated and re-installed. While regular maintenance of conventional systems can be possible when working with a few green roofs, it is likely to become prohibitive in citywide monitoring campaigns involving hundreds of roofs. Conversely, based on the authors' experience, the labor involved in maintaining the instrumentation required to implement the SWAM approach is minimal. Additionally, since sufficiently accurate results for both runoff and ET can be obtained with SWAM using only one or two observations of rainfall and soil moisture per day, the data storage requirements and associated costs for SWAM are also lower than those accompanying more conventional systems.

Because the SWAM method uses surrogate, and not direct, measurements to provide values of green roof runoff and ET, SWAM is not necessarily considered to be an appropriate alternative for research-based monitoring of green roofs, which often demands more extensive, and thus data intensive, monitoring protocols. Nonetheless, the SWAM method is believed to provide a robust monitoring approach for integrated studies

of green roof co-benefits, and one that can help to bridge the gap between research and more data informed city planning decisions regarding green infrastructure implementation.

Table 3.5. Estimated cost of a weir system used in the monitoring of green runoff and climate parameters needed for ET estimation, versus the collection of data required to run the SWAM algorithm. Note, that these costs are based on present day quotes (from a study in 2013), and might vary over time.

Typical Monitoring System			**SWAM Monitoring System**		
Sensor	**Appx. Cost (USD)**	**Labor (hours)**	**Sensor**	**Appx. Cost (USD)**	**Labor (hours)**
S-RGB-M002 0.2 mm Rainfall Smart Sensor	410		S-RGB-M002 0.2 mm Rainfall Smart Sensor	410	
Senix TSPC-30S1-232*	384		EC5 SMC Soil Moisture Smart Sensor	139	
Onset Hobo U30-GSM-VIA-10-S100-801*	978		Onset Hobo U30-GSM-VIA-10-S100-801*	978	
Weir components	300				
Runoff (weir)	**2072**				
S-LIB-M003 Solar Radiation Sensor	220				
S-THB-M002 Temperature/RH Sensor	189				
S-WSET-A Wind Sensor	560				
EC5 SMC Soil Moisture Smart Sensor	139				
Evapotranspiration (SMEF)	**1108**				
Weir construction		**6**			
Weir calibration		**4**			
Installation of weir and weather station		**8**	**Installation of monitoring system**		**4**
Total	**3180**	**18**	**Total**	**1527**	**4**

3.4. Conclusions

Current, widely used monitoring and modeling approaches to quantify green infrastructure performance can be time, material and labor intensive, and, thus, costly. As a result, the applicability of such approaches for citywide hydrologic performance monitoring campaigns in urban areas where green infrastructure is being adopted at scale is limited. This study addressed the growing need to develop new, resource efficient

methods for the widespread hydrologic performance monitoring of urban green infrastructure, such as green roofs. Results from the study indicate that extensive green roof runoff and evapotranspiration can successfully be estimated using an approach termed the Soil Water Apportioning Method (SWAM), which is based on a simplified water-balance method and requires only recorded rainfall, soil (substrate) moisture measurements, and the maximum water storage capacity of the substrate to provide robust performance data.

Validation of SWAM runoff estimations was undertaken via comparison with monitored runoff data obtained from three, full-scale green roofs located in New York City, referred to as *W118*, *USPS* and *ConEd*, respectively. The runoff performance of SWAM proved to be acceptable for calculation time-steps greater than 3 and up to 24-hours. While a general SWAM under-estimation bias was observed for small rainfall events (<20mm) and an over-estimation bias was observed for very high intensity rain events, these biases can likely be reduced by dynamically varying the maximum water storage capacity of the substrate based on factors such as storm characteristics or season and/ or including roof specific routing parameters in the model. Such steps, however, would require more data and more complex analyses. A comparison of SWAM estimated runoff from an array of nine soil moisture sensors installed on the *W118*, indicated relatively little variance (+/- 1mm) between estimations based on readings from each individual sensor, provided sensors were not located in the upstream portion of the monitored watershed or in areas where local ponding occurred. Thus, performance monitoring founded on data from one sensor per green roof drainage area could suffice for many applications, if the sensor location is chosen with care.

Validation of SWAM ET estimations was undertaken by comparing SWAM generated ET values with ET obtained using a modified form of the Soil Moisture Extraction Function (SMEF) for the *W118* green roof. The performance of SWAM proved to be acceptable for all calculation time steps. At smaller times steps, SWAM was able to estimate diurnal ET patterns, while total daily ET values were well estimated using only one or two soil moisture measurements per day. Since ET and runoff performance was relatively stable at time-steps of 6 to 24-hours, a data collection frequency of every 6-hours or greater is recommended for best ET, as well as runoff, estimation results. Unlike runoff, SWAM estimated ET values were less sensitive to sensor location, and displayed less total variation (+/- 0.5mm).

Overall, the work presented here provides supporting evidence that SWAM can provide a viable method for the long-term, low-cost monitoring of green roof hydrologic performance, with nominal instrumentation and computational effort.

Chapter 4

The relative effects of climate and land cover change on tropical hydrology

Abstract – Alongside deforestation and growing urbanization, the tropics are increasingly experiencing forest regeneration. These land cover changes can have significant effects on local and regional hydrology. Representative watershed scale research on this topic, however, has been limited. In this study, 60 years of hydro-climate data and two land cover maps from Puerto Rico, where extensive forest regeneration has occurred, were used to investigate the impact of land cover change on local climate and streamflow from 15 mesoscale watersheds. Changes in climate, notably increasing minimum temperatures leading to decreased diurnal temperature range (DTR), were partly attributed to land cover change and partly to natural variability and potential regional climate change. Total yearly streamflow and baseflow (normalized by precipitation) were negatively correlated with urbanization, indicating decreased soil infiltration and recharge in urbanizing watersheds. Reforestation did not significantly impact streamflow and baseflow in the studied watersheds, although there was a non-statistically-significant positive relationship between these factors. Changes in total yearly surface flow were more strongly associated with forest age than with increased forest cover, thus it may be many decades before reductions in surface flow as a results of increasing forest cover can be realized. Baseflow recession times increased in reforested watersheds and decreased in urbanized watersheds, demonstrating that land cover changes have altered the response of the studied watersheds – with greater soil infiltration and recharge in reforested watersheds leading to greater baseflow and longer recession times. Watershed topography impacted the relative effects of forest regeneration on baseflow recession times. Overall, this study provides evidence of improved subsurface conditions and longer recession times following forest regeneration in a tropical region.

Graphical Abstract – Main findings, with figure A) showing correlations between total streamflow and baseflow (normalized by precipitation) and the explanatory variables considered (statistical significance at p-value ≤ 0.05 is highlighted with a grey band) and figure B) illustrating changes in baseflow recession times following reforestation in one of the watersheds considered in this study.

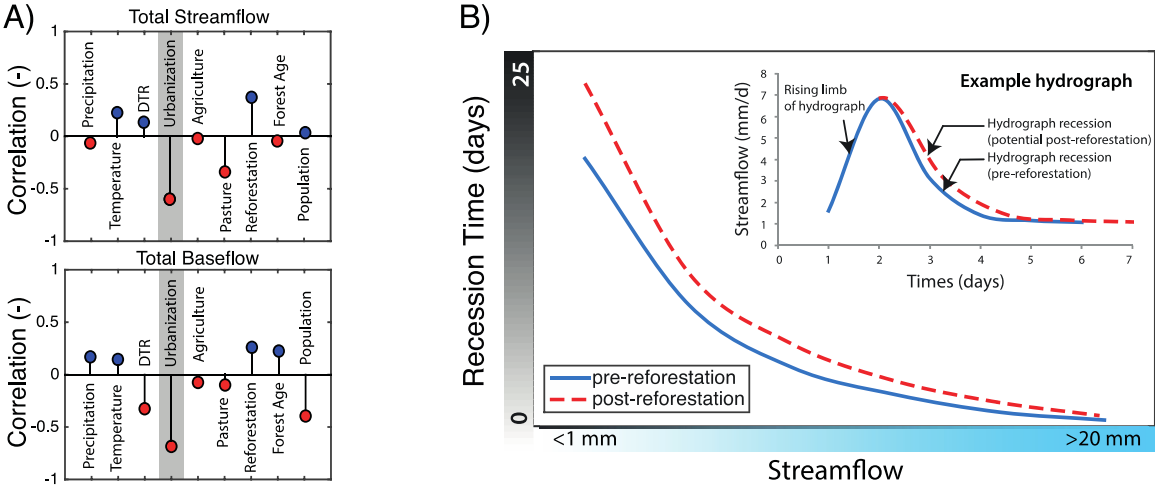

4.1. Introduction

Covering one-fifth of the global land surface, the tropics play a crucial role in the global continental hydrologic and carbon cycles (IPCC, 2014), while also being subject to the greatest intensity of land cover disturbance across the world (FAO, 2010). The effect of land cover change, and deforestation in particular, on water and climate in the tropics has been widely studied and debated over the past decades (Andressian, 2004; Bruijnzeel, 2004). Studies have recently also drawn attention to the growing emergence of secondary forests on previously deforested, abandoned agricultural lands ("A Large and Persistent Carbon Sink in the World's Forests," 2011; FAO, 2010; Giambelluca, 2002; Hölscher et al., 2005; Perz and Skole, 2003). Globally, secondary forests account for 70% of the total forested land in the tropics (Brown and Lugo, 1990; FAO, 2010). In Latin America and the Caribbean, secondary forests account for roughly 66% of the deforested land area (Aide et al., 2012). Yet despite their prevalence, there remains a dearth of knowledge regarding the impact of secondary forests on tropical hydrology at the watershed scale (Bruijnzeel, 2004; Ghimire et al., 2014). This is due largely to the lack of long-term observational hydro-climatic data in the tropics (Wohl et al., 2012). Given the importance of tropical hydrology to both global and regional hydro-climatic interactions, advancing the understanding of how natural and anthropogenic change impacts streamflow at the watershed scale in the humid tropics is paramount.

Streamflow can be divided into two components: 1) *surface flow*, which represents the *rapid* watershed response to rainfall, and 2) *baseflow*, which represents the *long-term* flow contribution fed from deep subsurface (including groundwater) and delayed shallow subsurface storage between rainfall events (Price, 2011). Land cover

change can disrupt the water balance of both streamflow components by affecting regional precipitation patterns and the partitioning of precipitation into evapotranspiration, runoff and groundwater flow (Ellison et al., 2012). The net effects of land cover change on surface flow and baseflow are largely dependent on the scale of the study area, the scale of the land cover disturbance, and the time passed after the initial land cover disturbance (Andressian, 2004; Ellison et al., 2012). Studies conducted at the local scale (1 – 100 km^2) suggest that reforestation reduces water yields due to the higher water demands of young forests (Andressian, 2004; Bosch and Hewlett, 1982; Brown et al., 2005; Calder, 2002; Farley et al., 2005; Jackson et al., 2005; Malmer et al., 2010; Zhang et al., 2001). However, small-scale studies, conducted over relatively short time-scales of 1 – 10 years, might not capture the potential influence of regional changes on rainfall (Ellison et al., 2012) or potential improvements in soil conditions over time when reforestation occurs on previously degraded land (Giambelluca, 2002). For example, Wilcox and Huang (2010), reported significantly increased baseflow following woodland regeneration on once degraded landscapes in Texas based on the analysis of a long-term dataset of 85 years. Regarding sub-surface improvements, a review of 14 sites by Ilstedt et al. (2007) found that infiltration capacity increased, on average, by a factor of three after afforestation or tree planting in agricultural fields. However, Ghimire et al. (2014) reported that the water use of a newly planted pine plantation (25 years old at the time of the study) in the Nepalese Lesser Himalaya led to decreases in streamflow. Thus, the impact of secondary forests on hydrology appears to be contingent on the trade-off between two things: 1) enhanced soil water storage capacity and recharge from improved infiltration through organic matter buildup during the forest maturing period (leading to

greater baseflow and total streamflow) (Bruijnzeel, 1989; Ghimire et al., 2013), and 2) decreased soil water reserves due to the higher water use of trees compared to crops, pasture, or shrub lands (leading to lower baseflow and total streamflow) (Bonell and Bruijnzeel, 2005; Bruijnzeel, 2004, 1989). This trade-off is also tied to the physical environment of the reforested region, namely on the soil type, underlying geology, climate, topography and existing land cover (Price, 2011; Wohl et al., 2012).

The Caribbean island of Puerto Rico provides a unique opportunity to study the regional hydrologic impact of natural forest regeneration (in this study also referred to as *reforestation*) on previously disturbed landscapes in the tropics. The island nation has experienced significant changes in land cover over the past 60 years, with extensive forest regeneration on abandoned agricultural lands and coffee plantations (Aide et al., 2012; López et al., 2001). Contrary to other regions in the humid tropics, and especially to its neighboring islands in the Caribbean basin (McGillis et al., 2015), Puerto Rico also has a strong record of publically available hydro-climatic and historical land cover data, which makes it possible to conduct analysis on historical water and land cover dynamics.

Findings from previous studies of land cover change on hydrology in Puerto Rico have been mixed. Beck et al., (2013) investigated 12 mesoscale watersheds across the island and did not find a statistically significant relationship between changes in forest and urban cover and runoff from 1950 to 2005. The authors did, however, note the presence of a weak relationship between increased forest cover and increased total streamflow, which they believed could suggest improvements in soil infiltration and water storage capacity. The lack of statistical significance was attributed to potential hydro-climatic data quality issues and to heterogeneities in catchment response due to the

simultaneous occurrence of reforestation and urbanization in most of the studied watersheds. Uriarte et al. (2011) also did not find a significant effect of land cover change on instantaneous runoff observations from 57 small sub-watersheds during the period of 1977 to 2000. Catchment modeling by Van Beusekom et al. (2014), however, revealed that the watershed scale and the scale of land cover disturbance played a major role in whether a trend between land cover and runoff could be detected or not. The authors found that runoff in highly altered small watersheds in Puerto Rico was, in fact, impacted by land cover changes, whereas over larger regions with localized areas of land cover change, there was a negligible effect on runoff. None of the previous studies in Puerto Rico focused specifically on changes in baseflow and watershed response at the mesoscale.

In this study, we investigate the impact of land cover change on tropical hydrology using 60 years of hydro-climatic data (1955 – 2015) and two land cover maps (1977 and 2000) from 15 watersheds of variable size (40 – 540 km^2) in Puerto Rico. Specifically, we test the following main hypotheses: 1) there is a relationship between forest regeneration and local climate (temperature, precipitation), 2) there is a positive relationship between forest regeneration and baseflow and a negative relationship between urbanization and baseflow, 3) there is a negative relationship between forest regeneration and surface flow and a positive relationship between urbanization and surface flow, and 4) baseflow recession times increase with forest regrowth on previously deforested/ cultivated land. In the proceeding sections, an overview of the study region and datasets and methodologies used for testing the main hypotheses are presented. This is followed by a discussion of the land cover and hydro-climatic trends during the study

period, and investigation of the relative contribution of several natural and anthropogenic factors to observed changes in annual and seasonal streamflow, surface flow and baseflow. The implication of changes in baseflow recession times of selected watersheds is then discussed. Finally, concluding remarks and recommendations for future research are made.

4.2. Study region

The island of Puerto Rico is the smallest of the Caribbean islands in the Greater Antilles, with a land area of 8 870 km^2. Puerto Rico experiences a seasonal rainfall pattern, with a winter dry season (from December to April) and an early (from May to June) and late (from August to November) rainfall season (Giannini et al., 2000; Jury et al., 2007). This small island spans six ecological life zones, ranging from subtropical dry forest to subtropical rain forest, with annual precipitation ranging from 600 to 5 000 millimeters and mean annual temperatures ranging from 19 °C to 26 °C (Ewel and Whitmore, 1973). These stark differences in precipitation on the island are due to the strong topographic gradients that create a barrier to the northeasterly trade winds, resulting in the southwest receiving less than half of the annual rainfall of the northeast (Daly et al., 2003). Regionally, Puerto Rico's climate is affected by the North Atlantic Oscillation, the El Niño Southern Oscillation and regular hurricane and tropical storm activity (Giannini et al., 2001; Jury et al., 2007). The geology is equally diverse and includes sedimentary rocks on the north and south coasts (with a karst region in the northeast and sand and alluvial soil in the central-north and central-south coasts) and old volcanic and sedimentary rocks in the central mountainous area (Grau et al., 2003).

Socioeconomic and policy changes over the past 60 years have transformed Puerto Rico's land cover. From 1940 to 1980, agricultural land in Puerto Rico decreased from 85% to 37% (Cruz-Báez and Boswell, 1997) as U.S. and Puerto Rican government policies shifted the focus of the island's economy from agriculture to industrial activities (Dietz, 1986). As a result, agriculture went from composing approximately 43% of the island's Gross National Product (GNP) in the 1930s to 1.2% in 1996, while industry grew from 7% to 41% during the same period (López et al., 2001). The change in policy also induced migration away from rural agricultural dominated areas and into urban areas on the island as well as to continental urban centers such as New York City, Chicago and Miami (Cruz-Báez and Boswell, 1997; Rudel et al., 2000). While this led to growing urbanization and urban sprawl in Puerto Rico, it also led to the growth of secondary forests on abandoned agricultural lands and coffee plantations (Aide et al., 2012; Grau et al., 2003; Helmer, 2004; López et al., 2001; Martinuzzi et al., 2007). Due to this shift, forest cover rose from less than 10% in the 1930s to 57% in 2003 (Brandeis et al., 2003). At the same time, nearly half of the island is estimated to be in some degree of urban sprawl (Martinuzzi et al., 2007). Consequently, most of the watersheds in this study experienced a combination of reforestation and urbanization during the study period.

4.3. Datasets

4.3.1. Hydro-climate data

4.3.1.1. Streamflow

Historical daily streamflow, Q, for the period from January 1, 1955 to January 1, 2015 was obtained from the U.S. Geological Survey (USGS) Caribbean Water Science

Center (http://pr.water.usgs.gov) for 111 available stations. In order to ensure that a sufficient record of data was available for trend analysis, the following criteria were used to pre-screen the suitability of the available stations: 1) at least 30 years of recorded data from 1955 to 2015, 2) at least 10 years of recorded data from 1955 to 1985 and at least 10 years of recorded data from 1986 to 2015, 3) no greater than 10 years of continuously missing data, 4) the watershed experienced no major changes in water extraction from municipal or agricultural water use. Changes in water extraction were assessed based on water use data from the USGS, as discussed in Section 3.3. Further, because the goal of the study was to investigate the impact of land cover change on hydrology, only watersheds that experienced relatively significant change in forest cover (>5% change in land area) and/ or urban cover (>2% change in land area) during the study period were considered. The last criteria led to the exclusion of three watersheds, located in the protected Loquillo Experimental Forest where little land cover change has occurred. A total of 15 watersheds were selected for analysis based on the above-mentioned criteria. As an additional data quality assurance measure, months where streamflow exceed 1.1 times the monthly precipitation were removed from the analysis. This threshold was applied in order to systematically remove data outliers in the time series and led to the removal of a small number of months for each station. Drainage areas and watershed boundary shapefiles for each of the suitable 15 stations were obtained from the USGS. Three of the watersheds contained dammed streams, however, with the exception of one dam constructed in 1974, all others were completed prior to or within one year of the start of the study period, thus this was not believed to impact the trend analysis. Figure 4.1 shows the location of the 15 watersheds used in this study and the location and dates of

construction for the dams in the three watersheds. Table 4.1 provides detailed information for the 15 watersheds, including the available record of data from each station.

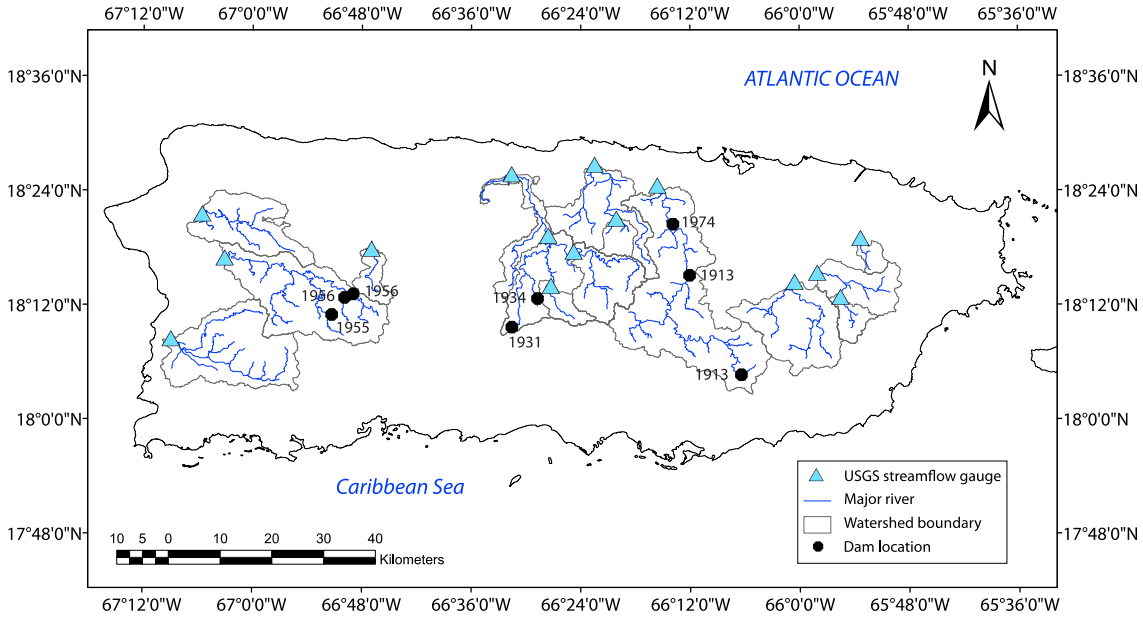

Figure 4.1. Map of Puerto Rico with the location of the 15 USGS streamflow gauges and watersheds used in this study and the location and date of construction of dams within the watersheds.

Table 4.1. Detailed information for the watersheds in this study.

Site Number	Site Name	Hydrologic Unit (8)	Hydrologic Unit (10)	Area (km^2)	Drainage Area (km^2)	Years of data	Streamflow Data Availability
50028000	RIO TANAMA NR UTUADO, PR	Cibuco-Guajataca	Rio Grande de Arecibo Watershed	47	47	56	1959-2015
50031200	RIO GRANDE DE MANATI NR MOROVIS, PR	Cibuco-Guajataca	Rio Grande de Manati Watershed	143	143	50	1965-2015
50034000	RIO BAUTA NR OROCOVIS, PR	Cibuco-Guajataca	Rio Grande de Manati Watershed	43	43	41	1969-1982; 1988-2015
50035000	RIO GRANDE DE MANATI AT CIALES, PR	Cibuco-Guajataca	Rio Grande de Manati Watershed	346	331	57	1956-2015
50038100	RIO GRANDE DE MANATI AT HWY 2 NR MANATI, PR	Cibuco-Guajataca	Rio Grande de Manati Watershed	429	413	45	1970-2015
50038320	RIO CIBUCO BLW COROZAL, PR	Cibuco-Guajataca	Rio Cibuco Watershed	39	39	46	1969-2015
50039500	RIO CIBUCO AT VEGA BAJA, PR	Cibuco-Guajataca	Rio Cibuco Watershed	227	227	42	1973-2015
50046000	RIO DE LA PLATA AT HWY 2 NR TOA ALTA, PR	Eastern Puerto Rico	Rio de la Plata Watershed	540	519	55	1960-2015
50055000	RIO GRANDE DE LOIZA AT CAGUAS, PR	Eastern Puerto Rico	Rio Grande de Loiza Watershed	232	232	56	1959-2015
50056400	RIO VALENCIANO NR JUNCOS, PR	Eastern Puerto Rico	Rio Grande de Loiza Watershed	43	43	44	1971-2015
50057000	RIO GURABO AT GURABO, PR	Eastern Puerto Rico	Rio Grande de Loiza Watershed	155	155	56	1959-2015
50061800	RIO CANOVANAS NR CAMPO RICO, PR	Eastern Puerto Rico	Rio Grande de Loiza Watershed	27	27	48	1967-2015
50138000	RIO GUANAJIBO NR HORMIGUEROS, PR	Culebrinas-Guanajibo	Rio Guanajibo Watershed	311	311	42	1973-2015
50144000	RIO GRANDE DE ANASCO NR SAN SEBASTIAN, PR	Culebrinas-Guanajibo	Rio Grande de Anasco Watershed	347	253	52	1963-2015
50147800	RIO CULEBRINAS AT HWY 404 NR MOCA, PR	Culebrinas-Guanajibo	Rio Culebrinas Watershed	183	183	48	1967-2015

4.3.1.2. Precipitation and temperature

Daily precipitation, P, and temperature, T, data were obtained from the NOAA National Climatic Data Center's GHCN-D database (http://www.ncdc.noaa.gov/). Precipitation data from an additional station, the El Verde station, located in the Luquillo Experimental Forest (which was not in the GHCN-D database) was also used to supplement the number of rainfall stations in the wettest part of the island. The temperature data included average, minimum and maximum daily air temperature: T_{avg}, T_{min}, T_{max}, respectively. Two criteria were used to assess the suitability of the precipitation stations for analysis: 1) the station had at least 25 years of data, and 2) rainfall was recorded past the year 1995. The second criterion was applied because records from a number of stations ended in the early to mid-1990's, during a drought period. The years of 1997, 1994 and 1991 were found to be the second, third and sixth driest years of the 20th century in Puerto Rico and annual rainfall accumulation averaged 87% of normal from 1990 to 1997 (Larsen, 2000), thus records that ended during this period could be biased toward a decreasing trend in precipitation. Incorporating the two criteria resulted in 61 stations out of 189 available stations with sufficient precipitation data, and 21 stations with sufficient temperature data, as not all of the GHCN-D stations recorded air temperature.

4.3.2. Land cover and forest age

Two land cover (LC) maps, one from 1977 to 1978 (referred to as 1977) and the other from 2000, were used to quantify: 1) changes in land cover before and after the transition point of 1985 and 2) the estimated age of forests in 2000. The transition point of 1985 was selected because it was believed to best represent conditions before and after

major land cover changes occurred in Puerto Rico's recent history. While the actual land cover transition point may differ for each region, the most dramatic shifts in land cover have been reported from 1940 to the mid and late-1980s (Grau et al., 2003). The 1977 land cover map was created using aerial photographs from 1977 and 1978 at 1:20,000 resolutions (Ramos and Lugo, 1994) and digitized to polygons at a 1:24,000 scale. The 2000 land cover and forest age map is based on Landsat TM and ETM+ mosaic images at 30×30 m resolution (Helmer et al., 2002; Kennaway and Helmer, 2007). Forest age is provided as a range of years.

All maps were rasterized to 30×30 m resolution and to a common geographic projection system. The 1977 map originally had 12 land cover classes, which were simplified to eight classes following the methodology from Crk et al. (2009): 1) Urban/developed, 2) Herbaceous/coffee/mixed woody agriculture, 3) Pasture/grass, 4) Forest/woodland/shrubland, 5) Forested wetland, 6) Non-forest wetland, 7) Non-vegetated, 8) Water. The 2000 map originally had 29 land cover classes, which were also reduced to the same eight classes, following methodology from Crk et al. (2009). Only the first four land cover classes were used in this study and were simplified to urban, agriculture, pasture and forest. Details of the re-classification methods and a discussion on the accuracy of the two maps can be found in Uriarte et al. (2011).

4.3.3. Additional datasets

State population and water-use data were obtained from the USGS (http://waterdata.usgs.gov/pr/nwis/wu). This data was available at a municipality level for the years of 1985, 1990, 1995, 2000, 2005 and 2010. Data on surface and groundwater withdraws for the public-supply facilities and surface and groundwater withdraws for

crop irrigation were used to assess the suitability of watersheds used for analysis. Changes in population, averaged across each of the 15 watersheds, were used to assess the potential growing demand on water supply due to migration away from or into the studied watersheds. Elevation data was obtained from a 30 m Digital Elevation Map (DEM) from the USGS (http://viewer.nationalmap.gov/launch/). Average elevation and slope were calculated for each of the 15 watersheds from the DEM. Figure 4.2 summarizes the duration of each dataset used in this study.

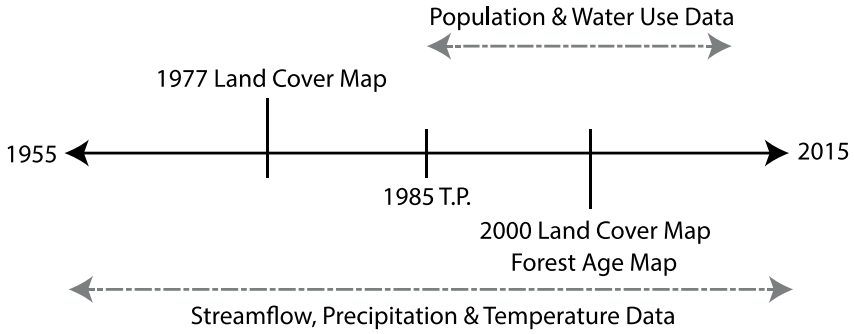

Figure 4.2. Timeline for the record of data from the main datasets used for analysis in this study. The transition point (T.P.) of 1985 was selected because it was believed to best represent conditions before and after major land cover changes occurred in Puerto Rico.

4.4. Methodology

4.4.1. Calculation and interpolation of hydro-climate variables

Streamflow was converted to an equivalent water depth (mm) by dividing the daily streamflow volume by the respective watershed drainage area for each of the 15 watersheds. To assess the impact of land cover change during both rainy and rainless periods, streamflow was separated into baseflow, BF, and surface flow, SF, using the USGS HYSEP local minimum method (Sloto and Crouse, 1996). With the local minimum method, baseflow values for each day are estimated by the connecting local minima – the lowest point based on 1.5 days before and after each day – of the

hydrograph dataset with straight lines. Precipitation across each watershed was interpolated and averaged using the Ordinary Kriging (O.K.) method. Only precipitation from stations that were 5 km or greater away from the coastline were used for O.K. interpolation. Since all of the studied watersheds were located inland, this criterion was imposed in order to reduce bias from coastal rainfall patterns resulting from sea breezes that may differ from inland precipitation (Rieck et al., 2015). This resulted in 39 stations available for interpolation. O.K. was used because of its high performance in mountainous tropical islands compared to other traditional and geo-statistical precipitation interpolation methods (Mair and Fares, 2011). Due to the relatively lower number of weather stations with a sufficient air temperature record, which restricted the applicability of interpolation methods, T_{avg}, T_{min}, and T_{max} from the station nearest to each watershed was used.

Although potential evapotranspiration is an important component of tropical hydrology, the lack of sufficient spatially distributed temperature and solar radiation data (among other parameters such as wind and relative humidity) could lead to unreliable calculations of potential evapotranspiration using common methods such as the Hargreaves or Penman-Monteith equations. Thus, in lieu of potential evapotranspiration, the Diurnal Temperature Range (DTR) was calculated by subtracting T_{min} from T_{max}. Changes in DTR reflects sensible heating and changes in the Bowen ratio (Gentine et al., 2011a, 2011b), which are driven mostly by changes in land cover, soil moisture, radiation and cloud cover (Dai et al., 1999). It is noted that tropical regions experience less fluctuation in solar radiation than in the mid-latitudes and DTR changes mostly reflect

changes in cloud cover. This makes DTR a useful tool in assessing potential changes in actual evaporation.

Daily Q and P were aggregated to monthly (in order to apply the streamflow threshold, $Q_{month} < 1.1\ P_{month}$) and yearly totals for the trend analysis. In addition to Q, SF and BF, four other normalized streamflow variables were calculated: Q/P, SF/P, BF/P, and BF/Q. Q/P is often referred to as the runoff coefficient and has previously been used to decipher between streamflow changes due to changes in precipitation and streamflow changes due to land cover change (ex. Costa et al., 2003; Le Tellier et al., 2009; Muñoz-Villers and McDonnell, 2013; Velpuri and Senay, 2013). Given this, Q/P, SF/P, and BF/P were used to represent normalized streamflow, surface flow and baseflow, whereby changes in the normalized values could be explained by factors other than precipitation or through the nonlinear response of the generated streamflow to precipitation. BF/Q represents the contribution of baseflow to total streamflow.

4.4.2. Hydro-climate trend analysis

To investigate the temporal changes in Puerto Rico's hydro-climate – based on Q, SF, BF, Q/P, SF/P, BF/P, BF/Q, P, T_{avg}, DTR – a Mann-Kendall non-parametric test was used. The Mann-Kendall test was run for the precipitation and streamflow components at 1) yearly, 2) dry season (December to April), and 3) rainy season (May to November) cumulated values. A similar analysis was carried out for T_{avg} and DTR using average values per year (seasonal analysis was not carried out). The Kendall's Tau-b, Sen's slope and the p-value were calculated at each step. The Sen's slope over the duration of the recorded dataset was used to represent the rate of change over that period. Statistical significance was determined at a p-value ≤ 0.05.

4.4.3. Evaluation of hypotheses

4.4.3.1. Hypothesis 1

Hypothesis 1 states that there is a relationship between forest regeneration, precipitation and temperature. This is based on the notion that the emergence of secondary forests would offset the effects of deforestation on regional precipitation and temperature, leading to an increase in precipitation and a decrease in maximum temperatures. To test the possible feedback between forest regeneration, rainfall and temperature, circular buffer zones of 500 m, 1 km, 3 km, and 5 km in diameter were created on ArcGIS and the percent of urbanization and reforestation from 1977 and 2000 within the buffer zones were calculated. A pixel was considered urbanized or reforested if it was urban or forested in 2000 but not in 1977. Linear correlations and p-values were calculated between the percent difference in the land cover area in each buffer zone and the rate of change of precipitation for each station. Correlations between the percent differences in the land cover area in each buffer zone and the rate of change of T_{avg}, T_{max}, T_{min}, and DTR were also calculated in order to assess the potential impact of land cover change on local temperature and evaporation. Statistical significance was determined at a p-value ≤ 0.05.

4.4.3.2. Hypotheses 2 and 3

Hypothesis 2 states that there is a positive relationship between forest regeneration and baseflow and a negative relationship between urbanization and baseflow. Hypothesis 3 states that there is a negative relationship between forest regeneration and surface flow and a positive relationship between urbanization and

surface flow. To test the relative effects of land cover change on baseflow, surface flow and total streamflow, a number of natural and anthropogenic explanatory variables, including land cover, were investigated. The natural explanatory variables included ΔP, ΔT_{avg}, and ΔDTR. The anthropogenic explanatory variables included changes in the four land cover classes from 1977 to 2000, ΔUrban, ΔAgriculture, ΔPasture, ΔForest, Forest Age and the change in population, ΔPopulation. The changes in hydro-climate variables represent the rate of change (Sen's slope) over the entire duration of available data for each station. Changes in land cover were calculated as a change in percent area in urban, agriculture, pasture and forest, from 1977 to 2000 for each watershed. The Forest Age was calculated as a weighted average for each watershed, using the average value from each age range. Change in population represents the rate of change of the average number of people living in each watershed from 1985 to 2010, noting that most watersheds were composed of several different municipalities.

To evaluate the impact of each explanatory variable on ΔQ, ΔSF, ΔBF, ΔQ/P, ΔSF/P, ΔBF/P, and ΔBF/Q, and test hypotheses 2 and 3, regression models were used. In order to avoid over-fitting the data in the models, the recommended limit of n/10 for the number of predictors recommended by Harrell (2001) was used. Since only 15 watersheds with a sufficient record of data were available for the analysis (n = 15), the models were restricted to 1 predictor (i.e. explanatory variable) and the linear (Pearson) correlations and p-values were calculated. Statistical significance was determined at a p-value ≤ 0.05. This analysis was done for yearly timescales.

4.4.3.3. Hypothesis 4

A baseflow recession curve describes the decay of streamflow with time during rainless periods. Baseflow recession slopes are particularly useful for understanding watershed response characteristics and for detecting change in watershed characteristics over time (Brutsaert and Nieber, 1977; Rupp and Selker, 2005; Troch et al., 2013; Wang and Cai, 2010a, 2010b). In this study, baseflow recession curves were created for each of the watersheds that exhibited a statistically significant change in Q/P, SF/P, or BF/P in the yearly Mann-Kendall trend analysis. Recession curves were calculated by separating each recession event in the streamflow time series and calculating the recession slope, K, for each segment via:

$$\ln(Q) = c - Kt \qquad [4.1]$$

where Q is the observed streamflow [mm], t is the time [days], and K and c are the linear regression coefficients. A Visual Basic program developed by Posavec et al. (2006) was used to calculate the baseflow recession curves (referred to in the program as master recession curves) and regression coefficients, K and c.

In order to evaluate potential changes in the recession behavior of the watersheds after land cover change, recession curves for the earlier period (1965 to 1985) and later period (1995 to 2015) were calculated and compared. Previous studies have demonstrated the applicability of this method for detecting the impact of human activities, such as groundwater pumping, on baseflow (Wang and Cai, 2010a, 2010b).

4.5. Results and discussion

4.5.1. Changes in land cover

Figure 4.3 displays the spatial pattern of total land cover change, urbanization or loss of urban land, reforestation or deforestation, and forest age across the island.

Individual pixels were considered urbanized or reforested if the pixel was non-urban or non-forest in 1977 and urban or forest in 2000. No change signified that the pixel was either forest or urban in both 1977 and 2000. Table 4.2 summarizes the percent change for the four land cover classes for each watershed. Figure 4.4 shows the elevations of the reforested and urbanized areas and the elevation distribution of each land cover change category.

From 1977 to 2000, Puerto Rico's land cover changed significantly; with 56% of the island experiencing some degree of land cover change. Of this change, 20% is attributed to reforestation and 7% is attributed to urbanization. Most of the forest regeneration occurred in the central western part of the island. Urbanization occurred at lower elevations and near existing urbanized areas, with the majority of this land cover change occurring at elevations of less than 250 meters. A notable amount of forest regeneration occurred at higher elevations, owing to the abandonment of coffee plantations and agricultural land that were in higher, less populated areas. However, substantial forest regeneration also occurred at lower elevations. These findings are in agreement with previous studies of land cover and elevation in Puerto Rico (Grau et al., 2003; Helmer, 2004; Martinuzzi et al., 2007). Change in forest cover for the studied watersheds ranged from -4% to 54%, while change in urban land area ranged from 3 to 10%. With the exception of two watersheds, all others had a loss in agricultural land and most experienced a loss in pasture. The average forest age for the 15 watersheds was 24 years; the heavily reforested central western part of the island also had some of the youngest forests.

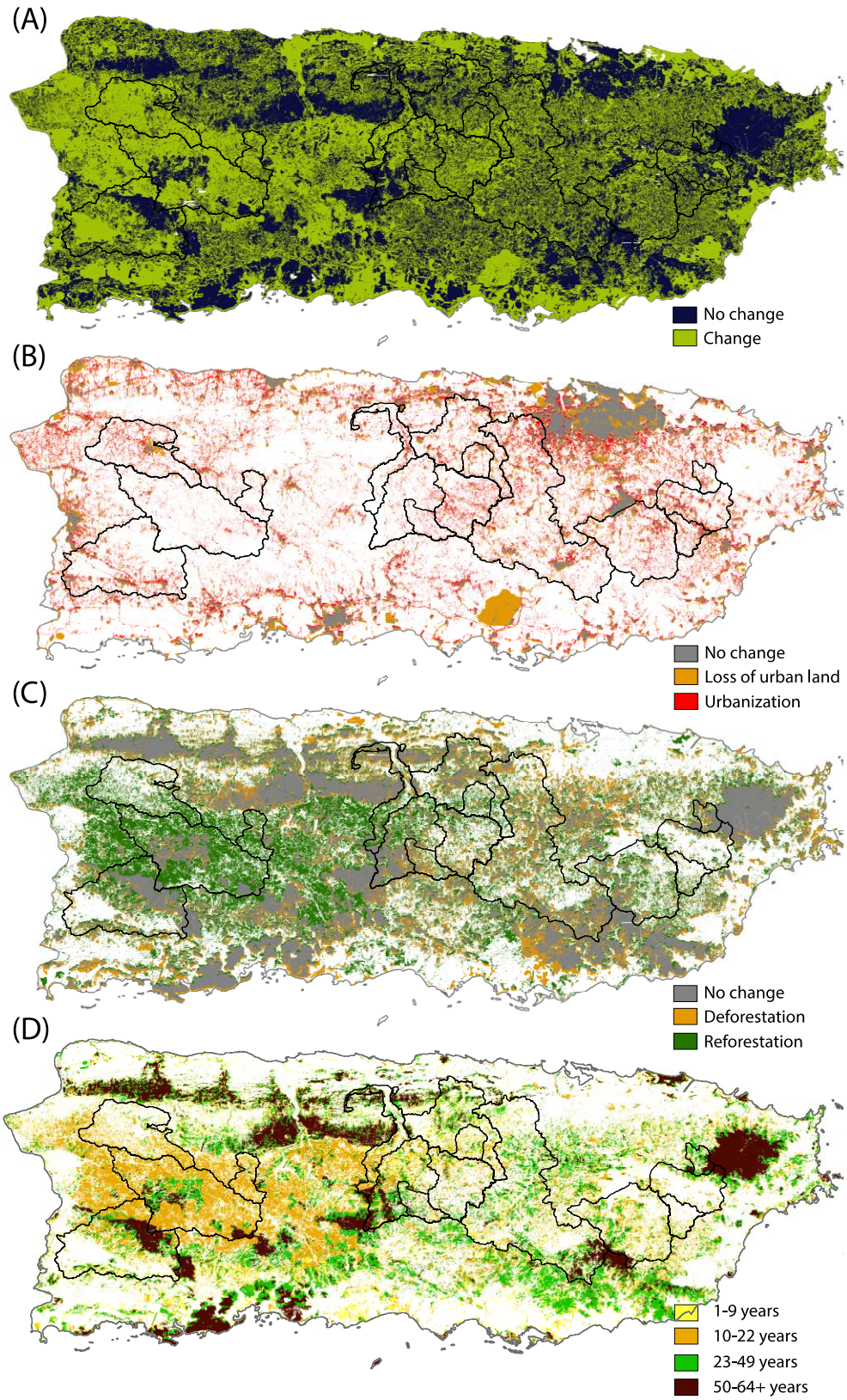

Figure 4.3. (A) Change in overall land cover, (B) change in urban land cover, and (C) change in forest cover from 1977 to 2000. (D) Forest age category.

Table 4.2. Land cover change, forest age, population change, average elevation and average slope for the watersheds in this study.

USGS ID	ΔUrban (%)	ΔAgriculture (%)	ΔPasture (%)	ΔForest (%)	Forest Age (years)	ΔPopulation (x1000)	Elev. (m)	Slope (deg.)
50028000	3	-57	0	54	16.65	192	571	16
50031200	10	-14	-6	11	21.76	207	588	18
50034000	7	13	-16	-4	28.78	55	732	22
50035000	6	-12	-7	13	27.21	140	577	20
50038100	6	-14	-6	14	27.67	149	518	19
50038320	3	-17	-9	24	16.14	307	248	13
50039500	4	-10	-4	10	22.82	240	189	13
50046000	5	-5	-2	2	27.40	191	412	16
50055000	5	-3	-21	17	22.02	412	265	14
50056400	8	-1	-17	10	16.67	572	168	9
50057000	7	-4	-13	9	25.06	577	173	10
50061800	6	1	-7	1	38.62	435	463	15
50138000	4	-37	14	19	28.72	-294	197	13
50144000	3	-56	2	53	22.46	82	467	18
50147800	6	-67	33	29	14.73	229	151	10

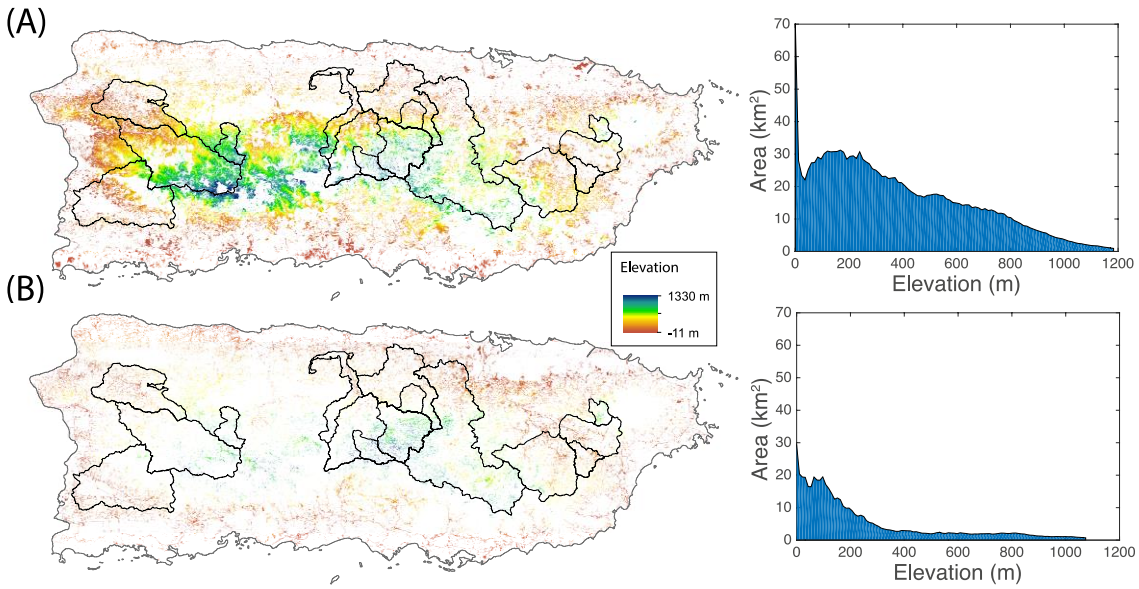

Figure 4.4. Spatial patterns and distribution of elevation under (A) reforested areas and (B) urbanized areas.

4.5.2. Hydro-climate trends

4.5.2.1. Precipitation and temperature trends

Over half of the temperature stations and over one-third of the precipitation stations exhibited a statistically significant change during the study period (Table A4, Figure 5). The number of statistically significant stations for P, T_{avg}, T_{max}, T_{min}, and DTR represented 38%, 52%, 76%, 67%, and 76% of the total number of stations, respectively. Of the 21 temperature recording stations, 17 experienced an increase in average yearly T_{min}, resulting in 14 of the 21 stations exhibiting a decreasing trend in DTR (see Figure 4.6). With the exception of one station in the northwest, all stations that had a significant change in T_{min}, experienced an increase in average minimum temperatures. On average, the rate of change of T_{max} was -0.026 °C/yr (-2.6 °C/100yr) for stations that exhibited a decreasing trend and 0.020 °C/yr (2 °C/100yr) for stations that exhibited an increasing trend. For T_{min}, negative values were on average -0.008 °C/yr (-0.8 °C/100yr) and positive values were on average 0.026 °C/yr (2.6 °C/100yr). Van Beusekom et al. (2015) reported a positive trend in minimum temperature of 0.02 °C/yr in northeastern Puerto Rico, which is in line with this study. Torres-valcárcel et al., (2014) reported on average an increase of 0.67 °C/100yr in T_{min} and 1.51 °C/100yr in T_{max} in Puerto Rico. The difference in average values between their study and the current study is attributed to their use of 57 stations in contrast to the 21 used in this study (the authors used FILNET-adjusted maximum and minimum temperature data instead of the raw station datasets used in this study) and the considerably longer study period spanning from 1901 to 2007. Decreasing DTR was on average -0.044 °C/yr (4.4 °C/100yr) and increasing DTR was on average 0.020 °C/yr (2 °C/100yr). Station 660246 exhibited an anomalously large

difference between the change in T_{max} and T_{min}, resulting in a much higher DTR rate of change than the other stations (see Table A4). This is likely due to errors in the recorded data. Overall, the decreasing trend in DTR is in agreement with previous global studies (ex. Easterling et al., 1997; Stone and Weaver, 2003; Zhou et al., 2010) and regional studies in the Caribbean (Aguilar et al., 2005; Peterson et al., 2002; Stephenson et al., 2014). This finding highlights the potential impact of climate variability and change in Puerto Rico (Braganza et al., 2004).

A greater number of stations in the coastal zones had a statistically significant change in precipitation (41%) than that inland stations (36%). Generally, precipitation in the southern part of the island increased, while rainfall in the north decreased, displaying disparity between the rainfall patterns on either side of the Cordillera Central mount range that spans central Puerto Rico. Similar results were reported by Beck et al. (2013), who hypothesized – based on evidence from previous studies (ex. Van der Molen et al., 2006) – that the spatial pattern could be attributed to changes in wind patterns induced by changing sea surface temperatures. The precipitation rate of change for the stations that had a statistically significant change in precipitation ranged from -3 to -28 mm/yr and 4 to 21 mm/yr. The distribution of the number of stations that experienced a decreasing trend in rainfall (29) and those that experienced an increasing trend in rainfall (32) was about equal, again drawing attention to the spatial pattern in precipitation changes across the island.

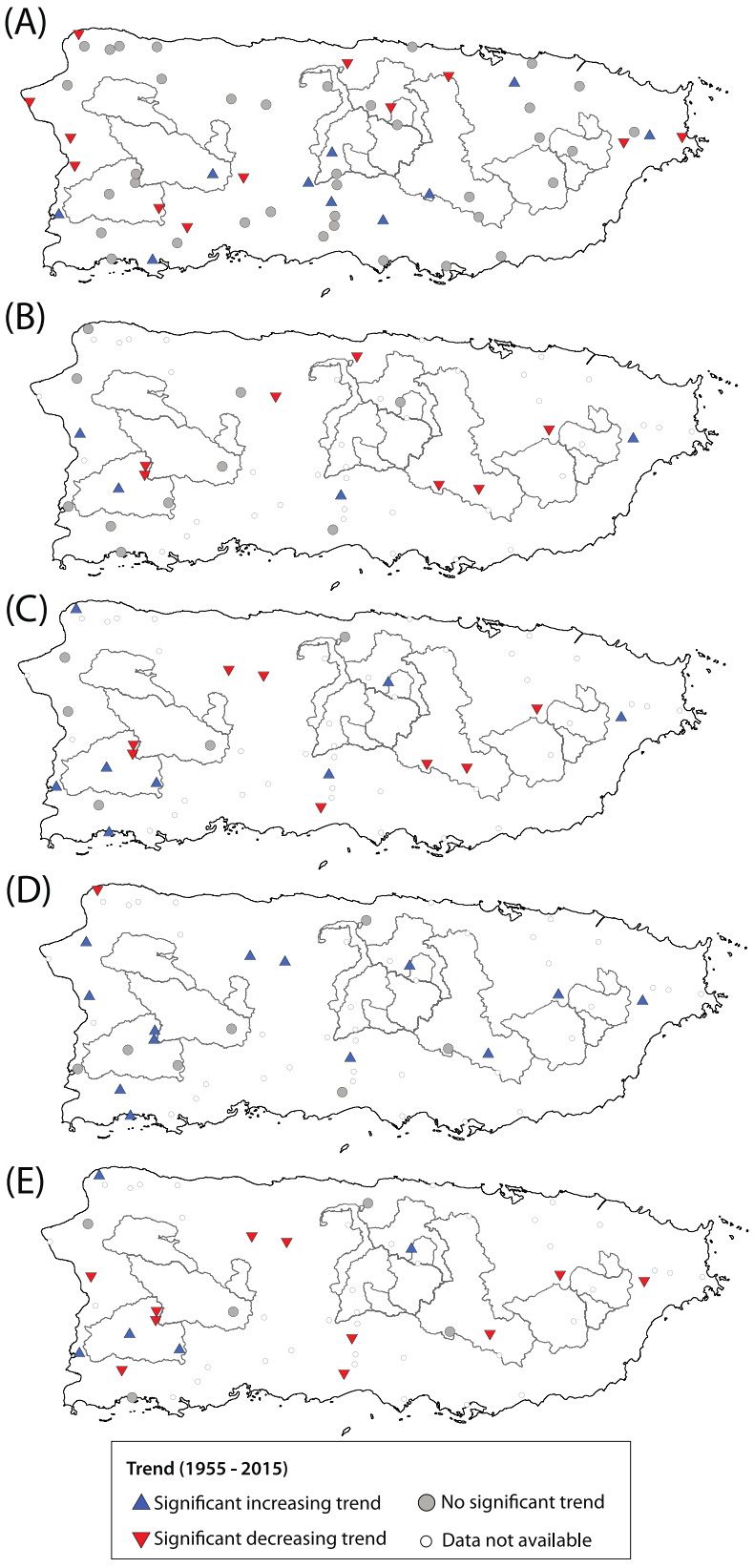

Figure 4.5. Trends in (A) total yearly precipitation, (B) average yearly air temperature, (C) maximum yearly air temperature, (D) minimum yearly air temperature, and E) average yearly DTR.

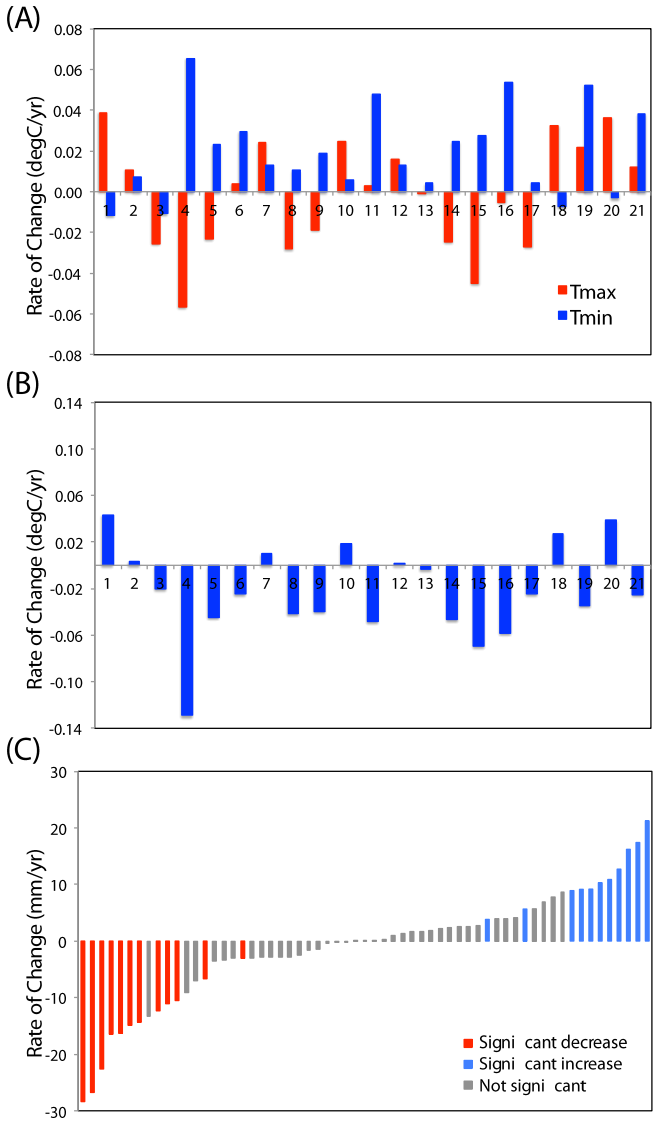

Figure 4.6. Rates of change for (A) T_{max} and T_{min}, (B) DTR, and (C) precipitation over the study period.

4.5.2.1. Streamflow trends

Table 4.3 summarizes the findings from the watershed-scale yearly and seasonal streamflow and precipitation trend analysis; Appendix Table A5 provides additional information including the means, Mann-Kendall Tao-b values, and p-values. A majority of the studied watersheds (8 of 15) experienced a statistically significant increase in

precipitation, particularly in the dry season (7 of 15). Only 20% (3 of 15) of the stations experienced a significant change in precipitation in the rainy season. Changes in total streamflow, surface flow and baseflow were significant for 20%, 27% and 33% of the stations, respectively. These values mainly reflected changes in the rainy season, whereas only 13%, or 2 out of 15, stations experienced significant changes in Q, SF, and BF in the dry season. Normalized streamflow and baseflow values, Q/P and BF/P, also changed markedly for many watersheds during the study period, with 5 of 15 and 7 of 15 stations exhibiting a significant change, respectively. These changes occurred in both the dry and rainy season. Changes in normalized surface flow, SF/P, were less apparent as only 1 of the 15 stations exhibited a statistically significant change overall. The contribution of baseflow to total streamflow, BF/Q, also changed significantly for many stations during the study period, with 8 of the 15 stations exhibiting a statistically significant change, but almost entirely during the rainy season.

Precipitation increased over all of the watersheds studied, during both the dry and rainy season (with the exception of one station that had a small decrease in the rainy season). The increase in rainfall averaged 8 mm/yr across the watersheds for all seasons and 3 mm/yr during the dry season. The finding that rainfall for all watersheds increased despite the fact that nearly half of the stations experienced a decrease in precipitation raised questions regarding the suitability of rainfall interpolation with the limited number of stations in Puerto Rico. To resolve this issue, the trend analysis was re-run using the nearest rainfall station to each watershed in lieu of interpolation. This resulted in 12 of the 15 watersheds experiencing an increase in precipitation, with the other three exhibiting a drying trend. It was, however, concluded that the interpolation method better

captured the spatial dynamics of rainfall across the watersheds given the wide orographic distributions in rainfall characteristic of small mountainous watersheds in the Caribbean (McGillis et al., 2015). The exclusion of coastal stations was believed to reduce the bias in rainfall interpolation, as per the discussion in Section 4.4.1.

For the watersheds that experienced increasing trends, total streamflow increased on average 3.7 mm/yr, surface flow increased on average 2.6 mm/yr and baseflow increased on average 1.9 mm/yr. Only one watershed had a decreasing trend in yearly streamflow (-1.4 mm/yr) and respectively three and four watersheds exhibited decreasing trends in surface flow (average -0.68 mm/yr) and baseflow (average -0.81 mm/yr).

Seven of the 15 watersheds were selected for further analysis. These stations were selected because they exhibited a statistically significant change in Q/P, SF/P or BF/P in both the yearly trend analysis and in at least one of the seasons. Figure 4.7 shows the annual time series of P, Q, SF, BF, Q/P, SF/P, and BF/P for the seven selected watersheds, and the corresponding fitted trend lines. For watersheds that had a significant increase in Q/P, SF/P, or BF/P, the increase in the streamflow component was greater than the increase in rainfall over the watershed. For watersheds that had a significant decrease in Q/P, SF/P, or BF/P, either the streamflow component decreased despite the increasing rainfall trend over the watershed or the amount of increase in the streamflow component was much less than the increasing rate of precipitation. The most pronounced decreasing trends occurred in watersheds B and G (watershed letters are also indicated in Table 4.3). In watershed B: Q, SF and BF decreased despite increasing P, resulting in significant declines in Q/P and BF/P, while SF/P did not show any significant change. On the other hand, in watershed G: Q, SF and BF were relatively constant during the study

period, despite increasing P, also resulting in a decline in Q/P, SF/P (not significant) and BF/P. The greatest increases in streamflow occurred in watersheds A, C and F. The seven selected watersheds are discussed in further detail in Sections 4.5.4 and 4.5.5.

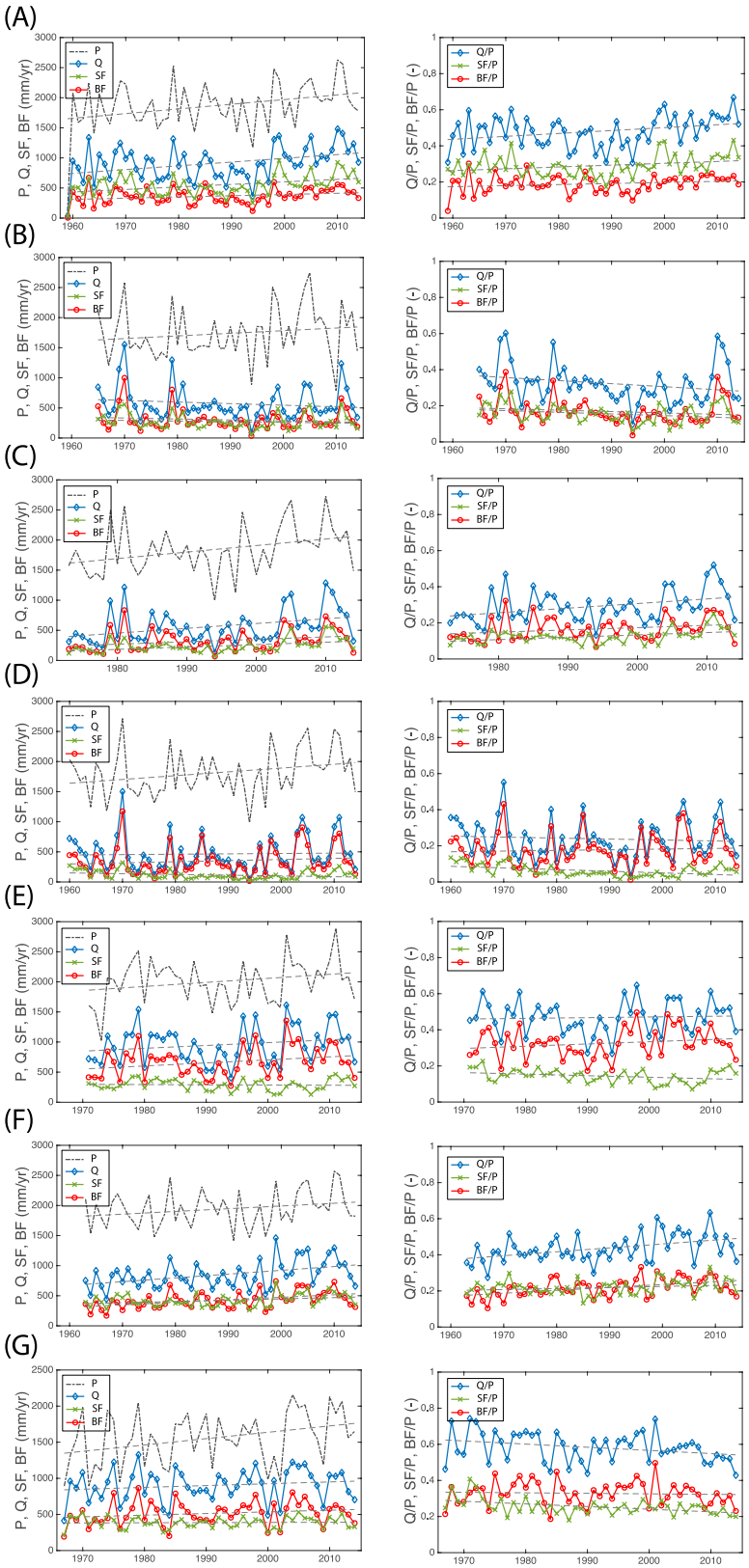

Figure 4.7. Time series of P, Q, SF, BF, Q/P, SF/P and BF/P for the seven watersheds that exhibited a significant change in Q/P, SF/P or BF/P. Watershed ID's are as follows: (A) 50028000, (B) 50031200, (C) 50039500, (D) 50046000, (E) 50057000, (F) 50144000, and (G) 50147800.

Table 4.3. Changes in (A) precipitation and streamflow components and (B) normalized streamflow components and contribution of baseflow to total streamflow over the study period for each of the selected watersheds. Statistically significant changes are highlighted in grey. Watersheds that were selected for further detailed analysis are denoted by letters A to G. ΔQ/P, ΔSF/P, ΔBF/P, and ΔQ/Q are in units of x1000.

(A)

			All Seasons				Dry Season				Rainy Season			
USGS ID	**Watershed Area (km²)**	**Record (yrs)**	**ΔP (mm/yr)**	**ΔQ (mm/yr)**	**ΔSF (mm/yr)**	**ΔBF (mm/yr)**	**ΔP (mm/yr)**	**ΔQ (mm/yr)**	**ΔSF (mm/yr)**	**ΔBF (mm/yr)**	**ΔP (mm/yr)**	**ΔQ (mm/yr)**	**ΔSF (mm/yr)**	**ΔBF (mm/yr)**
50028000[A]	47	56	5.56	6.09	2.37	3.99	1.29	0.82	0.24	0.66	3.72	4.13	1.70	2.72
50031200[B]	143	50	4.78	-1.43	-0.41	-1.17	1.67	-1.38	-0.60	-0.59	3.82	-0.16	0.43	-0.52
50034000	43	41	18.48	6.34	2.55	3.64	6.63	2.55	1.26	1.25	11.08	3.65	1.43	2.52
50035000	346	57	9.83	2.36	0.58	1.48	3.99	0.64	0.07	0.45	4.86	1.64	0.44	1.32
50038100	429	45	2.40	2.57	1.36	0.29	1.00	0.40	0.25	-0.12	-0.15	1.51	0.97	0.38
50038320	39	46	7.79	1.34	0.10	1.67	2.72	0.23	-0.16	0.65	3.08	1.65	0.46	0.87
50039500[C]	227	42	12.48	7.58	4.68	2.79	2.38	2.02	1.24	1.22	8.99	5.80	3.52	1.96
50046000[D]	540	55	6.84	0.51	1.21	-0.96	1.58	-0.65	-0.18	-0.49	3.93	0.72	1.07	-0.44
50055000	232	56	10.92	4.76	3.61	0.56	2.72	0.57	0.37	0.24	8.03	3.31	3.08	0.24
50056400	43	44	4.53	3.69	3.99	-0.48	0.66	1.24	1.32	-0.22	3.42	2.21	2.82	-0.74
50057000[E]	155	56	7.97	3.36	4.15	-0.62	2.76	0.49	0.59	-0.21	5.35	3.29	3.52	-0.42
50061800	27	48	11.75	2.98	-0.77	3.39	6.75	1.37	0.15	0.92	5.45	2.19	-0.84	2.41
50138000	311	42	4.36	0.96	-0.86	1.90	2.76	0.44	0.19	0.37	2.42	0.18	-0.98	1.58
50144000[F]	347	52	4.43	5.83	3.77	1.74	3.16	1.22	0.65	0.51	1.63	3.63	2.72	1.54
50147800[G]	183	48	9.45	3.09	2.52	0.02	3.55	0.88	0.60	0.24	6.17	1.85	1.95	0.38

(B)

			All Seasons				Dry Season				Rainy Season			
USGS ID	**Watershed Area (km^2)**	**Record (yrs)**	**Δ(Q/P) (-)**	**Δ(SF/P) (-)**	**Δ(BF/P) (-)**	**Δ(BF/Q) (-)**	**Δ(Q/P) (-)**	**Δ(SF/P) (-)**	**Δ(BF/P) (-)**	**Δ(BF/Q) (-)**	**Δ(Q/P) (-)**	**Δ(SF/P) (-)**	**Δ(BF/P) (-)**	**ΔBF/Q (-)**
50028000[A]	47	56	1.64	0.72	0.87	0.19	0.79	0.23	0.32	-0.10	1.80	0.67	0.67	0.50
50031200[B]	143	50	-2.27	-0.91	-1.03	-0.44	-3.96	-1.44	-1.83	-0.27	-1.09	-0.39	-0.39	-1.07
50034000	43	41	-0.06	-0.55	0.41	1.62	-0.73	0.28	-0.47	-1.22	-0.13	-0.61	-0.61	3.08
50035000	346	57	-0.82	-0.77	0.09	1.85	-1.88	-0.99	-0.43	0.87	-0.08	-0.40	-0.40	1.58
50038100	429	45	1.03	0.86	0.25	-0.22	-0.48	-0.16	-0.31	-0.27	0.88	0.43	0.43	0.43
50038320	39	46	0.57	-0.49	0.92	1.87	-1.20	-1.19	-0.14	1.55	1.61	0.39	0.39	1.09
50039500[C]	227	42	2.32	1.54	0.93	-0.04	2.28	1.38	1.07	-0.50	3.01	1.80	1.80	-0.71
50046000[D]	540	55	-0.67	0.17	-0.84	-2.87	-1.75	-0.62	-1.23	-1.98	-0.25	0.38	0.38	-2.81
50055000	232	56	0.32	0.78	-0.46	-1.53	-0.65	0.11	-0.89	-1.19	0.40	0.96	0.96	-1.57
50056400	43	44	0.46	1.09	-0.89	-2.48	1.83	2.35	-0.96	-4.95	-0.75	-0.18	-0.18	-1.96
50057000[E]	155	56	0.07	1.08	-0.81	-2.39	-0.28	0.38	-1.02	-2.65	0.81	1.65	1.65	-2.52
50061800	27	48	-0.15	-1.22	0.57	2.92	-1.04	-0.85	-0.38	1.36	0.63	-1.07	-1.07	3.51
50138000	311	42	-0.36	-0.90	0.59	2.19	-0.20	0.05	0.21	-0.50	-0.53	-1.13	-1.13	2.43
50144000[F]	347	52	2.07	1.66	0.47	-1.35	0.81	0.65	-0.08	-1.85	2.54	1.99	1.99	-1.17
50147800[G]	183	48	-2.31	-0.32	-1.22	-1.20	-1.47	0.51	-1.71	-2.53	-2.93	-1.55	-1.55	-0.95

4.5.3. Impact of land cover on climate

Land cover change can impact regional climate through changes on net radiation, changes in the partitioning between sensible and latent heat flux, changes in momentum exchange and the partitioning of precipitation into soil water, evapotranspiration and runoff (Douglas et al., 2009, 2006; Foley et al., 2005; Lawton et al., 2001a; Pielke et al., 1997, 1998; Pielke, 2001; Ray et al., 2006; Woldemichael et al., 2014). Removal of tropical forests and vegetation leads to a reduction in evapotranspiration, an increase in the surface albedo, higher sensible heating and lower roughness (Gentine et al., 2007; Snyder et al., 2004). The effect of reduced evapotranspiration increases surface temperatures and dries the planetary boundary layer, as less water is transpired to the atmosphere from the surface (Gentine et al., 2013; Snyder et al., 2004). Over wet tropical regions this reduces precipitation when deforestation occurs across large regions (Gentine et al., 2013). Modeling studies have provided evidence for this effect in the tropics (Costa and Foley, 2000; Snyder et al., 2004), although evidence of these effects is scale dependent and varies across regions depending on the degree of land-ocean coupling (Lawrence and Vandecar, 2015). We note that heterogeneity at the mesoscale can nonetheless alter this feedback loop and deforested, drier regions, typically generate more convective rainfall and higher cloud cover induced by mesoscale heterogeneities (Knox and Bisht, 2010; Lawton et al., 2001b; Rieck, 2014; Rieck et al., 2015; Taylor et al., 2012). We believe that that the heterogeneity induced by land use land cover changes in Puerto Rico occurs at a scale that is too small (see Figure 4.3) to strongly influence mesoscale circulations.

Based on the analysis, there was no statistically significant indication that forest regeneration at the buffer zone areas investigated was the cause of the changes in precipitation from 1955 to 2015 (see Figure 4.8 and Table 4.4). There was, however, a weak increasing trend of precipitation with reforestation at the smallest buffer distance investigated (500 m), as displayed in Figure 4.8A. There could be two possible explanations for the lack of correlation between rainfall and forest regeneration: 1) insufficient time has passed since the forest regeneration for the new young forests and vegetation to significantly impact rainfall patterns, 2) changes on precipitation patterns occurred at scales larger than those considered in this study.

There was a statistically significant correlation between decreasing precipitation trends and urbanization for buffer distances of 3 km and 5 km. This suggests that part of the precipitation changes highlighted in Section 4.5.2 may be due to land cover change rather than climate variability or climate change alone.

A significant positive correlation was also found between T_{max} and urbanization. Although not statistically significant, T_{min} had a negative correlation with urbanization and DTR had a positive correlation with urbanization. The positive correlation between urbanization and DTR (although weak) could represent the decreased evaporation in urbanized areas due to reduced vegetation and pervious cover. The trends with T_{max} and T_{min}, however, are somewhat counterintuitive from the state of knowledge regarding the "urban heat island" which is believed to typically take place at night, when buildings and streets release the solar heating absorbed during the day (Kalnay and Cai, 2003). Thus, this should mainly impact the minimum temperature, T_{min}. However, temperature changes in Puerto Rico appears to be more affected by the transport of heat and moisture

from the maritime sea breeze than by continental land cover change (Van der Molen et al., 2006). The strong positive correlation between T_{max} and urbanization is then partially attributed to location bias, where most urbanization has occurred in the low-lying coastal areas of the island.

Hypothesis 1 could neither be accepted nor rejected based on the findings presented in this study. Further investigation may be required to explore the feedback between forest regeneration and precipitation at different scales of land cover disturbance than those considered in this study. Mesoscale atmospheric modeling, also beyond the scope of the current study, could also help to decipher the effects of the maritime sea breeze from those of land cover change on temperatures across Puerto Rico.

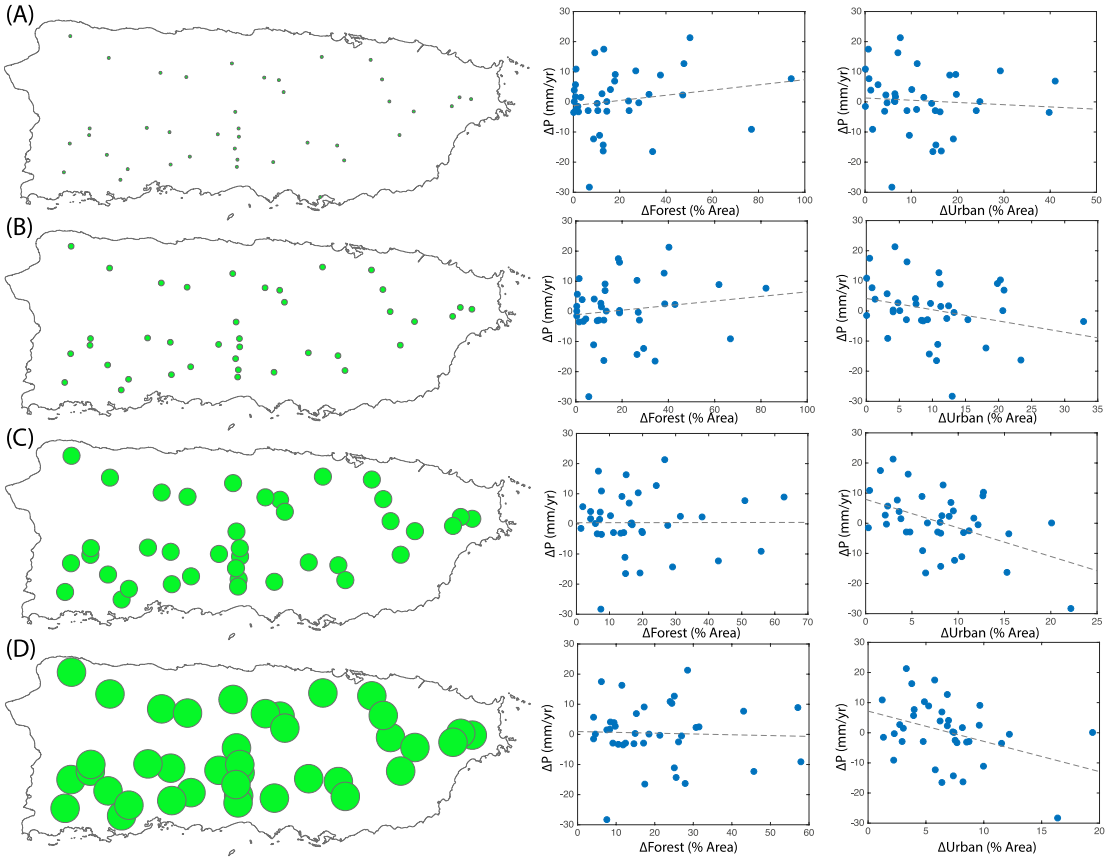

Figure 4.8. Spatial distribution and location of buffer distances of (A) 500 m, (B) 1 km, (C) 3 km, and (D) 5 km. Corresponding scatter plots display the change in precipitation versus change in forest and urban land area for the buffer distances evaluated.

Table 4.4. Correlations for urbanization and reforestation calculated at different buffer distances with changes in total yearly precipitation, P, yearly average temperatures, T_{avg}, yearly maximum temperatures, T_{max}, yearly minimum temperatures, T_{min}, and average yearly diurnal temperature range, DTR. Statistically significant changes are highlighted in grey.

	Buffer Distance			
	500 m	**1 km**	**3 km**	**5 km**
		P		
Urbanization	-0.07 (0.66)	-0.27 (0.10)	-0.48 (0.00)	-0.38 (0.02)
Reforestation	0.18 (0.27)	0.15 (0.38)	0.00 (0.99)	-0.04 (0.83)
		T_{avg}		
Urbanization	0.28 (0.23)	0.17 (0.47)	0.01 (0.98)	0.04 (0.86)
Reforestation	-0.24 (0.29)	-0.12 (0.59)	-0.03 (0.91)	-0.11 (0.64)
		T_{max}		
Urbanization	0.46 (0.04)	0.34 (0.13)	0.27 (0.23)	0.34 (0.13)
Reforestation	-0.26 (0.25)	-0.12 (0.60)	-0.16 (0.48)	-0.23 (0.31)
		T_{min}		
Urbanization	-0.16 (0.48)	-0.20 (0.39)	-0.17 (0.45)	-0.26 (0.25)
Reforestation	-0.12 (0.61)	-0.22 (0.34)	-0.15 (0.52)	-0.08 (0.74)
		DTR		
Urbanization	0.37 (0.10)	0.33 (0.14)	0.28 (0.22)	0.36 (0.11)
Reforestation	-0.09 (0.70)	0.06 (0.79)	0.00 (0.98)	-0.08 (0.74)

4.5.4. Impact of land cover on streamflow

Different biophysical and anthropogenic explanatory variables were tested in order to explore the factors contributing to the changes in streamflow, surface flow and baseflow and to test hypotheses 2 and 3. Table 4.5 summarizes the results of the correlation analysis and Figure 4.9 shows scatter plots of the changes in the normalized streamflow components, ΔQ/P, ΔSF/P, ΔBF/P, and ΔBF/Q versus selected biophysical

and anthropogenic explanatory variables. Of the anthropogenic explanatory variables, there was a significant correlation between the change in urban land area and ΔBF, ΔQ/P and ΔBF/P. There was also a significant relationship between ΔBF/Q and Forest Age. Of the biophysical explanatory variables, there was a significant correlation between ΔP and ΔQ, and ΔT_{avg} and ΔQ, as well as between ΔT_{avg} and ΔSF. Although not significant, there was a positive correlation between forest regeneration and all streamflow components (see Figure 4.9).

Hypothesis 2 is thus partially validated since there is a statistically significant negative correlation between urbanization and baseflow, however, there is no significant relationship between forest regeneration and baseflow (although the trend is positive). The relatively strong correlation between ΔUrban and ΔBF/P of -0.61 (with p-value 0.02) is an indication that urbanization of the previously forested or agricultural land has led to less soil infiltration and recharge due to increasing imperviousness of the landscape (Bruijnzeel, 2004). Watersheds that experienced between 5 to 7% increase in urban land area had a range of positive and negative ΔBF/P's, which is attributed to the fact that those watersheds also experienced some degree of forest regeneration that may or may not have buffered the effects of urbanization. The effects of urbanization on baseflow have been variable across the literature (Konrad and Booth, 2005; Nilsson et al., 2003; Roy et al., 2003), where the reduced infiltration from increasing impervious surfaces is in some cases counteracted by leakage of water supply or sewage infrastructure, which may import water from outside the catchment (Walsh et al., 2005). This however, was not believed to be the case with urbanization patterns in the studied watersheds and the decreased baseflow in urbanized regions was attributed to reduced soil infiltration.

Hypothesis 3 is rejected because ΔSF and ΔSF/P display the opposite relationship with urbanization and forest regeneration than expected – there is a non-significant positive relationship with forest regeneration and a non-significant negative relationship with urbanization. The contradictory relationship between surface flow and urbanization found in this study was also reported by Ramírez et al. (2009), where the authors found that urban streams in Puerto Rico were just as "flashy" – fast rising and draining surface flow hydrographs associated with urban land use (Walsh et al., 2005) – as non-urban ones. This implies that other factors such as topography may be governing storm flow response in the small mountainous watersheds of Puerto Rico. The contradictory relationship can further be explained by the relationship between ΔSF and Forest Age. Although not statistically significant at p-value ≤ 0.05, there was a relatively high negative correlation between ΔSF and Forest Age (-0.49), which means that the age of the secondary forests could be a greater indicator of surface flow change than merely the increase in forest cover. In fact, it has been reported that as forest regeneration occurs, it could take 40 years or more (depending on the level of landscape degradation prior to forest regeneration) for the secondary forests to have the density, basal area, and aboveground biomass similar to those of old growth forests (Aide et al., 2000). Thus, as secondary forests in Puerto Rico age, they will have a thicker canopy that could intercept rainfall as well as potentially soils with greater structure from increased aboveground biomass that could store the surface runoff. In addition to the (non-significant) negative relationship between Forest Age and surface flow, there was also some indication of a positive relationship between Forest Age and ΔBF, and Forest Age and ΔBF/P, and a statistically significant relationship between Forest Age and ΔBF/Q. The latter

relationship implies that as forests age, the contribution of baseflow to total streamflow increases, potentially owing to improved recharge from more structured soils. More research is required to investigate the relationship between the aging of secondary forests and increased baseflow. However, the findings regarding the relationships between Forest Age and the different streamflow components are noteworthy because they highlight the importance of considering forest age in multi-watershed studies of land cover change effects on hydrology.

Table 4.5. Correlations between changes in the difference streamflow components and biophysical and anthropogenic explanatory variables. Statistically significant changes are highlighted in grey.

		Yearly Rate of Change						
		ΔQ	**ΔSF**	**ΔBF**	**ΔQ/P**	**$\Delta Q_{SF}/P$**	**$\Delta Q_{BF}/P$**	**$\Delta Q_{BF}/Q$**
Biophysical Explanatory Variables	**ΔP**	0.52	0.32	0.29	-0.06	-0.04	0.03	0.13
		(0.05)	(0.24)	(0.29)	(0.84)	(0.88)	(0.91)	(0.64)
	ΔT_{avg}	0.54	0.57	0.05	0.21	0.36	-0.10	-0.23
		(0.04)	(0.03)	(0.85)	(0.45)	(0.19)	(0.72)	(0.42)
	ΔDTR	-0.06	0.02	-0.12	0.05	0.09	0.00	0.09
		(0.82)	(0.94)	(0.66)	(0.85)	(0.76)	(1.00)	(0.75)
Anthropogenic Explanatory Variables	**ΔUrban**	-0.41	-0.06	-0.52	-0.61	-0.39	-0.61	-0.11
		(0.13)	(0.82)	(0.05)	(0.02)	(0.15)	(0.02)	(0.69)
	ΔAgriculture	0.00	-0.01	-0.18	0.05	0.03	-0.05	0.09
		(0.99)	(0.98)	(0.52)	(0.86)	(0.92)	(0.85)	(0.74)
	ΔPasture	-0.24	-0.24	0.12	-0.38	-0.40	-0.06	0.05
		(0.40)	(0.40)	(0.68)	(0.16)	(0.14)	(0.84)	(0.86)
	ΔForest	0.23	0.18	0.25	0.31	0.31	0.22	-0.14
		(0.42)	(0.51)	(0.38)	(0.26)	(0.26)	(0.44)	(0.62)
	Forest Age	-0.14	-0.49	0.31	0.08	-0.19	0.35	0.51
		(0.61)	(0.06)	(0.26)	(0.77)	(0.50)	(0.20)	(0.05)
	ΔPopulation	0.27	0.50	-0.43	0.04	0.27	-0.43	-0.45
		(0.34)	(0.06)	(0.11)	(0.88)	(0.34)	(0.11)	(0.09)

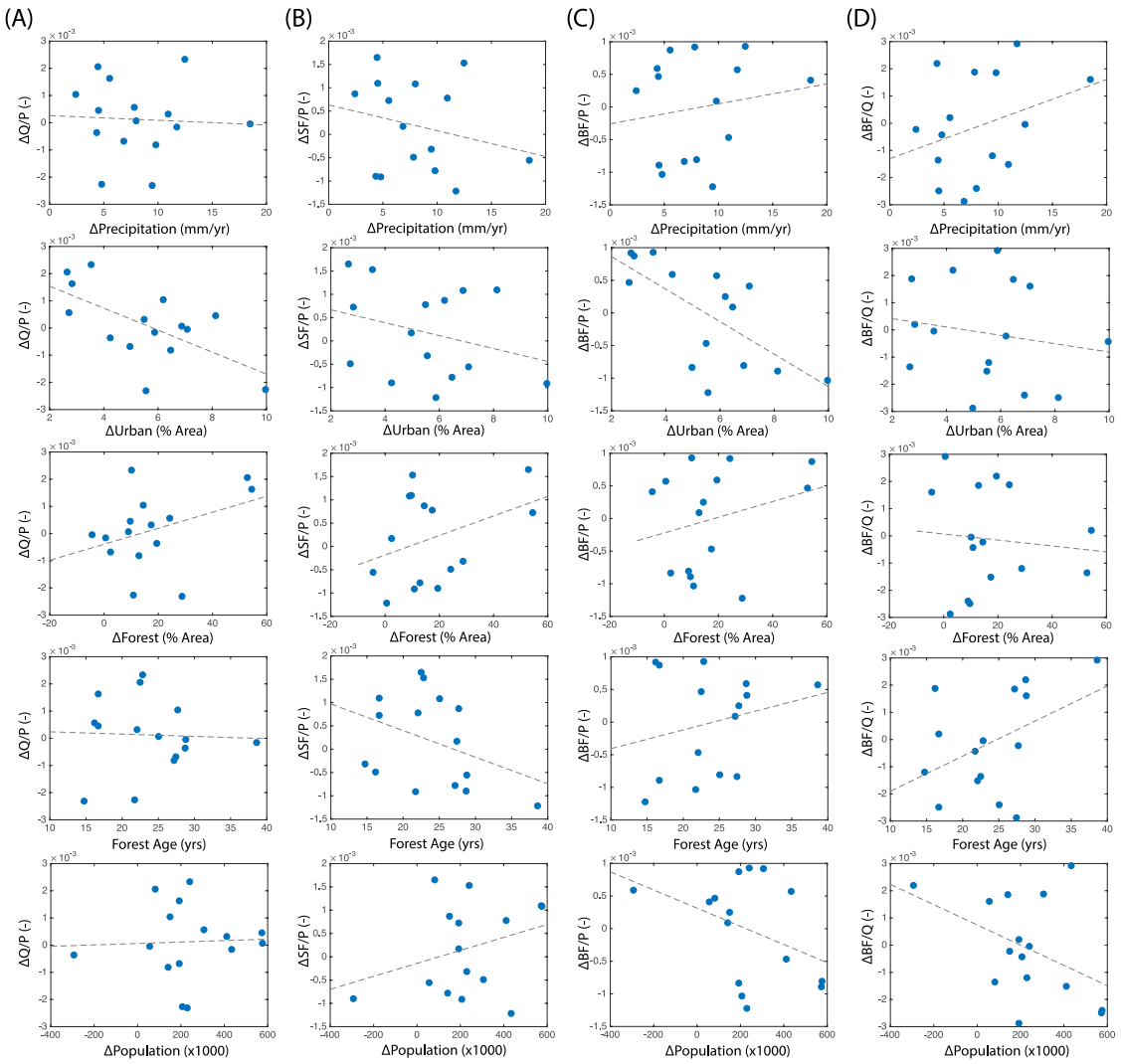

Figure 4.9. Scatter plots with linear regression lines (dotted line) of A) ΔQ/P, B) ΔSF/P, C) ΔBF/P, and D) ΔBF/Q versus selected biophysical and anthropogenic explanatory variables.

Changes in population density were generally not well correlated with the streamflow components, although there was a non-significant negative correlation with ΔBF/P and ΔBF/Q and a non-significant positive correlation with ΔSF. Thus, the change in population density in a watershed could potentially be used as an indicator of changes in streamflow components if used as a proxy for urbanization and subsequently greater demand on surface and subsurface water; however, further study is required to substantiate this. One limitation in using changes in population density as an explanatory

variable for streamflow trends was that the population dataset only dated back to 1985, whereas the streamflow datasets typically began in the late-1950's to early-1960's.

Figure 4.10 shows detailed changes in the normalized streamflow components and changes in the four land cover types for the seven watersheds that experienced a statistically significant change as described in Section 4.2.1. Watersheds A and F both experienced significant agricultural abandonment, which led to forest regeneration. Those watersheds also had increases in Q/P, SF/P and BF/P, although watershed F had a greater increase in normalized surface flow than normalized baseflow, while the opposite was true for watershed A. This is partly attributed to the larger catchment area of watershed F, where potential regional increases in rainfall would have a greater effect, and partly because watershed F had more existing forest area than watershed A, thus improvements to the baseflow recharge were likely to be less pronounced. Watershed B had the greatest urbanization rate of the studied watersheds, resulting in negative Q/P, SF/P and BF/P. Watersheds D and E had a relatively moderate amount of urbanization and very little forest regeneration, both experiencing a statistically significant decrease in normalized baseflow. Watershed C had a large increase in all streamflow components, despite comparatively smaller amounts of forest regeneration. This was believed to be because of the record of the streamflow dataset, which was shorter than that of the other six watersheds. Despite forest growth, $\Delta Q/P$ and $\Delta BF/P$ in watershed G significantly decreased. This result was connected to the marked increase in pasture area, where the imperviousness of the pasture from soil compaction would lead to less infiltration and recharge. Overall, these results reinforce the previous findings from the correlation analysis using all 15 watersheds.

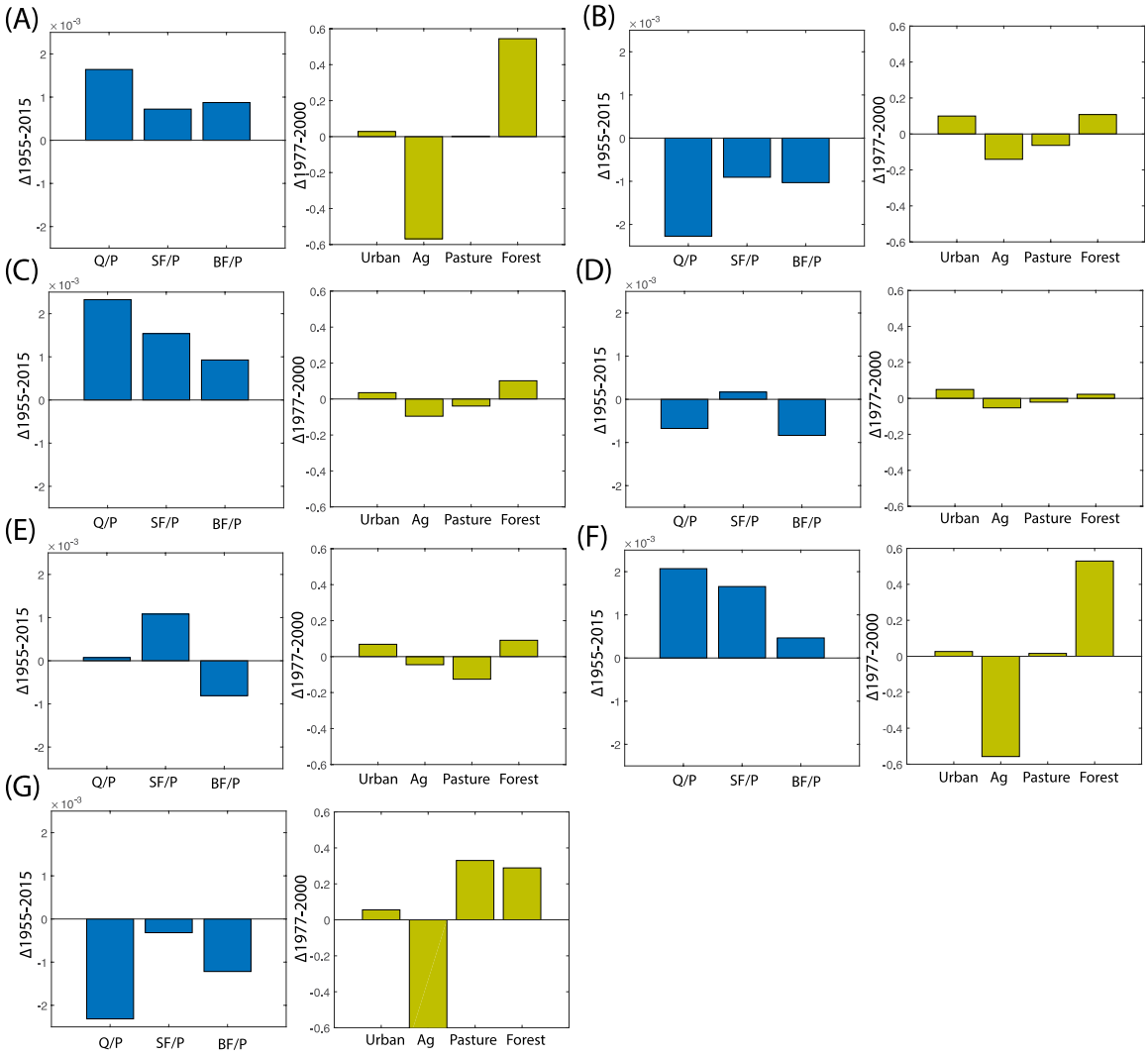

Figure 4.10. Changes in land cover and Q/P, SF/P and BF/P for the seven watersheds that exhibited a significant change in Q/P, SF/P or BF/P. Watershed ID's are as follows: (A) 50028000, (B) 50031200, (C) 50039500, (D) 50046000, (E) 50057000, (F) 50144000, and (G) 50147800.

4.5.5. Changes in baseflow recession behavior

A common attribute of urbanized streams is shorter hydrograph recession times as compared with forested streams (Walsh et al., 2005). Thus, it was believed that watersheds that became urbanized during the study period would exhibit faster baseflow recession times. Adversely, for watersheds that gained forest cover during the study period, an increase in the baseflow recession time would indicate improvements in the

soil structure, allowing greater soil storage capacity, while increased vegetation throughout the watershed would slow down the flow rate of water. This hypothesis was tested by quantifying the recession behavior of the seven watersheds that exhibited a statistically significant change in Q/P, SF/P or BF/P. Figure 4.11 displays the baseflow recession curves for two different periods – 1965 to 1985 and 1995 to 2015 – for the seven watersheds. The recession slopes were separated into six different streamflow bins – 1 to 3 mm, 3 to 5 mm, 5 to 10 mm, 10 to 20 mm, and greater than 20 mm – and the mean and median recession time for each bin was calculated. These values are provided in Table 4.6. Figure 4.12 displays boxplots of watershed the binned recession times.

Watersheds A and F, that had the greatest transition from agriculture to forest, also experienced longer recession times in the post-transition period, with the exception of the largest events for watershed F. Watershed A, in particular, displayed a fundamental change in the recession slope behavior from the earlier to the later period. Mean recession times for streamflows of less than 3 mm increased on average by about 2 days, and for the largest events they increased by an average of 109%. The less drastic change in the recession behavior of watershed F is attributed partly to the presence of existing aging forests (leading to greater evapotranspiration) in that watershed and partly to topographic differences between the two watersheds. Reforestation in watershed A occurred at higher elevations than in watershed F, however, watershed F is characterized by greater differences in topography (resulting in steeper slopes). Because watershed topography controls the rate at which soil water moves downslope, determining whether precipitation is flushed to the channel network or retained in the soil (Price, 2011), it could be expected that the reforested watershed with the greatest differences in elevation (watershed F)

would experience a less drastic increase in baseflow and baseflow recession times than the watershed with less dramatic changes in topography (watershed A), since more streamflow would naturally lead to surface flow than baseflow. This is illustrated by differences in the contribution of baseflow to total yearly streamflow (BF/Q) between the two watersheds, where average BF/Q was 0.57 in watershed A, while it was 0.46 in watershed F (see Table A5). Yet, even in watershed F, recession times for events of 1 to 3 mm increased by about 1 day. Longer recession slopes are attributed to increased groundwater storage and higher baseflows (Brutsaert, 2008), thus the longer recession slopes in the two extensively reforested watersheds are believed to indicate improvements in subsurface storage of precipitation and greater groundwater recharge.

Watershed G, which had a large increase in forest and pasture land cover, experienced shorter recession times at all streamflow values. Similarly, the watershed that experienced the greatest amount of urbanization, watershed B, also had shorter recession times at all streamflow values (with the exception of no change for the smallest streamflows). The moderate forest regeneration and urbanization in watershed C led to slightly increased recession times for streamflows of less than 10 mm and slightly decreased recession times for streamflows of greater than 10 mm. Watersheds D and E had a similar response, with recession times in watershed D decreasing at streamflows of less than 5 mm and increasing at streamflows of greater than 5 mm, and recession times in watershed E decreasing at streamflows of less than 3 mm and increasing at streamflows of greater than 3 mm. These findings indicate that the imperviousness of the landscape may be reducing the storage capacity of the soil, leading to diminished baseflow with faster recession times.

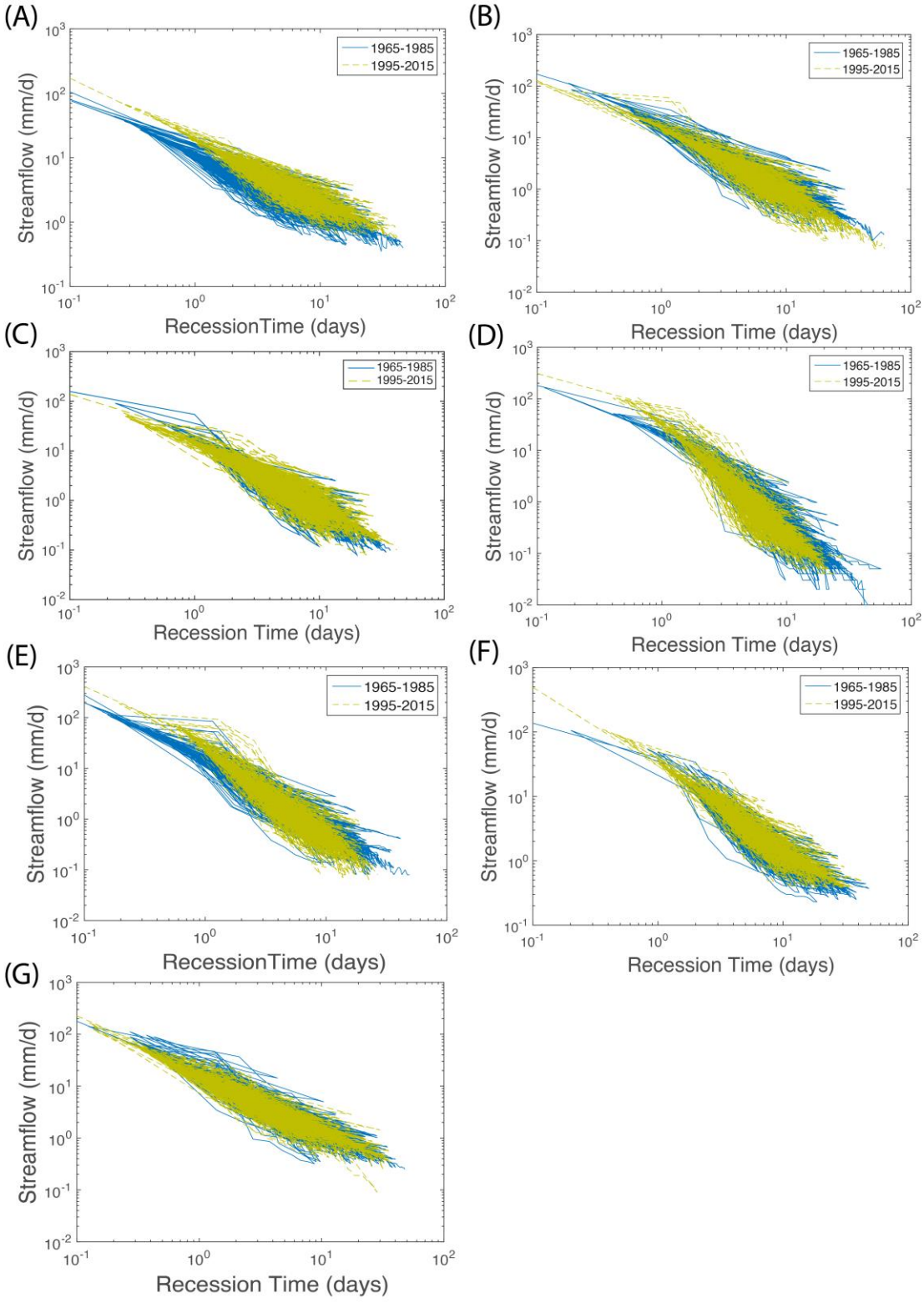

Figure 4.11. Baseflow recession curves for the seven watersheds that exhibited a significant change in Q/P, SF/P or BF/P for the pre-transition (1965-1985) and post-transition (1995-2015) periods. Watershed ID's are as follows: (A) 50028000, (B) 50031200, (C) 50039500, (D) 50046000, (E) 50057000, (F) 50144000, and (G) 50147800.

Table 4.6. Mean and median of binned recession times, K, based on streamflow for the period 1965 to 1985 and 1995 to 2015 for the selected watersheds A to G.

			Streamflow											
			< 1 mm		**1 - 3 mm**		**3 - 5 mm**		**5 -10 mm**		**10 - 20 mm**		**> 20mm**	
			K_{mean} (days)	**K_{median} (days)**	**K_{mean} (days)**	**K_{median} (days)**	**K_{mean} (days)**	**K_{median} (days)**	**K_{mean} (days)**	**K_{median} (days)**	**K_{mean} (days)**	**K_{median} (days)**	**K_{mean} (days)**	**K_{median} (days)**
A	**50028000**	1965-1985	18.87	17.74	8.72	7.99	4.44	3.83	2.33	2.03	0.97	0.88	0.31	0.36
		1995-2015	21.81	22.62	11.07	10.17	5.97	5.45	3.21	2.99	1.58	1.57	0.65	0.67
		Change	**16%**	**28%**	**27%**	**27%**	**35%**	**43%**	**38%**	**47%**	**63%**	**80%**	**109%**	**88%**
B	**50031200**	1965-1985	15.22	14.00	7.79	7.05	3.92	3.36	2.45	2.20	1.39	1.26	0.63	0.62
		1995-2015	15.30	13.17	7.45	6.93	3.96	3.58	2.41	2.30	1.35	1.28	0.62	0.58
		Change	**0%**	**-6%**	**-4%**	**-2%**	**1%**	**7%**	**-2%**	**5%**	**-3%**	**2%**	**-3%**	**-7%**
C	**50039500**	1965-1985	12.76	11.71	6.27	5.59	3.21	2.96	2.00	1.93	1.46	1.37	0.81	0.66
		1995-2015	13.15	11.72	6.69	6.14	3.64	3.28	2.24	2.05	1.34	1.20	0.67	0.53
		Change	**3%**	**0%**	**7%**	**10%**	**13%**	**11%**	**12%**	**6%**	**-8%**	**-12%**	**-17%**	**-20%**
D	**50046000**	1965-1985	12.74	11.18	5.48	5.20	3.48	3.20	2.52	2.38	1.68	1.55	0.79	0.78
		1995-2015	9.90	9.24	4.52	4.26	3.34	2.92	2.53	2.39	1.91	1.70	1.11	1.13
		Change	**-22%**	**-17%**	**-18%**	**-18%**	**-4%**	**-9%**	**0%**	**1%**	**14%**	**10%**	**40%**	**44%**
E	**50057000**	1965-1985	12.50	11.32	5.52	5.21	3.05	2.72	1.98	1.85	1.25	1.07	0.58	0.43
		1995-2015	10.09	9.33	5.36	4.96	3.15	2.99	2.21	2.07	1.61	1.48	0.99	0.89
		Change	**-19%**	**-18%**	**-3%**	**-5%**	**3%**	**10%**	**11%**	**12%**	**29%**	**39%**	**69%**	**107%**
F	**50144000**	1965-1985	17.63	16.55	8.73	7.98	4.57	4.44	3.17	3.04	2.22	2.01	1.33	1.39
		1995-2015	18.15	17.56	9.62	8.92	5.41	5.10	3.76	3.53	2.30	2.20	1.16	1.10
		Change	**3%**	**6%**	**10%**	**12%**	**18%**	**15%**	**19%**	**16%**	**4%**	**9%**	**-13%**	**-21%**
G	**50014700**	1965-1985	18.77	17.86	8.83	7.73	4.19	3.96	2.77	2.62	1.59	1.49	0.72	0.68
		1995-2015	18.72	17.70	8.14	7.17	3.83	3.57	2.30	2.18	1.35	1.21	0.59	0.53
		Change	**0%**	**-1%**	**-8%**	**-7%**	**-9%**	**-10%**	**-17%**	**-17%**	**-15%**	**-19%**	**-18%**	**-23%**

The results of the baseflow recession analysis provide evidence to support hypothesis 4. This study reveals that forest regeneration has over time altered the response of Puerto Rico's extensively reforested watersheds so that baseflow recession times have increased when compared to pre-regeneration periods. To the best knowledge of the author, this study is the first to provide evidence of altered baseflow recession behavior following forest regeneration in the tropics. The study also provides evidence that urbanization or transition from agriculture to pasture in watersheds shortens hydrograph response times in the tropics. Baseflow recession slope analysis can be an important tool for studying the hydrologic effects of land cover change under data limited conditions, where sufficient rainfall records may not be available for the normalization of streamflow and baseflow.

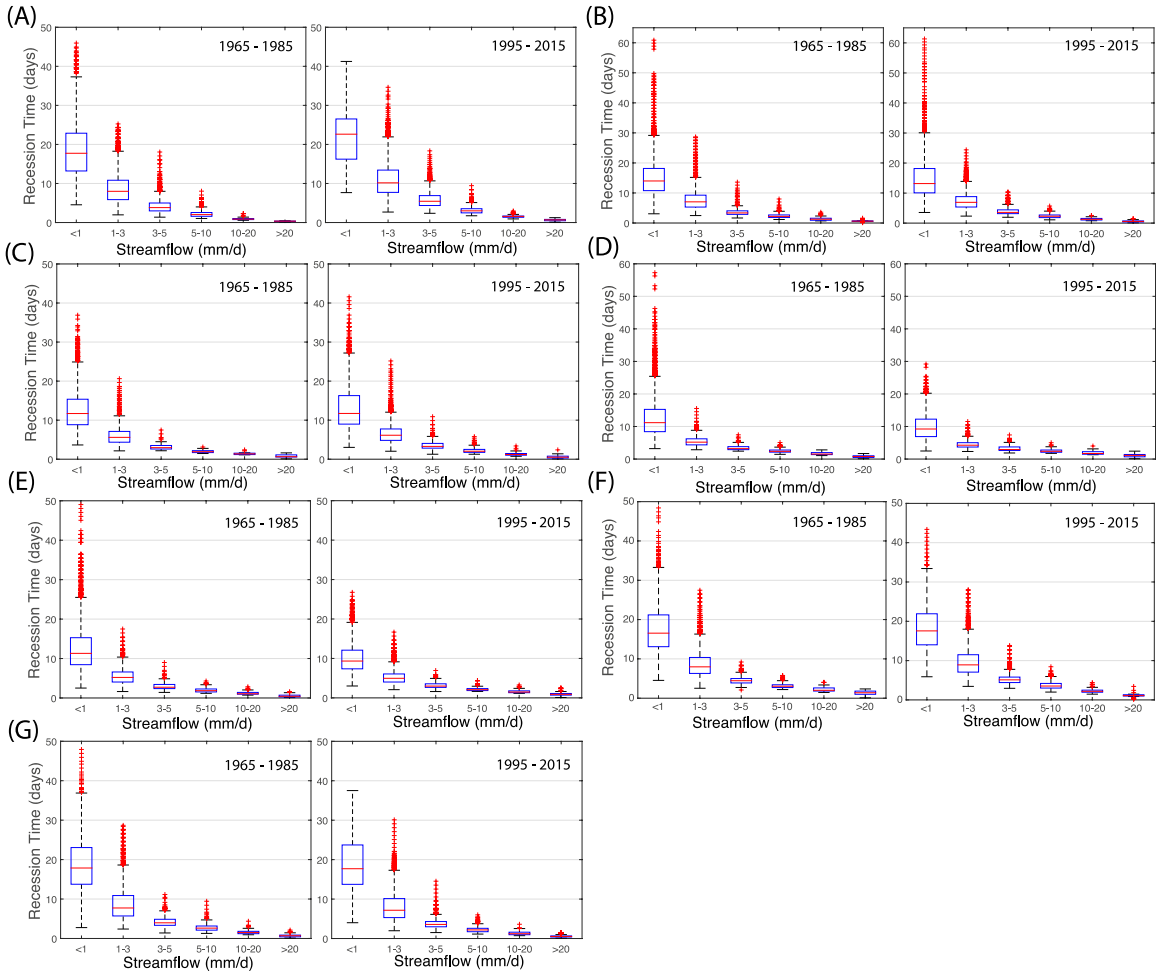

Figure 4.12. Binned recession time boxplots for the seven watersheds that exhibited a significant change in Q/P, SF/P or BF/P for the pre-transition (1965-1985) and post-transition (1995-2015) periods. Watershed ID's are as follows: (A) 50028000, (B) 50031200, (C) 50039500, (D) 50046000, (E) 50057000, (F) 50144000, and (G) 50147800.

4.6. Conclusions

Over the past 60 years, Puerto Rico has experienced extensive changes in land cover and hydro-climatology. Urbanization led to a decreasing trend in total yearly precipitation, yet, a significant relationship between forest regeneration and increased precipitation was not found. There was a distinct spatial pattern of precipitation change, as rainfall in the southern part of the island has generally increased, while rainfall in the northern part of the island has generally decreased. Minimum temperatures across the island have been rising (more than the rise in maximum temperatures), leading to a

decrease in the average diurnal temperature range. Urbanization was also associated with a significant increase in maximum yearly temperatures. A combination of regional climate and land cover changes are likely driving the observed trends in precipitation and temperature.

Changes in streamflow were also partly attributed to land cover. The statically significant negative correlation between the change in urban land cover and the change in normalized runoff and baseflow indicates that baseflow and consequently total streamflow has been decreasing as a result of urbanization. This is due to the increase in impervious surfaces, which inhibit infiltration and recharge. Although there was no significant relationship found between the change in yearly streamflow or baseflow as a result of forest regeneration, the reforested watersheds exhibited a fundamental change in the baseflow recession behavior. Over the study period, recession times in the most reforested, previously agricultural watershed increased by about 2 days for streamflows of less than 1 mm and 109% for streamflows of greater than 20 mm. This provides evidence for the theory that soil infiltration and watershed response to rainfall improve following forest regeneration. This finding also illustrates the importance of considering both water yields and recession behavior in quantifying the effects of land change on baseflow. Increases in baseflow recession times following forest regeneration are also connected to watershed topography, with reforested watersheds exhibiting less pronounced differences in elevation experiencing greater increases in baseflow recession times than those with large slopes. Baseflow recession times decreased following urbanization and the conversion of agricultural lands to pasture. This was attributed to increased imperviousness of the land surface, which would inhibit infiltration and

interception, leading to more direct runoff. Finally, forest age was found to play a more dominant role in the reduction of surface flow than did the change in forest cover between the two periods. This may prove useful for future research as well as policies. In terms of investments into reforestation programs, it would be important for decision makers to be aware that it may take many decades before reductions in surface flow are achieved. For future research looking at the impact of land cover change across multiple watersheds, forest age may be an important variable to consider. The consideration of forest age can be particularly important for studies of natural forest regeneration, since increasingly, tropical landscapes and watersheds will contain a mosaic of forests at different stages of succession (Chazdon, 2014).

Chapter 5

Contributions and Future Work

From densely populated cities to the deforested mountains that create the natural boundaries of watersheds, the impact of land cover change on hydrology transcends many scales. The water management challenges brought on by urbanization and deforestation, as described in this dissertation, have motivated the adoption of landscape re-greening on otherwise impervious or degraded (ex. poorly managed agricultural land) surfaces. As interest in the application of re-greening strategies grows, the question remains: how effectively can these strategies address problems such as flooding and water pollution and how do we evaluate their hydrological benefits? The research summarized in this dissertation addressed this question by evaluating the hydrological benefits of landscape re-greening from the city to the watershed-scale. Through this perspective, the research contained in the preceding three chapters provides several important contributions to the interdisciplinary fields of ecological hydrology and ecological engineering. Beyond the theoretical contributions of the work, the research also presents a number of tools that could be used to make more informed decisions regarding the implementation of different re-greening strategies. This chapter highlights the major contributions of the work described in this thesis as well as potential avenues for future research.

5.1. Green roof design considerations *(Chapter 2)*

Green roofs can be designed in many different ways. Depending on the needs of its end users and the initial implementation goals, a green roof can range from a simple single genus vegetated mat to more complex designs with various types of plants, walking paths, and other architectural elements. In terms of providing hydrological services, a green roof's performance is affected by the physical characteristics of the design and the roof over which it is placed, as well as local weather conditions and regional climate (Czemiel Berndtsson, 2010). *Chapter 2* addressed voids in the literature regarding both factors.

5.1.1. Significance of key findings

Prior work regarding the physical design characteristics of green roofs had not explicitly accounted for the effects of green roof drainage area. *Chapter 2* addressed this gap in research by investigating differences in hydrologic performance between three extensive green roofs in New York City. By controlling for all major physical characteristics of the green roofs – type, manufacturer, age, location (i.e. micro-climate) – except for monitored drainage area, the study enabled observed and modeled differences in hydrologic performance to be attributed to scale. Through event-based observations of individual storms, it was revealed that a larger green roof drainage area would result in greater runoff peak reduction, although it would not necessarily impact overall rainfall retention or the lag time from peak rainfall to peak runoff. The greater peak reduction on larger green roofs was considered to be due to the longer time it takes for water to travel from the outer parts of the rooftop drainage basin to the roof drain. By reducing peak runoff, green roofs can decrease the amount of stormwater entering a city's sewer system

during the height of a storm. This has notable design implications, as combined sewer overflows can be triggered by as little as 3 mm of rainfall in one hour (Montalto et al., 2007). It is suggested that if hydrological benefits are a consideration for the installment of green roofs, then designers and engineers should be cognizant of the green roof area covering individual rooftop drainage basins.

Storm event characteristics – rainfall depth, rainfall intensity, rainfall duration and antecedent dry weather period (ADWP) – were also found to impact green roof hydrologic performance. Overall, rainfall depth and duration exhibited the strongest relationship with rainfall retention and peak reduction, which agreed with previous reports. However, the study summarized in *Chapter 2* questioned the role of ADWP as an indicator of green roof performance. It is deduced from this work that future event-based models should place more emphasis on rainfall depth and duration as prediction parameters and consider the use of substrate moisture conditions in lieu of ADWP.

Predictive models are an increasingly important aspect of green roof research, as they allow for the hydrological benefits of green roofs to be scaled-up to represent the impact of citywide implementation. Models can also be used to optimize the design of individual green roofs for factors such as substrate depth, substrate properties and plant type. *Chapter 2* considered the efficacy of one popular model used in the prediction of green roof hydrology, HYDRUS-1D, in predicting extensive green roof runoff based on laboratory measured parameters. Similar to the observational data, the one dimensional infiltration model was affected by green roof drainage area. Green roof heterogeneities, leading to preferential flow paths in the different drainage areas, were believed to influence event-based runoff behavior, which the model was not able to capture. The use

of initial boundary conditions based on average substrate moisture instead of actual substrate moisture at the beginning of each simulation was also identified as a key issue leading to poor model performance for smaller rainfall events. This again stresses the importance of substrate moisture in predicting green roof hydrologic behavior. Overall, this chapter revealed the need for roof specific calibration parameters when using HYDRUS-1D to predict green roof event-based hydrology and acknowledged the importance of considering flow paths in event-based predictions of green roof runoff.

5.1.2. Avenues for future research

Standardized design guides for green roofs are generally lacking in the United States. The development of design standards for green roofs could help to pave a path for this rapidly emerging civil infrastructure to become a more accountable and commonly utilized tool. The findings from *Chapter 2* present an opportunity to develop green roof 'performance-design-curves' that could provide users with the optimum green roof drainage area based on desired or required reductions in rainfall retention and peak reduction. Figure 2.7 and the graphical abstract in *Chapter 2* illustrate the potential for the development of these curves. Additional monitoring and modeling of drainage areas different than those considered in the study should be undertaken to solidify the relationship between drainage area and green roof stormwater runoff reductions. In this manner, a direct link could be created between the work of green roof researchers and the needs of practitioners in better integrating green roofs into their building designs.

5.2. Long-term evaluation of green roof hydrologic performance *(Chapter 3)*

As the adoption of green infrastructure becomes more typical in cities, there is a greater need to develop resource efficient methods for their continuous performance evaluation of this infrastructure. *Chapter 3* addressed this need with the development of the Soil Water Apportioning Method (SWAM), which can predict green roof runoff and ET solely using measurements of substrate moisture, rainfall and the manufacturer provided green roof substrate water storage capacity.

5.2.1. Significance of key findings

Although SWAM incorporated findings from previous research studies, the methodology summarized in *Chapter 3*, to the best knowledge of the author, was the first to enable the prediction of *both* green roof runoff and evapotranspiration using minimally measured parameters, without the need for additional calibration. SWAM is not explicitly a predictive hydrological model. However, since it can be used to make hind-cast prediction of green roof performance, it is considered a hybrid monitoring-modeling tool. Unlike the event-based modeling with HYDRUS-1D that was discussed in *Chapter 2* and Section 5.1.1 in this chapter, the method proposed in *Chapter 3* aims to provide continuous data on aggregate green roof hydrologic behavior over the course of a green roof's life span.

SWAM performed well compared with directly measured runoff and modeled evapotranspiration for three different extensive green roof types – pre-vegetated mat, built-in-place and modular tray. Best results were achieved using processing time-steps of 3 to 24 hours. The analyses also revealed that estimates of runoff and evapotranspiration via SWAM could be obtained with the use of only one soil moisture sensor per green roof drainage area and as little as one measurement of substrate moisture per day. This makes

SWAM a cost and resource-efficient alternative to other commonly used monitoring methods. It is estimated that the installation costs of a SWAM network would be about one-half of those of a typical monitoring system (exclusive of the cost of labor and maintenance) and require nearly 5-times less labor-hours. The maintenance requirements of the SWAM network are also much less demanding than those of other typical systems, which require regular re-calibration and troubleshooting. In practice, the cost and maintenance requirements of typical monitoring networks limit their use outside of academic research.

As in the contributions of *Chapter 2*, highlighted above, SWAM provides a tool that can help to bridge the gap between research and more informed city planning decisions regarding green infrastructure implementation. Given the module's simplicity and robustness, SWAM could have utility for researchers from various fields of study as well as practitioners interested in the development of widespread green infrastructure monitoring and evaluation campaigns.

5.2.2. Avenues for future research

Expansion of SWAM's validation with additional field monitoring would strengthen the findings from *Chapter 3*. Specifically, direct measurements of ET would provide a good supplement to the comparison with the Soil Moisture Extraction Function (SMEF) model presented in *Chapter 3*. More direct measurements of runoff from the built-in-place and modular tray green roofs would also be useful for further validation of SWAM for different types of green roofs. Lastly, although two different low-cost soil moisture sensors were tested in this study, future work could investigate the sensitivity of additional sensors in measuring green roof substrate moisture. Having identified moisture

measurements as a key parameter to green roof performance predictions, there is great potential to incorporate ultra-low-cost soil moisture measuring devices in green roof studies. Bringing down the cost of instrumentation would also help to make large-scale performance evaluation of green infrastructure more realizable.

Perhaps the most important avenue for future research would be applying the SWAM methodology to green infrastructure other than green roofs. Green streets and right-of-way bioswales, which are both exceedingly popular components of city green infrastructure plans, would be excellent candidates for this method. By accounting for rainfall over these vegetated surfaces and the stormwater diverted to them via curbside flow, their water retention capacity could be calculated using changes in soil moisture. Depending on the depth of the soil, several sensors may be required to capture the vertical moisture profile. If successful in predicting the behavior of these other systems, SWAM could be used to create an integrated network of green infrastructure hydrologic monitoring citywide.

5.3. Hydrological benefits of reforestation *(Chapter 4)*

With the growing emergence of secondary forests on previously deforested, cultivated landscapes and greater investments going into targeted reforestation programs, there is a need to quantify the hydrological effects of reforestation on degraded land. *Chapter 4* addressed this issue through a case study of Puerto Rico, a country that has experienced extensive forest regeneration over the past 60 years.

5.3.1. Significance of key findings

The results summarized in *Chapter 4* present one of the first accounts of improved soil storage and recharge following forest regeneration in previously agricultural-intensive watersheds in the tropics. By investigating streamflow, precipitation and land cover changes in 15 mesoscale watersheds (27 m^2 to 540 m^2), it was found that baseflow recession times have increased in the most reforested watersheds, providing evidence of greater soil infiltration with forest regeneration. The scale of increase in baseflow recession times was dependent on the natural topography of the watershed as well as the previous soil conditions and presence of mature forests. For example, a reforested watershed with little existing forest cover and milder topographical differences would likely experience a relatively larger increase in baseflow recession times than one with mature forests and sharp topographic reliefs. Realizing the role of these factors in the hydrological benefits of reforestation is important for better managing expectations of investments into reforestation programs.

The hydrologic benefits of reforestation were also dependent on the age of the regenerated forests and the degree of urbanization in the studied watersheds. The study found that improved baseflow might not be apparent until several decades after initial forest regeneration, while there was evidence of poor soil infiltration in urbanized areas, leading to decreased baseflow. Thus, it's possible that growing urbanization may offset improvements in subsurface recharge due to forest regeneration at the watershed scale.

Island wide changes in temperature over the study period agreed with global and regional studies, with extreme temperatures having increased overall. The increasing temperature trends supported the reported effects of climate change observed in many other regions. In addition to climate change and variability, temperature and precipitation

trends were also partly attributed to land cover change. The consideration of climate factors was an important aspect of the analysis, which allowed for the isolation of streamflow changes likely due to natural variability from those that were likely due to land cover change.

The results presented in *Chapter 4* are a contribution to the interdisciplinary study of land cover change and hydrology. *Chapter 4* advances knowledge on the effects of forest regeneration on hydrology at the watershed scale by presenting evidence for the hydrological benefits of reforestation on previously degraded land in tropical regions. This chapter also addressed a gap in the literature regarding the impact of land cover change on baseflow (Bruijnzeel, 2004). Finally, the demonstrated use of baseflow recession analysis to investigate the effects of land cover change on streamflow provides an important tool for future research on this topic.

5.3.2. Avenues for future research

Even in data rich regions, studying the effects of land cover change on watershed-scale hydrology is challenging. Watershed modeling would be a good next step for the research presented in *Chapter 4*. Beck et al. (2013) demonstrated the ability of the HBV-light model, a spatially-lumped, conceptual rainfall-runoff model based on the original HBV model (Bergström, 1976), to predict daily streamflow in Puerto Rico. The study reported by Beck et al. (2013) did not explicitly consider changes in baseflow recession behavior as a result of land cover change at the watershed scale. Future work could expand on the modeling efforts of Beck et al. (2013) and the work summarized in *Chapter 4* of this dissertation by using a conceptual hydrologic model (such as the HBV-light) to investigate, in greater detail, the contributing physical factors in the landscape

that have led to changes in streamflow, surface flow, baseflow, and baseflow recession times. Recent studies (ex. Blöschl et al., 2007; Ellison et al., 2012) have also drawn attention to the importance of considering feedback loops between land cover change, climate and hydrology. The study in *Chapter 4* made an effort to address these feedback loops by investigating potential land cover change effects on precipitation and temperature and by normalizing streamflow, surface flow and baseflow by precipitation. However, without the use of predictive models, the study in this respect was limited. Considering the interconnected relationship between land cover change and potential changes in precipitation, evapotranspiration and streamflow would require a coupled hydro-climate model that could be applied at the mesoscale. Given the noted gap in research that addresses land cover change feedbacks on hydrology and climate (Ellison et al., 2012), this presents another path for future research to follow.

5.4. Concluding remarks

Landscape re-greening provides an opportunity to address water management challenges arising from land cover change through the use of natural systems. The research presented in this dissertation addressed the impact of land cover change on hydrology at various scales, from the city to the watershed scale. Implementing re-greening programs at different scales is important because the hydrological effects of upstream land cover change invariably impact downstream users. As it was demonstrated in the case study of Puerto Rico presented in *Chapter 4*, urbanization typically occurs in the lower elevations of a watershed, while deforestation typically occurs in more mountainous regions in the upper reaches of a watershed. The simultaneous occurrence of urbanization and deforestation within individual watersheds is something that many

regions in the world are facing. While the specific re-greening approach should be unique for each region based on its water management needs and goals, this dissertation provided valuable insight as well as a number of tools that can help to determine the hydrological benefits of citywide green infrastructure implementation and watershed scale reforestation.

References

(FLL), F.L.L., 2002. Guidelines for the planning, execution, and upkeep of green-roof sites. Boon, Germany.

A Large and Persistent Carbon Sink in the World's Forests, 2011. . Science (80-.). 333, 988–993.

Aguilar, E., Peterson, T.C., Ramı, P., Frutos, R., Retana, J.A., Solera, M., Soley, J., Gonza, I., Araujo, R.M., Santos, A.R., Valle, V.E., Brunet, M., Bautista, M., Castan, C., Aguilar, L., Herna, G.I., Obed, F., Salgado, J.E., Baca, M., Gutie, M., Centella, C., Espinosa, J., Martı, D., Haylock, M., Benavides, H., Mayorga, R., 2005. Changes in precipitation and temperature extremes in Central America and northern South America, 1961 – 2003. J. Geophys. Res. 110, 1–15. doi:10.1029/2005JD006119

Aide, T.M., Clark, M.L., Grau, H.R., Lopez-Carr, D., Levy, M. a, Redo, D., Bonilla-Moheno, M., Riner, G., Andrade-Nuñez, M.J., Muñiz, M., 2012. Deforestation and Reforestation of Latin America and the Caribbean (2001 – 2010). Biotropica 45, 262–271. doi:10.1111/j.1744-7429.2012.00908.x

Aide, T.M., Zimmerman, J.K., Pascarella, J.B., Rivera, L., Marcano-vega, H., 2000. Forest Regeneration in a Chronosequence of Tropical Abandoned Pastures: Implications for Restoration Ecology. Restor. Ecol. 8, 328–338.

Alfredo, K., Montalto, F., Goldstein, A., 2010. Observed and Modeled Performances of Prototype Green Roof Test Plots Subjected to Simulated Low- and High-Intensity Precipitations in a Laboratory Experiment. J. Hydrol. Eng. 15, 444–457. doi:10.1061/(ASCE)HE.1943-5584.0000135

Andressian, V., 2004. Waters and forests: from historical controversy to scientific debate. J. Hydrol. 291, 1–27. doi:10.1016/j.jhydrol.2003.12.015

ASTM International, 2009. Standard Test Method for Moisture Retention Curves of Porous Building Materials Using Pressure Plates. Designation: C1699-09.

Beck, H.E., Bruijnzeel, L.A., Dijk, A.I.J.M. van, McVicar, T.R., Scatena, F.N., Schellekens, J., 2013. The impact of forest regeneration on streamflow in 12 mesoscale humid tropical catchments. Hydrol. Earth Syst. Sci. 1, 2613–2635. doi:10.5194/hess-17-2613-2013

Bengtsson, L., 2005. Peak flows from thin sedum-moss roof. Nord. Hydrol.

Bengtsson, L., Grahn, L., OLlsson, J., 2004. Hydrological function of a thin extensive green roof in southern Sweden. Nord. Hydrol. 36, 259–268.

Berghage, R., Jarrett, A., Beattie, D., Kelley, K., Husain, S., Rezai, F., Long, B., Negassi, A., Cameron, R., Hunt, W., 2007. Quantifying Evaporation and Transpirational Water Losses from Green Roofs and Green Roof Media Capacity for Neutralizing Acid Rain.

Berghage, R.D., Beattie, D., Jarrett, A.R., Thuring, C., Razaei, F., O'Connor, T., Razaci, F., O'Connor, T.P., 2009. Green Roofs for Stormwater Runoff Control, EP A/600/R-09/026. Cincinnati, OH.

Berghage, R.D., Miller, C., Bass, B., Moseley, D., Weeks, K., 2010. Stormwater Runoff From a Large Commercial Roof In Chicago, in: CitiesAlive!: Eighth Annual Green Roof and Wall Conference. Vancouver, BC, pp. 1–13.

Bergström, S., 1976. Development and application of a conceptual runoff model for Scandinavian catchments. Swedish Meteorological and Hydrological Institute (SMHI).

Berndtsson, J.C., 2010. Green roof performance towards management of runoff water quantity and quality: A review. Ecol. Eng. 36, 351–360. doi:10.1016/j.ecoleng.2009.12.014

Berretta, C., Poë, S., Stovin, V., 2014. Moisture content behaviour in extensive green roofs during dry periods: The influence of vegetation and substrate characteristics. J. Hydrol. 511, 374–386. doi:10.1016/j.jhydrol.2014.01.036

Bliss, D.J., Neufeld, R.D., Ries., R.J., Ries, R.J., 2009. Storm Water Runoff Mitigation Using a Green Roof. Environ. Eng. Sci. 26, 407–418.

Bloomberg, M.R., Lloyd, E., 2013. NYC Green Infrastructure 2013 Annual Report.

Bloomberg, M.R., Strickland, C.H., 2012. NYC Green Infrastructure Plan : 2012 Green Infrastructure Pilot Monitoring Report.

Blöschl, G., Ardoin-bardin, S., Bonell, M., Dorninger, M., Goodrich, D., Gutknecht, D., Matamoros, D., Merz, B., Shand, P., Szolgay, J., 2007. At what scales do climate variability and land cover change impact on flooding and low flows? Hydrological 21, 1241–1247. doi:10.1002/hyp

Bonell, M., Bruijnzeel, L.A., 2005. Forests, Water and People in the Humid Tropics. Cambridge University Press, Cambridge.

Bosch, J.M., Hewlett, J.D., 1982. A review of catchment experiments to determine the effect of vegetation changes on water yield and evapotranspiration. J. Hydrol. 55, 3–23.

Bradshaw, C.J. a., Sodhi, N.S., Peh, K.S.-H., Brook, B.W., 2007. Global evidence that deforestation amplifies flood risk and severity in the developing world. Glob. Chang. Biol. 13, 2379–2395. doi:10.1111/j.1365-2486.2007.01446.x

Braganza, K., Karoly, D.J., Arblaster, J.M., 2004. Diurnal temperature range as an index of global climate change during the twentieth century. Geophys. Res. Lett. 31, 2–5. doi:10.1029/2004GL019998

Brandeis, T.J., Helmer, E.H., Oswalt, S.N., 2003. The Status of Puerto Rico's Forests, 2003.

Brooks, R.H., Corey, A.T., 1964. Hydraulic Properties of Porous Media. Hydrol. Pap. Color. State Univ.

Brown, A.E., Zhang, L., McMahon, T. a., Western, A.W., Vertessy, R. a., 2005. A review of paired catchment studies for determining changes in water yield resulting from alterations in vegetation. J. Hydrol. 310, 28–61. doi:10.1016/j.jhydrol.2004.12.010

Brown, L.R., 2001. Eco-economy: building an economy for the earth, 1st ed. W.W. Norton, New York.

Brown, S., Lugo, A.E., 1990. Tropical secondary forests. J. Trop. Ecol. 6, 1–32.

Bruijnzeel, L. a., 2004. Hydrological functions of tropical forests: Not seeing the soil for the trees? Agric. Ecosyst. Environ. 104, 185–228. doi:10.1016/j.agee.2004.01.015

Bruijnzeel, L.A., 1989. (De)forestation and dry season flow in the tropics: a closer look. J. Trop. For. Sci. 1, 229–243.

Brutsaert, W., 2008. Long-term groundwater storage trends estimated from streamflow records: Climatic perspective. Water Resour. Res. 44. doi:10.1029/2007WR006518

Brutsaert, W., Nieber, J.L., 1977. Regionalized drought flow hydrographs from a mature glaciated plateau. Water Resour. Res. 13, 637–643. doi:10.1029/WR013i003p00637

Calder, I.R., 2002. Forests and Hydrological Services: Reconciling public and science perceptions. L. Use Water Resour. Res. 2, 1–12.

Campbell Scientific, 1996. CS615 water content reflectometer instruction manual.

Carson, T.B., Marasco, D.E., Culligan, P.J., McGillis, W.R., 2013. Hydrological performance of extensive green roofs in New York City: observations and multi-year modeling of three full-scale systems. Environ. Res. Lett. 8, 024036. doi:10.1088/1748-9326/8/2/024036

Carter, T., Jackson, C.R., 2007. Vegetated roofs for stormwater management at multiple spatial scales. Landsc. Urban Plan. 80, 84–94. doi:10.1016/j.landurbplan.2006.06.005

Carter, T., Rasmussen, T., 2006. Hydrologic Behavior of Vegetated Roofs. J. Am. Water Resour. Assoc. 30602, 1261–1274.

Chazdon, R.L., 2008. Beyond Deforestation : Restoring Forests and Ecosystem Services on Degraded Lands. Science (80-.). 320, 1458–1460.

Chazdon, R.L., 2014. Second growth: The promise of tropical forest regeneration in an age of deforestation. University of Chicago Press.

Cobos, D.R., Chambers, C., 2010. Application Note: Calibrating ECH2O Soil Moisture Sensors.

Coffman, L., 2000. Low-Impact Development Design Strategies: An Integrated Design Approach. Prince George's County, Maryland.

Costa, M.H., Botta, A., Cardille, J.A., 2003. Effects of large-scale changes in land cover on the discharge of the Tocantins River, Southeastern Amazonia. J. Hydrol. 283, 206–217. doi:10.1016/S0022-1694(03)00267-1

Costa, M.H., Foley, J.A., 2000. Combined Effects of Deforestation and Doubled Atmospheric CO2 Concentrations on the Climate of Amazonia. J. Clim. 13, 18–34.

Coutts, A.M., Daly, E., Beringer, J., Tapper, N.J., 2013. Assessing practical measures to reduce urban heat: Green and cool roofs. Build. Environ. 70, 266–276. doi:10.1016/j.buildenv.2013.08.021

Crk, T., Uriarte, M., Corsi, F., Flynn, D., 2009. Forest recovery in a tropical landscape: what is the relative importance of biophysical, socioeconomic, and landscape variables? Landsc. Ecol. 24, 629–642. doi:10.1007/s10980-009-9338-8

Cruz-Báez, Á.D., Boswell, T.D., 1997. Atlas of Puerto Rico.

Culligan, P., Carson, T., Peterson, K., Odlin, M., Gaffin, S., McGillis, W., 2011. Quantifying Stormwater Runoff from Green Roofs in an Urban Environment, in: NSF CMMI Research and Innovation Conference. Atlanta, GA.

Culligan, P.J., Carson, T.B., Gaffin, S.R., Gibson, R.A., Hakimdavar, R., Hsueh, D.Y., Marasco, D.E., McGillis, W.R., 2014. Evaluation of Green Roof Water Quantity and Quality Performance in an Urban Climate.

Czemiel Berndtsson, J., 2010. Green roof performance towards management of runoff water quantity and quality: A review. Ecol. Eng. 36, 351–360. doi:10.1016/j.ecoleng.2009.12.014

Dai, A., Trenberth, K.E., Karl, T.R., 1999. Effects of Clouds, Soil Moisture, Precipitation, and Water Vapor on Diurnal Temperature Range. J. Clim. 12, 2451–2473.

Daly, C., Helmer, E.H., Quiñones, M., 2003. Mappin the Climate of Puerto Rico, Vieques and Culebra. Int. J. Climatol. 1381, 1359–1381. doi:10.1002/joc.937

DeFries, R., Eshleman, K.N., 2004. Land-use change and hydrologic processes: a major focus for the future. Hydrol. Process. 18, 2183–2186. doi:10.1002/hyp.5584

DeFries, R.S., Rudel, T., Uriarte, M., Hansen, M., 2010. Deforestation driven by urban

population growth and agricultural trade in the twenty-first century. Nat. Geosci. 3, 178–181. doi:10.1038/ngeo756

DeNardo, J.C., Jarrett, A.R., Manbeck, H.B., Beattie, D.J., Berghaghe, R.D., 2005. Stormwater mitigation and surface temperature reduction by green roofs. Trans. ASABE 48, 1491–1496.

Dietz, J.L., 1986. Economic history of Puerto Rico: institutional change and capitalist development.

DiGiovanni, K., Gaffin, S.R., Montalto, F., 2010. Green Roof Hydrology: Results from a Small-Scale Lysimeter Setup (Bronx, NY), in: Low Impact Development 2010: Redefining Water in the City. ASCE, San Francisco, CA, pp. 1328–1341.

Digiovanni, K., Montalto, F., Gaffin, S., Rosenzweig, C., 2013. Applicability of Classical Predictive Equations for the Estimation of Evapotranspiration from Urban Green Spaces : Green Roof Results. J. Hydrol. Eng. 18, 99–107. doi:10.1061/(ASCE)HE.1943-5584.0000572.

Douglas, E.M., Beltrán-przekurat, A., Niyogi, D., Sr, R.A.P., Vörösmarty, C.J., 2009. The impact of agricultural intensifi cation and irrigation on land-atmosphere interactions and Indian monsoon precipitation — A mesoscale modeling perspective. Glob. Planet. Change 67, 117–128. doi:10.1016/j.gloplacha.2008.12.007

Douglas, E.M., Niyogi, D., Frolking, S., Yeluripati, J.B., Pielke, R.A.S., Niyogi, N., Vörösmarty, C.J., Mohanty, U.C., 2006. Changes in moisture and energy fluxes due to agricultural land use and irrigation in the Indian Monsoon Belt. Geophys. Res. Lett. 33. doi:10.1029/2006GL026550

Easterling, D.R., Horton, B., Jones, P.D., Peterson, T.C., Karl, T.R., Parker, D.E., Salinger, M.J., Razuvayev, V., Plummer, N., Jamason, P., Folland, C.K., 1997. Maximum and Minimum Temperature Trends for the Globe. Science (80-.). 277, 364–368.

Ellison, D., Futter, M.N., Bishop, K., 2012. On the forest cover-water yield debate: From demand- to supply-side thinking. Glob. Chang. Biol. 18, 806–820. doi:10.1111/j.1365-2486.2011.02589.x

Ewel, J.J., Whitmore, J.L., 1973. The ecological life zones of Puerto Rico and the U.S.Virgin Islands, Forest Service Research.

FAO, 2010. Global Forest Resources Assessment 2010. Rome.

Farley, K.A., Jobbágy, E.G., Jackson, R.B., 2005. Effects of afforestation on water yield: a global synthesis with implications for policy. Glob. Chang. Biol. 11, 1565–1576. doi:10.1111/j.1365-2486.2005.01011.x

Fassman-Beck, E., Voyde, E., Simcock, R., Hong, Y.S., 2013. 4 Living Roofs in 3

Locations: Does Configuration Affect Runoff Mitigation? J. Hydrol. In Press. doi:http://dx.doi.org/10.1016/j.jhydrol.2013.03.004

Field, P.E.R., Sullivan, P.E.D., 2001. Overview of EPA's wet-weather flow research program. Urban Water 3, 165–169.

Fioretti, R., Palla, a., Lanza, L.G., Principi, P., 2010. Green roof energy and water related performance in the Mediterranean climate. Build. Environ. 45, 1890–1904. doi:10.1016/j.buildenv.2010.03.001

Foley, J. a, Defries, R., Asner, G.P., Barford, C., Bonan, G., Carpenter, S.R., Chapin, F.S., Coe, M.T., Daily, G.C., Gibbs, H.K., Helkowski, J.H., Holloway, T., Howard, E. a, Kucharik, C.J., Monfreda, C., Patz, J. a, Prentice, I.C., Ramankutty, N., Snyder, P.K., 2005. Global consequences of land use. Science (80-.). 309, 570–574. doi:10.1126/science.1111772

Gartner, T., Mulligan, J., Schmidt, R., Gunn, J., 2013. Natural Infrastructure: Investing in Forested Landscapes for Source Water Protection in the United States.

Gentine, P., Entekhabi, D., Chehbouni, A., Boulet, G., 2007. Analysis of evaporative fraction diurnal behaviour. Agric. For. Meteorol. 143, 13–29. doi:10.1016/j.agrformet.2006.11.002

Gentine, P., Entekhabi, D., Polcher, J., 2011a. The Diurnal Behavior of Evaporative Fraction in the Soil–Vegetation–Atmospheric Boundary Layer Continuum. J. Hydrometeorol. 12, 1530–1546. doi:10.1175/2011JHM1261.1

Gentine, P., Holtslag, A.A.M., D'Andrea, F., Ek, M., 2013. Surface and Atmospheric Controls on the Onset of Moist Convection over Land. J. Hydrometeorol. 14, 1443–1462. doi:10.1175/JHM-D-12-0137.1

Gentine, P., Polcher, J., Entekhabi, D., 2011b. Harmonic propagation of variability in surface energy balance within a coupled soil- vegetation- atmosphere system. Water Resour. Res. 47, 1–21. doi:10.1029/2010WR009268

Getter, K.L., Rowe, D.B., Andresen, J.A., 2007. Quantifying the effect of slope on extensive green roof stormwater retention. Ecol. Eng. 31, 225–31. doi:10.1016/j.ecoleng.2007.06.004

Ghimire, C.P., Bonell, M., Bruijnzeel, L.A., Coles, N.A., Lubczynski, M.W., 2013. Reforesting severely degraded grassland in the Lesser Himalaya of Nepal: Effects on soil hydraulic conductivity and overland fl ow production. J. Geophys. Res. Earth Surf. 118, 2528–2545. doi:10.1002/2013JF002888

Ghimire, C.P., Bruijnzeel, L.A., Lubczynski, M.W., Bonell, M., 2014. Negative trade-off between changes in vegetation water use and infiltration recovery after reforesting degraded pasture land in the Nepalese Lesser Himalaya. Hydrol. Earth Syst. Sci. 18, 4933–4949. doi:10.5194/hess-18-4933-2014

Giambelluca, T.W., 2002. Hydrology of altered tropical forest. Hydrol. Process. 16, 1665–1669. doi:10.1002/hyp.5021

Giannini, A., Kshnir, Y., Cane, M.A., 2000. Interannual Variability of Caribbean Rainfall, ENSO, and the Atlantic Ocean. J. Clim. 13, 297–311.

Giannini, A., Kushnir, Y., Cane, M.A., 2001. Seasonality Rainfall in the Impact of ENSO and the North Atlantic High on Caribbean Rainfall. Phys. Chem. Earth 26, 143–147.

Grau, H.R., Aide, T.M., Zimmerman, J.K., Thomlinson, J.R., Helmer, E., Zou, X., 2003. The Ecological Consequences of Socioeconomic and Land-Use Changes in Postagriculture Puerto Rico. Bioscience 53, 1159. doi:10.1641/0006-3568(2003)053[1159:TECOSA]2.0.CO;2

Grimm, N.B., Faeth, S.H., Golubiewski, N.E., Redman, C.L., Wu, J., Bai, X., Briggs, J.M., 2008. Global change and the ecology of cities. Science (80-.). 319, 756–760. doi:10.1126/science.1150195

Guo, Y., Liu, S., Baetz, B.W., 2012. Probabilistic rainfall-runoff transformation considering both infiltration and saturation excess runoff generation process. Water Resour. Res. 48.

Hakimdavar, R., Culligan, P.J., Finazzi, M., Barontini, S., Ranzi, R., 2014. Scale dynamics of extensive green roofs: Quantifying the effect of drainage area and rainfall characteristics on observed and modeled green roof hydrologic performance. Ecol. Eng. 73, 494–508. doi:10.1016/j.ecoleng.2014.09.080

Harrell, F.E., 2001. Regression Modeling Strategies With Applications to Linear Models, Logistic Regression, and Survival Analysis. Springer.

Helmer, E.H., 2004. Forest conservation and land development in Puerto Rico. Landsc. Ecol. 19, 29–40. doi:10.1023/B:LAND.0000018364.68514.fb

Helmer, E.H., Ramos, O., López, E. del M., Quiñones, M., Diaz, W., 2002. Mapping the Forest Type and Land Cover of Puerto Rico, a Component of the Caribbean Biodiversity Hotspot. Caribb. J. Sci. 38, 165–183.

Hilten, R.N., Lawrence, T.M., Tollner, E.W., 2008. Modeling stormwater runoff from green roofs with HYDRUS-1D. J. Hydrol. 358, 288–293. doi:10.1016/j.jhydrol.2008.06.010

Hobbs, R.J., Arico, S., Aronson, J., Baron, J.S., Cramer, V.A., Epstein, P.R., Ewel, J.J., Klink, C.A., Lugo, A.E., Norton, D., Ojima, D., Richardson, D.M., 2006. Novel ecosystems : theoretical and management aspects of the new ecological world order. Glob. Ecol. Biogeogr. 15, 1–7. doi:10.1111/j.1466-822x.2006.00212.x

Hoffman, L., 2006. Combatting combined sewer flow: green roof storm water modeling. Biocycle 37, 38–40.

Hölscher, D., Mackensen, J., Roberts, J.M., 2005. Forest recovery in the humid tropics: changes in vegetation structure , nutrient pools and the hydrological cycle, in: Forests, Water and People in the Humid Tropics. pp. 598–621.

Hummel & Co, I., 2007. Materials Test Report for Roof Top Soil Media.

Ilstedt, U., Malmer, A., Verbeeten, E., Murdiyarso, D., 2007. The effect of afforestation on water infiltration in the tropics: A systematic review and meta-analysis. For. Ecol. Manage. 251, 45–51. doi:10.1016/j.foreco.2007.06.014

IPCC, 2014. Climate Change 2014: Impacts, Adaptation, and Vulnerability. Part A: Global and Sectoral Aspects. Contribution of Working Group II to the Fifth Assessment Report of the Intergovernmental Panel on Climate Change [Field, C.B., V.R. Barros, D.J. Dokken, K.J. Cambridge University Press, Cambridge, United Kingdom and New York, NY, USA.

Jackson, R.B., Jobba, E.G., Roy, S.B., Barrett, D.J., Cook, C.W., Farley, K.A., Maitre, D.C., Mccarl, B.A., Murray, B.C., 2005. Trading Water for Carbon with Biological Carbon Sequestration. Science (80-.). 310, 1944–1947.

Jim, C.Y., Peng, L.L.H., 2012a. Substrate moisture effect on water balance and thermal regime of a tropical extensive green roof. Ecol. Eng. 47, 9–23. doi:10.1016/j.ecoleng.2012.06.020

Jim, C.Y., Peng, L.L.H., 2012b. Substrate moisture effect on water balance and thermal regime of a tropical extensive green roof. Ecol. Eng. 47, 9–23. doi:10.1016/j.ecoleng.2012.06.020

Jury, M., Malmgren, B. a., Winter, A., 2007. Subregional precipitation climate of the Caribbean and relationships with ENSO and NAO. J. Geophys. Res. 112, D16107. doi:10.1029/2006JD007541

Kalnay, E., Cai, M., 2003. Impact of urbanization and land-use change on climate. Nature 423, 528–532. doi:10.1038/nature01649.1.

Karl, T.R., Koss, W.J., 1984. Regional and National Monthly, Seasonal, and Annual Temperature Weighted by Area, 1895-1983. Asheville.

Kasmin, H., Stovin, V.R., Hathway, E. a., 2010. Towards a generic rainfall-runoff model for green roofs. Water Sci. Technol. 62, 898–905. doi:10.2166/wst.2010.352

Kennaway, T., Helmer, E.H., 2007. The Forest Types and Ages Cleared for Land Development in Puerto Rico. GIScience Remote Sens. 44, 356–382.

Knox, R., Bisht, G., 2010. Precipitation Variability over the Forest-to-Nonforest Transition in Southwestern Amazonia. J. Clim. 24, 2368–2377. doi:10.1175/2010JCLI3815.1

Konrad, C.P., Booth, D.B., 2005. Hydrologic Changes in Urban Streams and Their

Ecological Significance. Am. Fish. Soc. Symp. 47, 157–177.

Lall, R.R., 2013. Haiti to plant millions of trees to boost forests and help tackle poverty. Guard.

Lamb, D., Erskine, P.D., Parrotta, J.A., 2005. Restoration of Degraded Tropical Forest Landscapes 1628–1633.

Larsen, M.C., 2000. Analysis of 20th Century Rainfall and Streamflow to Characterize Drought and Water Resources in Puerto Rico. Phys. Geogr. 21, 494–521. doi:10.1080/02723646.2000.10642723

Laurance, W.F., 2007. Forests and floods. Nature 449, 409–410. doi:10.1111/j.1365-2486.2007.01446.x

Lawrence, D., Vandecar, K., 2015. The impact of tropical deforestation on climate and links to agricultural productivity. Nat. Publ. Gr. 5, 174. doi:10.1038/nclimate2430

Lawton, R.O., Nair, U.S., Pielke, R., Welch, R.M., 2001a. Climatic Impact of Tropical Lowland Deforestation on Nearby Montane Cloud Forests. Science (80-.). 294, 584–588.

Lawton, R.O., Nair, U.S., Sr, R.A.P., Welch, R.M., 2001b. Climatic Impact of Tropical Lowland Deforestation on Nearby Montane Cloud Forests. Science (80-.). 294, 584–588.

Le Tellier, V., Carrasco, A., Asquith, N., 2009. Attempts to determine the effects of forest cover on stream flow by direct hydrological measurements in Los Negros, Bolivia. For. Ecol. Manage. 258, 1881–1888. doi:10.1016/j.foreco.2009.04.031

Locatelli, L., Mark, O., Steen, P., Arnbjerg-nielsen, K., Bergen, M., John, P., 2014. Modelling of green roof hydrological performance for urban drainage applications 519, 3237–3248.

López, T.M., Aide, T.M., Thomlinson, J.R., 2001. Urban expansion and the loss of prime agricultural lands in Puerto Rico. Ambio 30, 49–54. doi:10.1579/0044-7447-30.1.49

Lovett, G.M., Burns, D. a., Driscoll, C.T., Jenkins, J.C., Mitchell, M.J., Rustad, L., Shanley, J.B., Likens, G.E., Haeuber, R., 2007. Who needs environmental monitoring? Front. Ecol. Environ. 5, 253–260. doi:10.1890/1540-9295(2007)5[253:WNEM]2.0.CO;2

Mair, A., Fares, A., 2011. Comparison of Rainfall Interpolation Methods in a Mountainous Region of a Tropical Island. J. Hydrol. Eng. 16, 371–383. doi:10.1061/(ASCE)HE.1943-5584.0000330

Malmer, A., Murdiyarso, D., Bruijnzeel, L.A., Ilstedt, U., 2010. Carbon sequestration in tropical forests and water: a critical look at the basis for commonly used generalizations. Glob. Chang. Biol. 16, 599–604. doi:10.1111/j.1365-

2486.2009.01984.x

Marasco, D.E., Hunter, B.N., Culligan, P.J., Ga, S.R., Mcgillis, W.R., 2014. Quantifying Evapotranspiration from Urban Green Roofs : A Comparison of Chamber Measurements with Commonly Used Predictive Methods.

Marsalek, J., Jimenez-Cisneros, B.E., Malmquist, P.A., 2006. Urban water cycle and interactions. Paris, France.

Martinuzzi, S., Gould, W. a., Ramos González, O.M., 2007. Land development, land use, and urban sprawl in Puerto Rico integrating remote sensing and population census data. Landsc. Urban Plan. 79, 288–297. doi:10.1016/j.landurbplan.2006.02.014

McGillis, W.R., Hsueh, D.Y., Zheng, Y., Markowitz, M., Gibson, R., Bolduc, G., Fevrin, F.J., Thys, J.E., Noel, W., Paine, J.K., Wang, Z.A., Hoering, K., Hakimdavar, R., Culligan, P.J., 2015. Carbon transport in rivers of southwest Haiti. Appl. Geochemistry 63, 563–572. doi:10.1016/j.apgeochem.2015.09.004

Mentens, J., Raes, D., Hermy, M., 2006. Green roofs as a tool for solving the rainwater runoff problem in the urbanized 21st century? Landsc. Urban Plan. 77, 217–226. doi:10.1016/j.landurbplan.2005.02.010

Montalto, F., Behr, C., Alfredo, K., Wolf, M., Arye, M., Walsh, M., 2007. Rapid assessment of the cost-effectiveness of low impact development for CSO control. Landsc. Urban Plan. 82, 117–131. doi:10.1016/j.landurbplan.2007.02.004

Moriasi, D.N., Arnold, J.G., Van Liew, M.W., Bringner, R.L., Harmel, R.D., Veith, T.L., 2007. Model evaluation guidelines for systematic quantification of accuracy in watershed simulations. Trans. … 50, 885–900.

Mualem, Y., 1976. A new model for predicting the hydraulic conductivity of unsaturated porous media. Water Resour. Res. 12.

Muñoz-Villers, L.E., McDonnell, J.J., 2013. Land use change effects on runoff generation in a humid tropical montane cloud forest region. Hydrol. Earth Syst. Sci. 17, 3543–3560. doi:10.5194/hess-17-3543-2013

Nash, J.E., Sutcliffe, J.V., 1970. River flow forecasting through conceptual models part I—A discussion of principles. J. Hydrol. 0.

National Oceanic and Atmospheric Administration, 2007. Storm Data Preparation NWSI 10-1605. Asheville.

National Research Council Committee on Reducing Stormwater Discharge Contributions to Water Pollution, 2009. Urban Stormwater Management in the United States. The National Academies Press.

Niachou, A., Papakonstantinou, K., Santamouris, M., Tsangrassoulis, A., Mihalakakou, G., 2001. Analysis of the green roof thermal properties and investigation of its

energy performance 33, 719–729.

Nilsson, C., Pizzuto, J.E., Moglen, G.E., Palmer, M.A., Stanley, E.H., Bockstael, N.E., Thompson, L.C., 2003. Ecological Forecasting and the Urbanization of Stream Ecosystems: Challenges for Economists, Hydrologists, Geomorphologists, and Ecologists. Ecosystems 6, 659–674. doi:10.1007/s10021-002-0217-2

Palla, a., Gnecco, I., Lanza, L.G., 2009. Unsaturated 2D modelling of subsurface water flow in the coarse-grained porous matrix of a green roof. J. Hydrol. 379, 193–204. doi:10.1016/j.jhydrol.2009.10.008

Palla, a., Gnecco, I., Lanza, L.G., 2012. Compared performance of a conceptual and a mechanistic hydrologic models of a green roof. Hydrol. Process. 26, 73–84. doi:10.1002/hyp.8112

Palla, A., Sansalone, J.J., Gnecco, I., Lanza, L.G., 2011. Storm water infiltration in a monitored green roof for hydrologic restoration. Water Sci. Technol. 64, 766. doi:10.2166/wst.2011.171

Paul, M.J., Meyer, J.L., 2001. Streams in the Urban Landscape. Annu. Rev. Ecol. Syst. 32, 333–365.

Perz, S.G., Skole, D.L., 2003. Secondary Forest Expansion in the Brazilian Amazon and the Refinement of Forest Transition Theory Secondary Forest Expansion in the Brazilian Amazon and the Re ¢ nement of Forest Transition Theory. Soc. Nat. Resour. 16. doi:10.1080/08941920390178856

Peterson, K.A., 2009. Observations of the Hydrological Performance of Green Roofs. Columbia University.

Peterson, T.C., Taylor, M.A., Demeritte, R., Duncombe, D.L., Burton, S., Thompson, F., Porter, A., Mercedes, M., Villegas, E., Fils, R.S., Tank, A.K., Martis, A., Warner, R., Joyette, A., Mills, W., Alexander, L., Gleason, B., 2002. Recent changes in climate extremes in the Caribbean region. J. Geophys. Res. 107, 1–9. doi:10.1029/2002JD002251

Pielke, R. a. S., 2005. Land Use and Climate Change. Science (80-.). 310, 1625–1626.

Pielke, R.A., Zag, X., Lee, T.J., Dalu, G.A., 1997. Mesoscale fluxes over heterogeneous flat landscapes for use in larger scale models. J. Hydrol. 190, 317–336.

Pielke, R.A.S., 2001. Influence of the spatial distribution of vegetation and soils on the prediction of cumulus convective rainfall. Rev. Geophys. 39, 151–177.

Pielke, R.A.S., Avissar, R., Raupach, M., Dolman, A.J., Zeng, X., Denning, A.S., 1998. Interactions between the atmosphere and terrestrial ecosystems: influence on weather and climate. Glob. Chang. Biol. 4, 461–475.

Posavec, K., Bacani, A., Nakic, Z., 2006. A Visual Basic Spreadsheet Macro for

Recession Curve Analysis. Gound Water 44, 764–767. doi:10.1111/j.1745-6584.2006.00226.x

Price, K., 2011. Effects of watershed topography , soils, land use, and climate on baseflow hydrology in humid regions: A review. Prog. Phys. Geogr. 35, sa. doi:10.1177/0309133311402714

Ramírez, A., Jesús-crespo, R. De, Martinó-cardona, D.M., Martínez-, N., Burgos-caraballo, S., Jesu, R. De, Martino, D.M., Ramı, A., 2009. Urban streams in Puerto Rico: what can we learn from the tropics? J. North Am. Benthol. Soc. 28, 1070–1079. doi:10.1899/08-165.1

Ramos, O.M., Lugo, A.E., 1994. Mapa de la vegetación de Puerto Rico. Acta Cient. 8, 63–66.

Ray, D.K., Nair, U.S., Lawton, R.O., Welch, R.M., Pielke, R.A.S., 2006. Impact of land use on Costa Rican tropical montane cloud forests: Sensitivity of orographic cloud formation to deforestation in the plains. J. Geophys. 111, 1–16. doi:10.1029/2005JD006096

Rieck, M., 2014. The Influence of Land Surface Heterogeneities on Cloud Size Development. Mon. Weather Rev. 142, 3830–3846. doi:10.1175/MWR-D-13-00354.1

Rieck, M., Hohenegger, C., Gentine, P., 2015. The effect of moist convection on thermally induced mesoscale circulations. Q. J. R. Meteorol. Soceity 2418–2428. doi:10.1002/qj.2532

Roy, A.H., Rosemond, A.D., Paul, M.J., Leigh, D.S., Wallace, J.B., 2003. Stream macroinvertebrate response to catchment urbanisation (Georgia, U.S.A.). Freshw. Biol. 48, 329–346.

Rudel, T.K., Perez-lugo, M., Zichal, H., 2000. When Fields Revert to Forest: Development and Spontaneous Reforestation in Post-War Puerto Rico. Prof. Geogr. 52, 386–397. doi:10.1111/0033-0124.00233

Rupp, D.E., Selker, J.S., 2005. Information, artifacts, and noise in the dQ/dt - Q recession analysis. Adv. Water Resour. 1–7. doi:10.1016/j.advwatres.2005.03.019

Shalikaran, L., Madani, K., Naeeni, S.T.., 2011. World Environmental and Water Resources Congress 2011: Bearing Knowledge for Sustainability, ASCE 2011. Find. Soc. Optim. Solut. California's Sacramento-San Joaquin Delta Probl. 3190–3197.

Sherrard, J. a., Jacobs, J.M., 2012. Vegetated Roof Water-Balance Model: Experimental and Model Results. J. Hydrol. Eng. 17, 858–868. doi:10.1061/(ASCE)HE.1943-5584.0000531

Simmons, M.T., Gardiner, B., Windhager, S., Tinsley, J., 2008. Green roofs are not created equal: the hydrologic and thermal performance of six different extensive

green roofs and reflective and non-reflective roofs in a sub-tropical climate. Urban Ecosyst. 11, 339–348. doi:10.1007/s11252-008-0069-4

Šimůnek, J., Šejna, M., Sakai, M., van Genuchten, M.T., 2009. The HYDRUS-1D Software Package for Simulating the One-Dimensional Movement of Water, Heat, and Multiple Solutes in Variably Saturated Media (ver. 4.08). Riverside.

Sloto, R. a., Crouse, M.Y., 1996. Hysep: a computer program for streamflow hydrograph separation and analysis. U.S. Geol. Surv. Water-Resources Investig. Rep. 96-4040 54.

Snodgrass, E.C., McIntyre, L., 2010. The Green Roof Manual: A Professional Guide to Design, Installation and Maintenance. Timber Press, Portland.

Snyder, P.K., Delire, C., Foley, J.A., 2004. Evaluating the influence of different vegetation biomes on the global climate. Clim. Dyn. 23, 279–302. doi:10.1007/s00382-004-0430-0

Stephenson, T.S., Vincent, L.A., Allen, T., Meerbeeck, C.J. Van, Mclean, N., Peterson, T.C., Taylor, M.A., Aaron-morrison, A.P., Auguste, T., Bernard, D., Boekhoudt, J.R.I., Blenman, R.C., George, C., Brown, G., Butler, M., Cumberbatch, C.J.M., Lake, D.E., Martin, D.E., Mcdonald, J.L., Zaruela, O., Porter, A.O., Ramirez, S., Tamar, G.A., Roberts, B.A., Mitro, S., Shaw, A., Spence, J.M., Trotman, A.R., 2014. Changes in extreme temperature and precipitation in the Caribbean region, 1961 – 2010. Int. J. Climatol. 2971, 2957–2971. doi:10.1002/joc.3889

Stone, D.A., Weaver, A.J., 2003. Factors contributing to diurnal temperature range trends in twentieth and twenty-first century simulations of the CCCma coupled model. Clim. Dyn. 20, 435–445. doi:10.1007/s00382-002-0288-y

Stovin, V., 2010. The potential of green roofs to manage urban stormwater. Water Environ. J. 24, 192–199. doi:10.1111/j.1747-6593.2009.00174.x

Stovin, V., Poë, S., Berretta, C., 2013. A modelling study of long term green roof retention performance. J. Environ. Manage. 131, 206–15. doi:10.1016/j.jenvman.2013.09.026

Sun, T., Bou-Zeid, E., Wang, Z.-H., Zerba, E., Ni, G.-H., 2012. Hydrometeorological determinants of green roof performance via a vertically resolved model for heat and water transport. Build. Environ. 60, 211–224.

Sun, T., Bou-Zeid, E., Wang, Z.-H., Zerba, E., Ni, G.-H., 2013. Hydrometeorological determinants of green roof performance via a vertically-resolved model for heat and water transport. Build. Environ. 60, 211–224. doi:10.1016/j.buildenv.2012.10.018

Susca, T., Gaffin, S.R., Dell'osso, G.R., 2011. Positive effects of vegetation: urban heat island and green roofs. Environ. Pollut. 159, 2119–26. doi:10.1016/j.envpol.2011.03.007

Takebayashi, H., Moriyama, M., 2007. Surface heat budget on green roof and high reflection roof for mitigation of urban heat island. Build. Environ. 42, 2971–2979. doi:10.1016/j.buildenv.2006.06.017

Taylor, C.M., Jeu, R.A.M. De, Guichard, F., Harris, P.P., Dorigo, W.A., 2012. Afternoon rain more likely over drier soils. Nature 489, 423–426. doi:10.1038/nature11377

Timmerman, Raes, D., Hermy, A., Mentens, J., 2006. GreenRoof - Water balance model manual.

Torres-Valcárcel, Á.R., Harbor, J., Torres-Valcárcel, A.L., González-Avilés, C.J., 2014. Historical differences in temperature between urban and non-urban areas in Puerto Rico. Int. J. Climatol. 35, 1648–1661. doi:10.1002/joc.4083

Troch, P.A., Berne, A., Bogaart, P., Harman, C., Hilberts, A.G.J., Lyon, S.W., Paniconi, C., Pauwels, V.R.N., Rupp, D.E., Selker, J.S., Teuling, A.J., Uijlenhoet, R., Verhoest, N.E.C., 2013. The importance of hydraulic groundwater theory in catchment hydrology: The legacy of Wilfried Brutsaert and Jean-Yves Parlange. Water Resour. Res. 49, 5099–5116. doi:10.1002/wrcr.20407

Tzoulas, K., Korpela, K., Venn, S., Yli-pelkonen, V., Ka, A., Niemela, J., James, P., 2007. Promoting ecosystem and human health in urban areas using Green Infrastructure : A literature review 81, 167–178. doi:10.1016/j.landurbplan.2007.02.001

United Nations, 2014. World Urbanization Prospects. doi:10.4054/DemRes.2005.12.9

Uriarte, M., Yackulic, C.B., Lim, Y., Arce-Nazario, J. a., 2011. Influence of land use on water quality in a tropical landscape: A multi-scale analysis. Landsc. Ecol. 26, 1151–1164. doi:10.1007/s10980-011-9642-y

Van Beusekom, A.E., Gonz, G., Rivera, M.M., 2015. Short-Term Precipitation and Temperature Trends along an Elevation Gradient in Northeastern Puerto Rico. Earth Interact. 19. doi:10.1175/EI-D-14-0023.1

Van Beusekom, A.E., Hay, L.E., Viger, R.J., Gould, W.A., Collazo, J.A., Khalyani, A.H., 2014. The Effects of Changing Land Cover on Streamflow Simulation in Puerto Rico. J. Am. Water Resour. Assoc. 50, 1575–1593. doi:10.1111/jawr.12227

Van der Molen, M.K., Dolman, A.J., Waterloo, M.J., Bruijnzeel, L.A., 2006. Climate is affected more by maritime than by continental land use change: A multiple scale analysis. Glob. Planet. Change 54, 128–149. doi:10.1016/j.gloplacha.2006.05.005

Van Dijk, A.I.J.M., Van Noordwijk, M., Calder, I.R., Bruijnzeel, S.L. a., Schellekens, J., Chappell, N. a., 2009. Forest-flood relation still tenuous - comment on "Global evidence that deforestation amplifies flood risk and severity in the developing world" by C. J. A. Bradshaw, N.S. Sodi, K. S.-H. Peh and B.W. Brook. Glob. Chang. Biol. 15, 110–115. doi:10.1111/j.1365-2486.2008.01708.x

Van Genuchten, M.T., 1980. A closed-form equation for predicting the hydraulic conductivity of unsaturated soils. Soil Sci. Soc. Am. J. 44, 892–898.

Van Renterghem, T., Botteldooren, D., 2009. Reducing the acoustical façade load from road traffic with green roofs. Build. Environ. 44, 1081–1087. doi:10.1016/j.buildenv.2008.07.013

Van Renterghem, T., Botteldooren, D., 2011. In-situ measurements of sound propagating over extensive green roofs. Build. Environ. 46, 729–738. doi:10.1016/j.buildenv.2010.10.006

Van Spengen, J., 2010. The effects of large-scale green roof implementation on the rainfall-runoff in a tropical urbanized subcatchment. Delft University of Technology.

VanWoert, N.D., Rowe, D.B., Andresen, J. a, Rugh, C.L., Fernandez, R.T., Xiao, L., 2005. Green roof stormwater retention: effects of roof surface, slope, and media depth. J. Environ. Qual. 34, 1036–44. doi:10.2134/jeq2004.0364

Velpuri, N.M., Senay, G.B., 2013. Analysis of long-term trends (1950–2009) in precipitation, runoff and runoff coefficient in major urban watersheds in the United States. Environ. Res. Lett. 8, 024020. doi:10.1088/1748-9326/8/2/024020

Vesuviano, G., Stovin, V., 2013. A generic hydrological model for a green roof drainage layer. Water Sci. Technol. 68, 769–775.

Villarreal, E.L., Bengtsson, L., 2005. Response of a Sedum green-roof to individual rain events. Ecol. Eng. 25, 1–7. doi:10.1016/j.ecoleng.2004.11.008

Villarreal, E.L., Semadeni-Davies, A., Bengtsson, L., 2004. Inner city stormwater control using a combination of best management practices. Ecol. Eng. 22, 279–298. doi:10.1016/j.ecoleng.2004.06.007

Vörösmarty, C.J., Green, P., Salisbury, J., Lammers, R.B., 2000. Global Water Resources: Vulnerability from Climate Change and Population Growth. Science (80-.). 289, 284–289.

Vose, R.S., Easterling, D.R., Gleason, B., 2005. Maximum and minimum temperature trends for the globe: An update through 2004. Geophys. Res. Lett. 32, 1–5. doi:10.1029/2005GL024379

Walsh, C.J., Roy, A.H., Feminella, J.W., Cottingham, P.D., Peter, M., Ii, R.P.M., Ii, R.A.P.M.O., 2005. The urban stream syndrome : current knowledge and the search for a cure The urban stream syndrome : current knowledge and. J. North Am. Benthol. Soc. 24, 706–723.

Wang, D., Cai, X., 2010a. Comparative study of climate and human impacts on seasonal baseflow in urban and agricultural watersheds. Geophys. Res. Lett. 37, 1–6. doi:10.1029/2009GL041879

Wang, D., Cai, X., 2010b. Recession slope curve analysis under human interferences. Adv. Water Resour. 33, 1053–1061. doi:10.1016/j.advwatres.2010.06.010

Wilcox, B.P., Huang, Y., 2010. Woody plant encroachment paradox: Rivers rebound as degraded grasslands convert to woodlands. Geophys. Res. Lett. 37, 1–5. doi:10.1029/2009GL041929

Wohl, E., Barros, A., Brunsell, N., Chappell, N. a., Coe, M., Giambelluca, T., Goldsmith, S., Harmon, R., Hendrickx, J., Juvik, J., McDonnell, J.J., Ogden, F., 2012. The hydrology of the humid tropics. Nat. Clim. Chang. 2, 655–662. doi:10.1038/nclimate1556

Woldemichael, A.T., Hossain, F., Pielke, R.S., 2014. Impacts of Postdam Land Use / Land Cover Changes on Modification of Extreme Precipitation in Contrasting Hydroclimate and Terrain Features. J. Hydrometeorol. 777–800. doi:10.1175/JHM-D-13-085.1

Wong, N., Chen, Y., Leng, C., Sia, A., 2003. Investigation of thermal beneÿts of rooftop garden in the tropical environment 38, 261–270.

Yang, J., Yu, Q., Gong, P., 2008. Quantifying air pollution removal by green roofs in Chicago. Atmos. Environ. 42, 7266–7273. doi:10.1016/j.atmosenv.2008.07.003

Zhang, L., Dawes, W.R., Walker, G.R., 2001. Response of mean annual evapotranspiration to vegetation changes at catchment scale. Water Resour. Res. 37, 701–708.

Zhao, L., Xia, J., Xu, C., Wang, Z., Sobkowiak, L., Long, C., 2013. Evapotranspiration estimation methods in hydrological models. J. Geogr. Sci. 23, 359–369. doi:10.1007/s11442-013-1015-9

Zhou, L., Dickinson, R.E., Dai, A., Dirmeyer, P., 2010. Detection and attribution of anthropogenic forcing to diurnal temperature range changes from 1950 to 1999 : comparing multi-model simulations with observations. Clim. Dyn. 35, 1289–1307. doi:10.1007/s00382-009-0644-2

Appendices

Appendix Figures

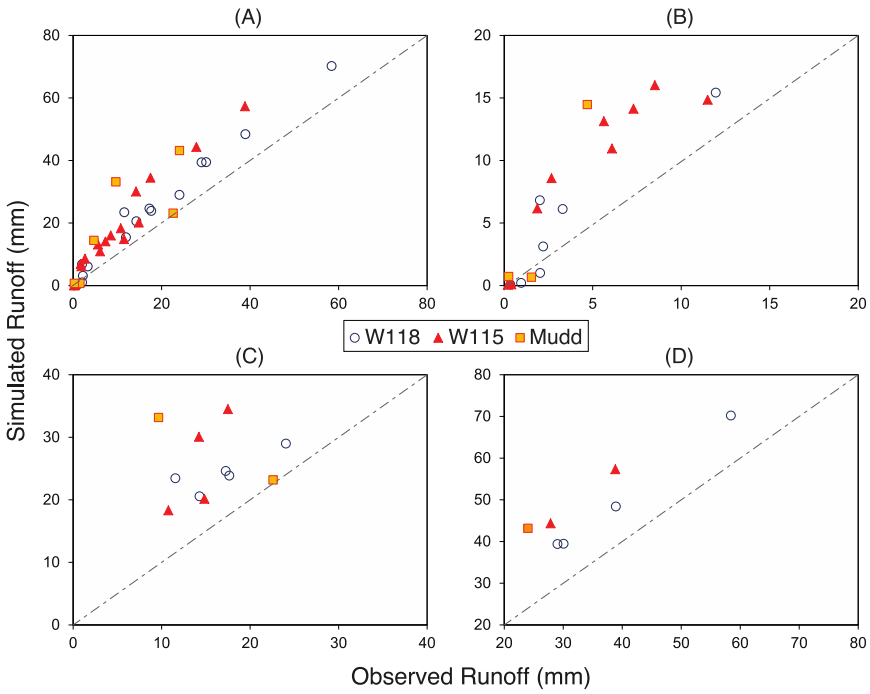

Figure A1. Observed versus simulated total runoff volume per unit rooftop area for the investigated green roof sites during (A) all modeled events, (B) small events (<20mm), (C) medium events (20-40mm), and (D) large events (>40mm). The dashed lines indicate perfect match between measurements and model outputs.

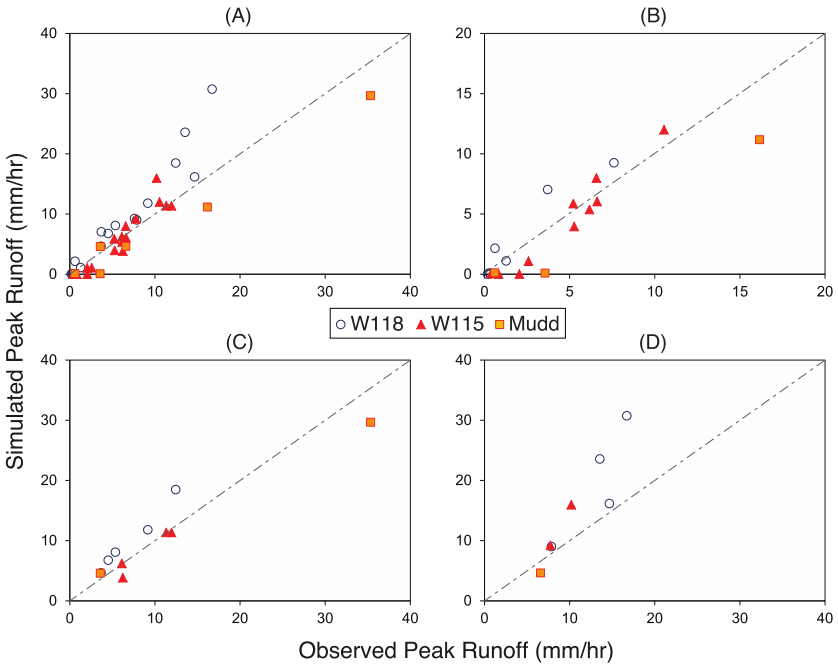

Figure A2. Observed versus simulated peak runoff rate for the investigated green roof sites during (A) all modeled events, (B) small events (<20mm), (C) medium events (20-40mm), and (D) large events (>40mm). The dashed lines indicate perfect match between measurements and model outputs.

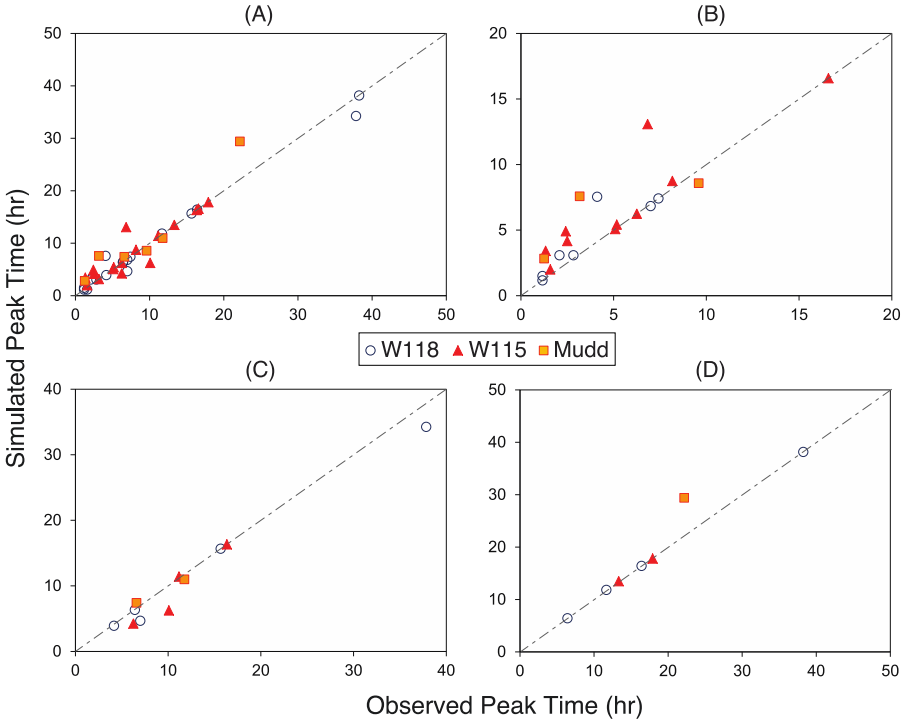

Figure A3. Observed versus simulated peak time for the investigated green roof sites during (A) all modeled events, (B) small events (<20mm), (C) medium events (20-40mm), and (D) large events (>40mm). The dashed lines indicate perfect match between measurements and model outputs.

Appendix Tables

Table A1. Summary statistics for Figure 2.5.

	Rainfall Retention (%)			Peak Reduction (%)			Lag (hr)		
Total Rainfall Depth (mm)									
	<20	20-40	>40	<20	20-40	>40	<20	20-40	>40mm
Mean	85	48	32	89	62	51	1.79	3.97	0.33
Median	98	49	34	98	64	52	0.29	2.54	0.083
St. Dev.	21	16	13	18	21	12	3.02	4.32	0.69
Rainfall Intensity (mm/hr)									
	<1	1-3	>3	<1	1-3	>3	<1	1-3	>3
Mean	87	78	77	88	79	84	3.61	1.7	0.86
Median	97	87	97	95	91	97	2.33	0.21	0.17
St. Dev.	21	25	28	16	26	22	4.2	3.38	1.15
Rainfall Duration (hr)									
	<10	10-20	>20	<10	10-20	>20	<10	10-20	>20
Mean	85	66	43	89	67	55	0.99	3.62	2.79
Median	100	77	41	100	80	52	0.25	0.75	0.25
St. Dev.	22	23	21	18	26	14	1.2	4.25	4.88
Antecedent Dry Weather Period (hr)									
	<50	50-100	>100	<50	50-100	>100	<50	50-100	>100
Mean	74	76	71	80	84	78	1.4	2.34	3.08
Median	85	92	79	91	93	82	0.25	1.08	0.38
St. Dev.	28	28	30	23	21	21	2.25	3.18	4.72

Table A2. Summary statistics for Figure 2.6.

	Rainfall Retention (%)			Peak Reduction (%)			Lag (hr)		
	W118	*W115*	*Mudd*	*W118*	*W115*	*Mudd*	*W118*	*W115*	*Mudd*
Small Events									
Mean	81	89	75	92	88	60	1.44	2.10	0.78
Median	99	100	75	99	99	61	0.25	0.33	1.00
St. Dev.	26	16	19	14	18	35	2.36	3.48	0.46
Medium Events									
Mean	46	52	46	71	56	27	3.76	5.45	1.62
Median	47	54	46	68	50	27	3.08	2.42	1.62
St. Dev.	16	9	39	13	20	33	3.67	6.51	1.24
Large Events									
Mean	25	43	-	54	50	-	0.46	0.06	-
Median	27	41	-	54	51	-	0.08	0.08	-
St. Dev.	11	7	-	12	6	-	0.90	0.05	-

Table A3. Hydrologic characteristics for all simulated rainfall events. ADWP is the Antecedent Dry Weather Period. NSE is the Nash-Sutcliffe Efficiency index. [a] Events that meet the statistical performance criteria of NSE>0.5 and RSR ≤ 0.7. [b] This event has been identified as an outlier and is not included in the statistics calculations for NSE, RSR and PBIAS.

	Atmospheric Data				**Runoff Depth**		**Efficiency**		
Rainfall event	Rainfall depth (mm)	Rainfall duration (h)	Rainfall intensity (mm/h)	ADWP (h)	Obs. (mm)	Sim. (mm)	NSE (-)	RSR (-)	PBIAS (%)
(a) *W118*									
8/3/11	26.92	14.08	1.91	117.75	11.56	23.44	0.29	0.71	103
8/6/11[b]	10.16	15.25	0.67	66.83	2.01	6.82	-7.27	8.27	238
8/7/11[a]	8.38	7.75	1.08	15.00	3.30	6.12	0.65	0.35	85
9/28/11[a]	26.92	52.00	0.52	99.58	17.25	24.61	0.79	0.21	43
9/30/11[a]	32.51	58.33	0.56	25.42	24.04	31.09	0.83	0.17	21
10/3/11	2.29	12.75	0.18	23.67	2.03	1.01	-0.01	1.01	-50
10/19/11[a]	42.16	31.08	1.36	107.42	29.03	39.40	0.79	0.21	36
10/27/11[a]	24.13	15.67	1.54	167.58	14.29	20.56	0.59	0.41	44
11/16/11	26.16	52.00	0.50	122.17	17.64	23.86	0.16	0.84	35
11/29/11[a]	17.27	25.58	0.68	141.92	11.95	15.43	0.56	0.44	29
12/6/11[a]	72.90	42.33	1.72	153.25	58.42	70.21	0.82	0.18	20
12/21/11[a]	5.59	9.33	0.60	6.08	2.20	3.13	0.65	0.35	42
12/27/11[a]	41.15	22.17	1.86	105.75	30.06	39.47	0.77	0.23	31
1/1/12	2.03	7.08	0.29	117.58	0.96	0.21	-0.28	1.28	-78
1/11/12[a]	51.82	27.08	1.91	241.67	38.93	48.41	0.85	0.15	24
1/16/12	2.29	5.92	0.39	93.00	0.35	0.08	-0.11	1.11	-77
Mean	24.54	24.90	0.99	100.29	16.50	22.12	0.49	0.51	21
Median	25.15	18.92	0.68	106.59	13.12	22.00	0.65	0.35	31
St. Dev.	20.20	17.51	0.63	62.73	16.35	20.01	0.38	0.38	52
(b) *W115*									
8/3/11[a]	17.78	5.67	3.14	117.83	7.30	14.14	0.76	0.24	94
9/29/11[a]	14.48	19.67	0.74	6.58	6.08	10.96	0.73	0.27	80
9/30/11	18.54	9.00	2.06	25.42	11.49	14.86	0.28	0.72	29
10/12/11	12.45	10.83	1.15	214.42	2.67	8.59	-2.64	3.64	222
10/14/11	2.03	2.00	1.02	13.75	0.21	0.07	-0.04	1.04	-66
10/19/11[a]	33.53	20.67	1.62	107.50	14.22	30.09	0.60	0.40	112
11/16/11	16.76	12.17	1.38	122.17	5.63	13.14	0.21	0.79	133
11/22/11[a]	48.01	33.33	1.44	10.17	27.85	44.37	0.74	0.26	59
11/29/11	9.91	12.75	0.78	141.00	1.87	6.17	-0.81	1.81	230
12/22/11	19.81	6.17	3.21	24.08	8.51	16.02	0.40	0.60	88
12/27/11[a]	23.88	7.08	3.37	105.92	14.84	20.16	0.84	0.16	36
1/11/12	37.85	18.75	2.02	237.00	17.48	34.51	0.41	0.59	97

1/13/12	2.29	0.67	3.43	7.42	0.40	0.10	-0.03	1.03	-76
1/17/12	3.05	3.67	0.83	6.25	0.37	0.29	-0.23	1.23	-20
4/22/12 [a]	61.47	19.42	3.17	10.50	38.83	57.34	0.75	0.25	48
6/12/12 [a]	21.34	14.50	1.47	57.20	10.77	18.32	0.54	0.46	70
Mean	21.45	12.27	1.93	75.45	10.53	18.07	0.16	0.84	71
Median	18.16	11.50	1.55	41.31	7.91	14.50	0.41	0.60	75
St. Dev.	16.57	8.57	1.01	76.40	10.61	16.23	0.87	0.87	85
(c) *Mudd*									
9/27/09	36.00	20.42	1.24	67.42	9.65	33.18	-1.30	2.30	244
9/28/09	3.53	1.83	0.74	31.17	1.53	0.67	-0.04	1.04	-56
10/7/09	4.06	6.58	1.57	74.67	0.25	0.73	-0.17	1.17	193
10/23/09	18.66	8.92	3.07	19.72	4.69	14.47	-0.84	1.84	209
10/24/09	27.58	11.42	3.45	6.00	22.58	23.18	-0.20	1.20	3
10/27/09	47.02	32.25	6.88	71.83	24.02	43.20	-0.13	1.13	80
Mean	22.81	13.57	2.83	56.77	10.45	19.24	-0.45	1.45	111
Median	23.12	10.17	2.32	27.33	7.17	18.83	-0.19	1.19	136
St. Dev.	17.45	11.03	2.25	91.45	10.48	17.28	0.51	0.51	122

Table A1. Mann-Kendal trend analysis results for all stations in the study.

		P_{tot} (mm/yr)				T_{avg} (C)				T_{max} (C)				T_{min} (C)				DTR (C)		
Station ID	Sen's Slope	MK τ_b	p-value	Trend	Sen's Slope	MK τ_b	p-value	Trend	Sen's Slope	MK τ_b	p-value	Trend	Sen's Slope	MK τ_b	p-value	Trend	Sen's Slope	MK τ_b	p-value	Trend
11603[C]	-6.6823	-0.2237	0.0118	-1	-0.0043	-0.0731	0.4174	0	0.0388	0.3957	0.0000	1	-0.0114	-0.2028	0.0237	-1	0.0434	0.3723	0.0000	1
11630[C]	-10.5250	-0.2263	0.0123	-1	-	-	-	-	-	-	-	-	-	-	-	-	-	-	-	-
11641[C]	2.5920	0.0836	0.3485	0	-	-	-	-	-	-	-	-	-	-	-	-	-	-	-	-
660040	0.2467	0.0022	0.9851	0	-	-	-	-	-	-	-	-	-	-	-	-	-	-	-	-
660053	-12.3464	-0.3027	0.0006	-1	-	-	-	-	-	-	-	-	-	-	-	-	-	-	-	-
660061	8.9211	0.2193	0.0324	1	0.0192	0.1188	0.2480	0	0.0109	0.1981	0.0534	0	0.0071	0.0609	0.5572	0	0.0034	0.0435	0.6770	0
660152[C]	-0.2852	-0.0158	0.8633	0	-	-	-	-	-	-	-	-	-	-	-	-	-	-	-	-
660158	12.7250	0.2348	0.0219	1	-0.0855	-0.6715	0.0000	-1	-0.0254	-0.3082	0.0026	-1	-0.0106	-0.1227	0.2329	0	-0.0204	-0.1304	0.2045	0
660426	2.6971	0.0444	0.7130	0	-0.0024	-0.0254	0.8381	0	-0.0566	-0.5619	0.0000	-1	0.0654	0.3748	0.0016	1	-0.1289	-0.4857	0.0000	-1
661142	21.2500	0.2946	0.0208	1	-	-	-	-	-	-	-	-	-	-	-	-	-	-	-	-
661345	-2.8506	-0.1096	0.2183	0	-	-	-	-	-	-	-	-	-	-	-	-	-	-	-	-
661536	-28.3800	-0.3279	0.0034	-1	-	-	-	-	-	-	-	-	-	-	-	-	-	-	-	-
661590[C]	4.2040	0.1246	0.1578	0	-	-	-	-	-	-	-	-	-	-	-	-	-	-	-	-
661901	-3.0410	-0.0680	0.4959	0	-0.0386	-0.3316	0.0009	-1	-0.0233	-0.3298	0.0010	-1	0.0232	0.3706	0.0002	1	-0.0445	-0.4468	0.0000	-1
662336	10.8960	0.2156	0.0401	1	-	-	-	-	-	-	-	-	-	-	-	-	-	-	-	-
662723	9.1571	0.2228	0.0245	1	-	-	-	-	-	-	-	-	-	-	-	-	-	-	-	-
662801[C]	-1.6423	-0.0710	0.4221	0	0.0034	0.0568	0.5215	0	0.0037	0.0656	0.4590	0	0.0296	0.2820	0.0014	1	-0.0248	-0.1519	0.0848	0
662934	-14.3432	-0.3430	0.0001	-1	0.0063	0.0926	0.3079	0	0.0240	0.4664	0.0000	1	0.0131	0.2934	0.0012	1	0.0101	0.2123	0.0189	1
663023	7.7654	0.2000	0.0540	0	-	-	-	-	-	-	-	-	-	-	-	-	-	-	-	-
663409[C]	-6.9630	-0.1749	0.0714	0	-	-	-	-	-	-	-	-	-	-	-	-	-	-	-	-
663431	-0.2175	-0.0087	0.9256	0	-0.0925	-0.4780	0.0000	-1	-0.0282	-0.4712	0.0000	-1	0.0106	0.2847	0.0013	1	-0.0416	-0.5401	0.0000	-1
663532[C]	3.8297	0.1770	0.0444	1	-	-	-	-	-	-	-	-	-	-	-	-	-	-	-	-
663657	-2.8681	-0.0634	0.5668	0	-	-	-	-	-	-	-	-	-	-	-	-	-	-	-	-
663904	-2.8403	-0.0994	0.2644	0	-	-	-	-	-	-	-	-	-	-	-	-	-	-	-	-
664126	-3.3174	-0.0943	0.3224	0	-	-	-	-	-	-	-	-	-	-	-	-	-	-	-	-
664193[C]	1.6733	0.0383	0.6676	0	-0.0529	-0.5235	0.0000	-1	-0.0188	-0.3246	0.0002	-1	0.0188	0.5301	0.0000	1	-0.0397	-0.5541	0.0000	-1

664276	2.2219	0.0780	0.3822	0	0.0186	0.2075	0.0206	1	0.0248	0.4972	0.0000	1	0.0058	0.0870	0.3292	0	0.0188	0.2633	0.0030	1
664330	0.1000	0.0010	0.9924	0	-	-	-	-	-	-	-	-	-	-	-	-	-	-	-	-
664702	-2.8322	-0.0881	0.3229	0	-	-	-	-	-	-	-	-	-	-	-	-	-	-	-	-
664867	-2.5605	-0.0667	0.4515	0	-	-	-	-	-	-	-	-	-	-	-	-	-	-	-	-
665020	-3.5316	-0.1480	0.0960	0	-	-	-	-	-	-	-	-	-	-	-	-	-	-	-	-
665064	4.0443	0.1016	0.2496	0	-0.0051	-0.0776	0.3803	0	0.0031	0.0798	0.3669	0	0.0479	0.5519	0.0000	1	-0.0483	-0.4426	0.0000	-1
665097	1.4340	0.0531	0.5531	0	0.0004	0.0045	0.9644	0	0.0162	0.4463	0.0000	1	0.0131	0.1853	0.0370	1	0.0013	0.0260	0.7741	0
665693[C]	-3.0287	-0.1974	0.0307	-1	-0.0449	-0.4198	0.0000	-1	-0.0010	-0.0201	0.8310	0	0.0043	0.0489	0.5961	0	-0.0037	-0.0401	0.6645	0
665807[C]	1.0583	0.0230	0.7986	0	-0.0425	-0.3945	0.0000	-1	-0.0247	-0.4361	0.0000	-1	0.0245	0.4699	0.0000	1	-0.0467	-0.4962	0.0000	-1
665908	-9.1395	-0.1343	0.1913	0	-0.0477	-0.4841	0.0000	-1	-0.0451	-0.5034	0.0000	-1	0.0275	0.3739	0.0003	1	-0.0694	-0.5401	0.0000	-1
665911	-11.0860	-0.2305	0.0094	-1	-	-	-	-	-	-	-	-	-	-	-	-	-	-	-	-
666073[C]	-22.6169	-0.4561	0.0000	-1	0.0477	0.4141	0.0000	1	-0.0052	-0.0852	0.3527	0	0.0537	0.5363	0.0000	1	-0.0580	-0.4900	0.0000	-1
666083[C]	0.2058	0.0091	0.9252	0	-	-	-	-	-	-	-	-	-	-	-	-	-	-	-	-
666270	1.6628	0.0303	0.8162	0	-	-	-	-	-	-	-	-	-	-	-	-	-	-	-	-
666361[C]	-3.0236	-0.0949	0.2868	0	-	-	-	-	-	-	-	-	-	-	-	-	-	-	-	-
666390	2.5663	0.0497	0.5790	0	-	-	-	-	-	-	-	-	-	-	-	-	-	-	-	-
666514	16.2281	0.2476	0.0348	1	-	-	-	-	-	-	-	-	-	-	-	-	-	-	-	-
666805	6.8876	0.1209	0.1743	0	-	-	-	-	-	-	-	-	-	-	-	-	-	-	-	-
666983	-1.4464	-0.0366	0.7446	0	-	-	-	-	-	-	-	-	-	-	-	-	-	-	-	-
666992[C]	-13.2175	-0.1081	0.3531	0	0.0155	0.1291	0.2663	0	-0.0270	-0.2643	0.0221	-1	0.0045	0.0871	0.4560	0	-0.0247	-0.2943	0.0108	-1
667292[C]	5.6600	0.2285	0.0108	1	-0.0003	-0.0041	0.9687	0	0.0324	0.5932	0.0000	1	-0.0073	-0.1023	0.2552	0	0.0273	0.4845	0.0000	1
667492[C]	2.4083	0.0546	0.5948	0	-	-	-	-	-	-	-	-	-	-	-	-	-	-	-	-
667843[C]	-14.8780	-0.3507	0.0006	-1	-	-	-	-	-	-	-	-	-	-	-	-	-	-	-	-
668126[C]	-26.7639	-0.4503	0.0000	-1	0.0572	0.3738	0.0008	1	0.0219	0.2780	0.0089	1	0.0523	0.2957	0.0054	1	-0.0344	-0.2248	0.0345	-1
668144	17.4343	0.2158	0.0151	1	-	-	-	-	-	-	-	-	-	-	-	-	-	-	-	-
668306	-16.4455	-0.3872	0.0000	-1	0.0047	0.0316	0.7384	0	0.0361	0.6067	0.0000	1	-0.0031	-0.0532	0.5712	0	0.0388	0.4788	0.0000	1
668536	-0.4176	-0.0175	0.8846	0	-	-	-	-	-	-	-	-	-	-	-	-	-	-	-	-
668815	5.7187	0.0824	0.4029	0	-	-	-	-	-	-	-	-	-	-	-	-	-	-	-	-
668940[C]	1.8860	0.0589	0.5220	0	-	-	-	-	-	-	-	-	-	-	-	-	-	-	-	-

668955	3.9917	0.1355	0.1243	0	-	-	-	-	-	-	-	-	-	-	-	-	-	-	-	-
669432	0.1470	0.0000	0.9876	0	-	-	-	-	-	-	-	-	-	-	-	-	-	-	-	-
669521	10.2929	0.2173	0.0250	1	0.0318	0.4645	0.0000	1	0.0121	0.2204	0.0230	1	0.0382	0.5075	0.0000	1	-0.0250	-0.3914	0.0001	-1

Table A2. Watershed scale Mann-Kendal trend analysis results for precipitation and streamflow components for (A) all seasons, (B) dry season, (C) rainy season.

A1)

			ΔP (mm/yr)					ΔQ (mm/yr)					ΔSF (mm/yr)					ΔBF (mm/yr)				
USGS ID	Watershed Area (km^2)	Record (yrs)	Mean	Sen's Slope	MK τ_b	p-value	Trend	Mean	Sen's Slope	MK τ_b	p-value	Trend	Mean	Sen's Slope	MK τ_b	p-value	Trend	Mean	Sen's Slope	MK τ_b	p-value	Trend
50028000	47	56	1864	5.56	0.18	0.05	1	909	6.09	0.23	0.01	1	364	2.37	0.19	0.04	1	545	3.99	0.25	0.01	1
50031200	143	50	1737	4.78	0.12	0.23	0	573	-1.43	-0.09	0.38	0	301	-0.41	-0.05	0.64	0	272	-1.17	-0.13	0.18	0
50034000	43	41	1784	18.48	0.34	0.00	1	682	6.34	0.15	0.16	0	390	2.55	0.12	0.29	0	292	3.64	0.25	0.02	1
50035000	346	57	1803	9.83	0.23	0.01	1	621	2.36	0.11	0.22	0	351	0.58	0.05	0.62	0	269	1.48	0.18	0.04	1
50038100	429	45	1692	2.40	0.05	0.63	0	747	2.57	0.08	0.44	0	415	1.36	0.07	0.50	0	333	0.29	0.02	0.85	0
50038320	39	46	1807	7.79	0.18	0.08	0	667	1.34	0.07	0.50	0	391	0.10	0.00	0.98	0	276	1.67	0.13	0.21	0
50039500	227	42	1838	12.48	0.30	0.01	1	561	7.58	0.25	0.02	1	324	4.68	0.24	0.03	1	237	2.79	0.28	0.01	1
50046000	540	55	1810	6.84	0.18	0.05	0	464	0.51	0.02	0.83	0	348	1.21	0.09	0.34	0	116	-0.96	-0.16	0.09	0
50055000	232	56	1943	10.92	0.28	0.00	1	835	4.76	0.16	0.08	0	507	3.61	0.20	0.03	1	327	0.56	0.05	0.59	0
50056400	43	44	2008	4.53	0.11	0.32	0	955	3.69	0.09	0.41	0	666	3.99	0.12	0.24	0	289	-0.48	-0.04	0.68	0
50057000	155	56	2128	7.97	0.20	0.03	1	739	3.36	0.11	0.23	0	522	4.15	0.16	0.08	0	218	-0.62	-0.07	0.45	0
50061800	27	48	2504	11.75	0.20	0.05	1	920	2.98	0.08	0.42	0	544	-0.77	-0.03	0.77	0	376	3.39	0.25	0.01	1
50138000	311	42	1777	4.36	0.12	0.28	0	537	0.96	0.04	0.73	0	305	-0.86	-0.07	0.53	0	231	1.90	0.17	0.11	0
50144000	347	52	1940	4.43	0.13	0.17	0	850	5.83	0.25	0.01	1	427	3.77	0.29	0.00	1	423	1.74	0.19	0.05	0
50147800	183	48	1554	9.45	0.22	0.03	1	901	3.09	0.12	0.22	0	514	2.52	0.16	0.11	0	387	0.02	0.01	0.95	0

A2)

			ΔQ / P (-)					ΔSF / P (-)					ΔBF / P (-)					ΔBF / Q (-)				
USGS ID	Watershed Area (km^2)	Record (yrs)	Mean	Sen's Slope	MK τ_b	p-value	Trend	Mean	Sen's Slope	MK τ_b	p-value	Trend	Mean	Sen's Slope	MK τ_b	p-value	Trend	Mean	Sen's Slope	MK τ_b	p-value	Trend

50028000	47	56	0.4792	0.0016	0.2013	0.0290	1	0.1895	0.0007	0.1623	0.0784	0	0.2896	0.0009	0.1909	0.0384	1	0.6073	0.0002	0.0390	0.6767	0
50031200	143	50	0.3234	-0.0023	-0.2310	0.0183	1	0.1683	-0.0009	-0.1902	0.0523	0	0.1551	-0.0010	-0.1967	0.0447	1	0.4856	-0.0004	-0.0465	0.6395	0
50034000	43	41	0.3661	-0.0001	-0.0073	0.9552	0	0.2075	-0.0006	-0.0439	0.6942	0	0.1586	0.0004	0.0756	0.4933	0	0.4506	0.0016	0.1683	0.1239	0
50035000	346	57	0.3330	-0.0008	-0.0977	0.2860	0	0.1880	-0.0008	-0.1479	0.1057	0	0.1451	0.0001	0.0226	0.8096	0	0.4463	0.0018	0.2293	0.0120	1
50038100	429	45	0.4370	0.0010	0.0788	0.4513	0	0.2406	0.0009	0.0828	0.4281	0	0.1964	0.0003	0.0323	0.7617	0	0.4641	-0.0002	-0.0283	0.7917	0
50038320	39	46	0.3588	0.0006	0.0512	0.6225	0	0.2026	-0.0005	-0.0454	0.6632	0	0.1562	0.0009	0.2174	0.0339	1	0.4423	0.0019	0.1923	0.0608	0
50039500	227	42	0.2903	0.0023	0.2427	0.0242	1	0.1655	0.0015	0.2009	0.0623	0	0.1249	0.0009	0.2427	0.0242	1	0.4382	0.0000	-0.0012	0.9914	0
50046000	540	55	0.2391	-0.0007	-0.0694	0.4590	0	0.1772	0.0002	0.0195	0.8389	0	0.0619	-0.0008	-0.2566	0.0058	1	0.2801	-0.0029	-0.2552	0.0061	1
50055000	232	56	0.4165	0.0003	0.0312	0.7398	0	0.2479	0.0008	0.1156	0.2110	0	0.1686	-0.0005	-0.1506	0.1026	0	0.4161	-0.0015	-0.2000	0.0300	1
50056400	43	44	0.4681	0.0005	0.0296	0.7848	0	0.3244	0.0011	0.1036	0.3266	0	0.1436	-0.0009	-0.1882	0.0734	0	0.3116	-0.0025	-0.2495	0.0175	1
50057000	155	56	0.3336	0.0001	0.0078	0.9380	0	0.2315	0.0011	0.1026	0.2672	0	0.1022	-0.0008	-0.2857	0.0019	1	0.3240	-0.0024	-0.2922	0.0015	1
50061800	27	48	0.3562	-0.0001	-0.0106	0.9221	0	0.2077	-0.0012	-0.1472	0.1425	0	0.1485	0.0006	0.1436	0.1524	0	0.4325	0.0029	0.2411	0.0160	1
50138000	311	42	0.2941	-0.0004	-0.0337	0.7615	0	0.1667	-0.0009	-0.1568	0.1464	0	0.1274	0.0006	0.1661	0.1238	0	0.4378	0.0022	0.2869	0.0077	1
50144000	347	52	0.4352	0.0021	0.2640	0.0059	1	0.2169	0.0017	0.3183	0.0009	1	0.2183	0.0005	0.1222	0.2039	0	0.5048	-0.0014	-0.2187	0.0226	1
50147800	183	48	0.5828	-0.0023	-0.2163	0.0308	1	0.3283	-0.0003	-0.0443	0.6632	0	0.2545	-0.0012	-0.2855	0.0043	1	0.4394	-0.0012	-0.1631	0.1038	0

B1)

			ΔP (mm/yr)					ΔQ (mm/yr)					ΔSF (mm/yr)					ΔBF (mm/yr)				
USGS ID	Watershed Area (km^2)	Record (yrs)	Mean	Sen's Slope	MK τ_b	p-value	Trend	Mean	Sen's Slope	MK τ_b	p-value	Trend	Mean	Sen's Slope	MK τ_b	p-value	Trend	Mean	Sen's Slope	MK τ_b	p-value	Trend
50028000	47	56	487	1.29	0.10	0.29	0	241	0.82	0.11	0.24	0	75	0.24	0.07	0.42	0	166	0.66	0.12	0.19	0
50031200	143	50	545	1.67	0.09	0.38	0	211	-1.38	-0.14	0.16	0	98	-0.60	-0.11	0.28	0	114	-0.59	-0.15	0.12	0
50034000	43	41	522	6.63	0.31	0.00	1	199	2.55	0.21	0.05	0	93	1.26	0.17	0.11	0	106	1.25	0.21	0.05	0
50035000	346	57	529	3.99	0.23	0.01	1	205	0.64	0.07	0.45	0	102	0.07	0.01	0.94	0	103	0.45	0.11	0.22	0
50038100	429	45	537	1.00	0.05	0.63	0	248	0.40	0.04	0.74	0	121	0.25	0.01	0.90	0	127	-0.12	-0.03	0.77	0
50038320	39	46	625	2.72	0.11	0.28	0	253	0.23	0.03	0.79	0	138	-0.16	-0.03	0.76	0	114	0.65	0.14	0.17	0
50039500	227	42	590	2.38	0.11	0.31	0	209	2.02	0.22	0.04	1	116	1.24	0.15	0.17	0	93	1.22	0.29	0.01	1
50046000	540	55	540	1.58	0.13	0.17	0	131	-0.65	-0.10	0.28	0	89	-0.18	-0.04	0.66	0	42	-0.49	-0.23	0.01	1
50055000	232	56	535	2.72	0.25	0.01	1	215	0.57	0.08	0.39	0	99	0.37	0.10	0.26	0	116	0.24	0.08	0.36	0
50056400	43	44	546	0.66	0.05	0.63	0	211	1.24	0.17	0.11	0	111	1.32	0.21	0.04	1	100	-0.22	-0.06	0.58	0

50057000	155	56	608	2.76	0.18	0.06	0	165	0.49	0.07	0.44	0	94	0.59	0.16	0.08	0	72	-0.21	-0.09	0.33	0
50061800	27	48	788	6.75	0.27	0.01	1	300	1.37	0.12	0.22	0	148	0.15	0.02	0.81	0	153	0.92	0.15	0.13	0
50138000	311	42	425	2.76	0.21	0.05	1	85	0.44	0.10	0.36	0	33	0.19	0.10	0.36	0	52	0.37	0.15	0.17	0
50144000	347	52	480	3.16	0.27	0.01	1	160	1.22	0.23	0.02	1	51	0.65	0.24	0.01	1	109	0.51	0.16	0.09	0
50147800	183	48	496	3.55	0.26	0.01	1	192	0.88	0.09	0.38	0	82	0.60	0.12	0.22	0	109	0.24	0.09	0.37	0

B2)

			ΔQ / P (mm/yr)					ΔSF / P (mm/yr)					ΔBF / P (mm/yr)					ΔBF / Q (mm/yr)				
USGS ID	Watershed Area (km^2)	Record (yrs)	Mean	Sen's Slope	MK τ_b	p-value	Trend	Mean	Sen's Slope	MK τ_b	p-value	Trend	Mean	Sen's Slope	MK τ_b	p-value	Trend	Mean	Sen's Slope	MK τ_b	p-value	Trend
50028000	47	56	0.4887	0.0008	0.0844	0.3619	0	0.1452	0.0002	0.0325	0.7291	0	0.3435	0.0003	0.0481	0.6059	0	0.7051	-0.0001	-0.0117	0.9044	0
50031200	143	50	0.3930	-0.0040	-0.2424	0.0133	1	0.1761	-0.0014	-0.1412	0.1502	0	0.2169	-0.0018	-0.2098	0.0322	1	0.5591	-0.0003	-0.0188	0.8540	0
50034000	43	41	0.3757	-0.0007	-0.0415	0.7109	0	0.1609	0.0003	0.0244	0.8310	0	0.2148	-0.0005	-0.0537	0.6291	0	0.6021	-0.0012	-0.0488	0.6614	0
50035000	346	57	0.3805	-0.0019	-0.1416	0.1214	0	0.1836	-0.0010	-0.1053	0.2503	0	0.1969	-0.0004	-0.0840	0.3599	0	0.5404	0.0009	0.0677	0.4614	0
50038100	429	45	0.4523	-0.0005	-0.0254	0.8161	0	0.2083	-0.0002	-0.0085	0.9436	0	0.2440	-0.0003	-0.0402	0.7082	0	0.5583	-0.0003	-0.0148	0.8954	0
50038320	39	46	0.3995	-0.0012	-0.0808	0.4396	0	0.2048	-0.0012	-0.1313	0.2070	0	0.1946	-0.0001	-0.0081	0.9454	0	0.4931	0.0015	0.0848	0.4168	0
50039500	227	42	0.3443	0.0023	0.2149	0.0461	1	0.1778	0.0014	0.1452	0.1790	0	0.1666	0.0011	0.1498	0.1654	0	0.4961	-0.0005	-0.0197	0.8623	0
50046000	540	55	0.2334	-0.0017	-0.1973	0.0340	1	0.1547	-0.0006	-0.0923	0.3235	0	0.0786	-0.0012	-0.3199	0.0006	1	0.3553	-0.0020	-0.1582	0.0894	0
50055000	232	56	0.3975	-0.0007	-0.0961	0.2988	0	0.1741	0.0001	0.0130	0.8932	0	0.2234	-0.0009	-0.1610	0.0809	0	0.5699	-0.0012	-0.1000	0.2795	0
50056400	43	44	0.3787	0.0018	0.1860	0.0767	0	0.1905	0.0024	0.2389	0.0229	1	0.1882	-0.0010	-0.1501	0.1538	0	0.5126	-0.0050	-0.2727	0.0093	1
50057000	155	56	0.2651	-0.0003	-0.0390	0.6767	0	0.1427	0.0004	0.0727	0.4327	0	0.1224	-0.0010	-0.2779	0.0025	1	0.4906	-0.0027	-0.1701	0.0651	0
50061800	27	48	0.3897	-0.0010	-0.0621	0.5397	0	0.1857	-0.0009	-0.1099	0.2743	0	0.2040	-0.0004	-0.0621	0.5397	0	0.5341	0.0014	0.0887	0.3789	0
50138000	311	42	0.2002	-0.0002	-0.0383	0.7287	0	0.0745	0.0001	0.0105	0.9309	0	0.1257	0.0002	0.0383	0.7287	0	0.6301	-0.0005	-0.0314	0.7781	0
50144000	347	52	0.3326	0.0008	0.0860	0.3726	0	0.1010	0.0006	0.1629	0.0898	0	0.2316	-0.0001	-0.0060	0.9559	0	0.7001	-0.0019	-0.1327	0.1673	0
50147800	183	48	0.3880	-0.0015	-0.1188	0.2372	0	0.1500	0.0005	0.0621	0.5397	0	0.2379	-0.0017	-0.2482	0.0131	1	0.6297	-0.0025	-0.1560	0.1198	0

C1)

			ΔP (mm/yr)					ΔQ (mm/yr)					ΔSF (mm/yr)					ΔBF (mm/yr)				
USGS ID	Watershed Area (km^2)	Record (yrs)	Mean	Sen's Slope	MK τ_b	p-value	Trend	Mean	Sen's Slope	MK τ_b	p-value	Trend	Mean	Sen's Slope	MK τ_b	p-value	Trend	Mean	Sen's Slope	MK τ_b	p-value	Trend
50028000	47	56	1402	3.72	0.16	0.09	0	681	4.13	0.19	0.04	1	295	1.70	0.16	0.08	0	386	2.72	0.22	0.02	1

50031200	143	50	1192	3.82	0.12	0.24	0	361	-0.16	-0.01	0.95	0	203	0.43	0.04	0.68	0	158	-0.52	-0.08	0.39	0
50034000	43	41	1262	11.08	0.27	0.01	1	483	3.65	0.14	0.20	0	297	1.43	0.08	0.47	0	186	2.52	0.24	0.03	1
50035000	346	57	1275	4.86	0.15	0.11	0	416	1.64	0.09	0.31	0	249	0.44	0.04	0.66	0	167	1.32	0.18	0.05	1
50038100	429	45	1167	-0.15	0.00	0.99	0	505	1.51	0.06	0.55	0	296	0.97	0.06	0.54	0	208	0.38	0.07	0.51	0
50038320	39	46	1196	3.08	0.10	0.32	0	420	1.65	0.09	0.39	0	256	0.46	0.03	0.75	0	164	0.87	0.13	0.22	0
50039500	227	42	1248	8.99	0.24	0.03	1	352	5.80	0.28	0.01	1	208	3.52	0.26	0.02	1	144	1.96	0.25	0.02	1
50046000	540	55	1269	3.93	0.16	0.09	0	334	0.72	0.04	0.70	0	260	1.07	0.07	0.48	0	74	-0.44	-0.09	0.32	0
50055000	232	56	1408	8.03	0.29	0.00	1	619	3.31	0.15	0.11	0	408	3.08	0.20	0.03	1	211	0.24	0.02	0.80	0
50056400	43	44	1462	3.42	0.10	0.37	0	744	2.21	0.08	0.45	0	555	2.82	0.09	0.40	0	189	-0.74	-0.08	0.42	0
50057000	155	56	1520	5.35	0.18	0.06	0	574	3.29	0.12	0.21	0	428	3.52	0.18	0.05	0	146	-0.42	-0.06	0.50	0
50061800	27	48	1716	5.45	0.12	0.22	0	619	2.19	0.06	0.53	0	396	-0.84	-0.04	0.70	0	223	2.41	0.29	0.00	1
50138000	311	42	1352	2.42	0.08	0.44	0	451	0.18	0.01	0.97	0	272	-0.98	-0.08	0.44	0	179	1.58	0.16	0.14	0
50144000	347	52	1459	1.63	0.06	0.53	0	690	3.63	0.20	0.04	1	375	2.72	0.21	0.03	1	314	1.54	0.17	0.08	0
50147800	183	48	1058	6.17	0.15	0.12	0	709	1.85	0.08	0.45	0	431	1.95	0.12	0.22	0	278	0.38	0.03	0.76	0

C2)

			ΔQ / P (mm/yr)					ΔSF / P (mm/yr)					ΔBF / P (mm/yr)					ΔBF / Q (mm/yr)				
USGS ID	Watershed Area (km^2)	Record (yrs)	Mean	Sen's Slope	MK τ_b	p-value	Trend	Mean	Sen's Slope	MK τ_b	p-value	Trend	Mean	Sen's Slope	MK τ_b	p-value	Trend	Mean	Sen's Slope	MK τ_b	p-value	Trend
50028000	47	56	0.4782	0.0018	0.2067	0.0263	1	0.2051	0.0007	0.1556	0.0950	0	0.2731	0.0012	0.2027	0.0294	1	0.5722	0.0005	0.0761	0.4162	0
50031200	143	50	0.2889	-0.0011	-0.1494	0.1279	0	0.1599	-0.0004	-0.0710	0.4719	0	0.1290	-0.0009	-0.1657	0.0911	0	0.4570	-0.0011	-0.0873	0.3753	0
50034000	43	41	0.3593	-0.0001	-0.0098	0.9373	0	0.2197	-0.0006	-0.0488	0.6614	0	0.1396	0.0008	0.1561	0.1537	0	0.4067	0.0031	0.2610	0.0167	1
50035000	346	57	0.3085	-0.0001	-0.0050	0.9616	0	0.1833	-0.0004	-0.0739	0.4206	0	0.1252	0.0003	0.0877	0.3386	0	0.4172	0.0016	0.1805	0.0482	1
50038100	429	45	0.4167	0.0009	0.0707	0.4997	0	0.2405	0.0004	0.0303	0.7767	0	0.1763	0.0005	0.0626	0.5507	0	0.4440	0.0004	0.0283	0.7917	0
50038320	39	46	0.3329	0.0016	0.1150	0.2639	0	0.1936	0.0004	0.0377	0.7190	0	0.1394	0.0008	0.1652	0.1075	0	0.4327	0.0011	0.0628	0.5445	0
50039500	227	42	0.2616	0.0030	0.2451	0.0229	1	0.1532	0.0018	0.2381	0.0270	1	0.1084	0.0011	0.2056	0.0565	0	0.4206	-0.0007	-0.0662	0.5439	0
50046000	540	55	0.2372	-0.0003	-0.0209	0.8276	0	0.1824	0.0004	0.0384	0.6844	0	0.0549	-0.0006	-0.1933	0.0379	1	0.2580	-0.0028	-0.2391	0.0102	1
50055000	232	56	0.4204	0.0004	0.0364	0.6975	0	0.2721	0.0010	0.0896	0.3329	0	0.1483	-0.0004	-0.1026	0.2672	0	0.3668	-0.0016	-0.2195	0.0172	1
50056400	43	44	0.5000	-0.0007	-0.0782	0.4603	0	0.3713	-0.0002	-0.0169	0.8794	0	0.1287	-0.0010	-0.1966	0.0613	0	0.2595	-0.0020	-0.2178	0.0381	1
50057000	155	56	0.3570	0.0008	0.0545	0.5575	0	0.2622	0.0017	0.1558	0.0912	0	0.0948	-0.0007	-0.2494	0.0068	1	0.2821	-0.0025	-0.3026	0.0010	1

50061800	27	48	0.3434	0.0006	0.0426	0.6761	0	0.2163	-0.0011	-0.0922	0.3599	0	0.1270	0.0010	0.2465	0.0138	1	0.3893	0.0035	0.2376	0.0176	1
50138000	311	42	0.3231	-0.0005	-0.0383	0.7287	0	0.1942	-0.0011	-0.1545	0.1526	0	0.1289	0.0008	0.1940	0.0720	0	0.4039	0.0024	0.2706	0.0119	1
50144000	347	52	0.4696	0.0025	0.2911	0.0024	1	0.2537	0.0020	0.2790	0.0036	1	0.2158	0.0006	0.1267	0.1876	0	0.4624	-0.0012	-0.1599	0.0959	0
50147800	183	48	0.6846	-0.0029	-0.1879	0.0607	0	0.4111	-0.0015	-0.1259	0.2101	0	0.2735	-0.0011	-0.1809	0.0712	0	0.4015	-0.0010	-0.1188	0.2372	0